Unconventional Superconductivity in Correlated Fermion Systems

Jan Kaczmarczyk

Rozprawa doktorska
Promotor: Prof. dr hab. Józef Spałek

Uniwersytet Jagielloński
Instytut Fizyki im. Mariana Smoluchowskiego
Zakład Teorii Materii Skondensowanej i Nanofizyki

Kraków, maj 2011

Abstract

We study unconventional superconductivity in strongly correlated electron systems and in applied magnetic (Zeeman) field. The strong correlations among quasiparticles are accounted for by means of the Gutzwiller approximation within the statistically-consistent scheme proposed recently in our group. We analyze the situation for a gas of heavy quasiparticles and obtain a phase diagram on the magnetic field-temperature plane (for both two- and three-dimensional cases, including the s-wave- and d-wave-gap symmetry solutions). In low magnetic fields the system is in the Bardeen-Cooper-Schrieffer (BCS) phase, whereas for the increasing magnetic field a transition to the Fulde-Ferrell-Larkin-Ovchinnikov (FFLO) phase with nonzero Cooper pair momentum takes place. To distinguish novel features of the case with strong correlations we compare our results with those for a non-correlated situation. In all analyzed situations the FFLO phase is more robust for the case with strong correlations, which implies that *strong correlations stabilize the FFLO phase* (and possibly other high-field low-temperature unconventional phases). We explain the stabilization mechanism.

Next, we study conductance of a normal metal - strongly-correlated superconductor junction in order to provide an experimental test of our results. The conductance spectra in the cases with and without strong correlations differ essentially, and the differences should be easily observable experimentally, providing a *hallmark of strong correlations in the superconducting state*. Namely, correlations alter the distance between the conductance peaks for carriers with spin-up and spin-down. In the non-correlated case this distance is twice the Zeeman energy. In the correlated case this distance is about 30-50% smaller, but in other models it may be larger, depending on details of the electronic structure.

Additionally, we perform analysis of the coexistence of antiferromagnetism (AF) and superconductivity (SC) within t-J model for a system with strong correlations and in applied magnetic field in the Pauli limit. The coexisting phase exhibits two superconducting gaps (a consequence of the AF and SC coexistence): singlet and staggered-triplet. The triplet component has a nonzero Cooper pair momentum, and can be viewed as an analogue of the FFLO phase. We obtain a phase diagram on the band filling - magnetic field plane. For band filling close to unity (i.e., close to the half-filled band situation) *our results resemble those obtained recently in the heavy fermion system* $CeCo(In_{1-x}Cd_x)_5$. Namely, with the increasing magnetic field the system evolves from the coexisting phase, through AF phase, towards the spin-polarized normal state. Moreover, the onset of superconducting order decreases antiferromagnetic magnetization.

Keywords: strongly correlated electrons, unconventional superconductivity, heavy fermions, Fulde-Ferrell-Larkin-Ovchinnikov (FFLO) phase, spin-dependent masses, Andreev reflection, Andreev-reflection spectroscopy, Gutzwiller approach, antiferromagnetism, $CeCoIn_5$, d-wave superconductivity, t-J model, statistically-consistent Gutzwiller approximation (SGA).

Streszczenie

W rozprawie rozważono niekonwencjonalne nadprzewodnictwo w układach silnie skorelowanych elektronów w polu magnetycznym (typu Zeemana). Silne korelacje między kwaziczą̨stkami uwzględniono poprzez przybliżenie Gutzwillera w ramach statystycznie-konsystentnego podejścia zaproponowanego ostatnio w naszym zespole. Poddano analizie sytuację gazu ciężkich kwaziczą̨stek i otrzymano diagram fazowy w funkcji pola magnetycznego i temperatury (dla przypadku dwu- i trój-wymiarowego oraz uwzględniając symetrię przerwy typu s-wave oraz d-wave). W niskich polach magnetycznych układ jest w stanie Bardeena-Coopera-Schrieffera (BCS), natomiast przy zwiększaniu pola magnetycznego następuje przejście do fazy typu Fulde-Ferrell-Larkin-Ovchinnikov (FFLO) z niezerowym pędem środka masy par Coopera. Celem wyodrębnienia nowych cech przypadku z silnymi korelacjami, wyniki zostały porównane z otrzymanymi dla przypadku bez korelacji. We wszystkich analizowanych sytuacjach faza FFLO występuje w szerszym przedziale temperatur i pól w przypadku silnych korelacji co implikuje, że *silne korelacje stabilizują fazę FFLO* (i prawdopodobnie inne niekownencjonalne fazy pojawiające się w silnych polach i niskich temperaturach). W rozprawie wytłumaczono także mechanizm stabilizacji tego stanu.

Przeanalizowano także przewodność złącza typu normalny metal - silnie-skorelowany nadprzewodnik w celu sformułowania eksperymentalnego testu naszych wyników. Przebiegi przewodności w przypadkach z obecnością i absencją silnych korelacji różnią się znacznie. Różnice te powinny być łatwo mierzalne doświadczalnie, dostarczając *testu występowania silnych korelacji w stanie nadprzewodzącym*. Mianowicie, korelacje zmieniają odległość pomiędzy maksimami przewodności pochodzącymi od nośników o spinie w górę i tych o spinie w dół. W sytuacji braku korelacji ta odległość jest równa podwojonej energii Zeemana. Dla przypadku z korelacjami, odległość ta jest 30-50% mniejsza, ale w innych modelach może też być większa w zależności od szczegółów struktury elektronowej.

Dodatkowo, rozważono koegzystencję antyferromagnetyzmu (AF) i nadprzewodnictwa (SC) w ramach modelu t-J dla układu z silnymi korelacjami oraz w polu magnetycznym, w granicy Pauliego. Faza z koegzystencją wykazuje się dwiema przerwami: singletową oraz przerwą trypletową typu *staggered-triplet*. Składowa trypletowa charakteryzuje się niezerowym pędem środka masy par Coopera i może być postrzegana jako analogon fazy FFLO. Otrzymano diagram fazowy w funkcji wypełnienia pasma i pola magnetycznego. Dla sytuacji pasma prawie do połowy wypełnionego nasze wyniki *przypominają otrzymane ostatnio w układzie ciężkofermionowym* $CeCo(In_{1-x}Cd_x)_5$. Mianowicie, przy zwiększaniu pola magnetycznego układ ewoluuje z fazy z koegzystencją, poprzez fazę AF, ku spinowo-spolaryzowanemu stanowi normalnemu. Co więcej, pojawienie się przerwy nadprzewodzącej zmniejsza magnetyzację podsieci w stanie AF+SC.

Słowa kluczowe: silnie skorelowane elektrony, niekonwencjonalne nadprzewodnictwo, ciężkie fermiony, faza Fulde-Ferrell-Larkin-Ovchinnikov (FFLO), spinowo-zależne masy, odbicie Andreeva, metoda Gutzwillera, $CeCoIn_5$, antyferromagnetyzm, statystycznie konsystentne przybliżenie Gutzwillera (SGA), nadprzewodnictwo typu d-wave, model t-J.

Contents

Acknowledgements

I would like to express my gratitude to Prof. Józef Spałek for supervising the Thesis, for being a continuous source of motivation and inspiration during my scientific carrier, and for reading thoroughly the text of this Thesis.

Discussions with Prof. Krzysztof Byczuk, Prof. Maciej Maśka, Dr hab. Mariusz Sadzikowski, and my colleagues: Marcin Abram, Olga Howczak, Jakub Jędrak, Michał Heller, Tomasz Partyka, Marcin Wysokiński, and Zygmunt Starypan are also appreciated.

The work was supported by Ministry of Science and Higher Education under Grants Nos. N N202 173735 and N N202 128736.

I acknowledge that during the work on my Thesis I have been a scholarship fellow of the "Doctus – Małopolski fundusz stypendialny dla doktorantów" project cofunded by EU funds within European Social Fund.

I also acknowledge being a scholarship fellow within "Małopolskie Stypendium Doktoranckie" project financed by European Social Fund and Polish national budget under the Integrated Regional Operational Programme 2004-2006.

The results presented in this Thesis constituted part of the motivation for applying for the *TEAM* project by Prof. Spałek. This grant has been awarded by Foundation for Polish Science (FNP) for the years 2011-14.

List of abbreviations

AF	Antiferromagnetism (or antiferromagnetic)
ALFL	Almost Localized Fermi Liquid
AR	Andreev reflection
AW	Andreev window
BCS	Bardeen-Cooper-Schrieffer
BdG	Bogolyubov-de Gennes
FF	Fulde-Ferrell
FFLO	Fulde-Ferrell-Larkin-Ovchinnikov
FM	Ferromagnetic
GA	Gutzwiller approximation
GSL	GNU Scientific Library
HFLT	High-field low-temperature (phase)
IC	Incommensurate
LO	Larkin-Ovchinnikov
MF	Mean-field
NS	Normal state
NSJ	Normal metal - superconductor junction
PAM	Periodic Anderson Model
RMFT	Renormalized Mean-Field Theory
SB	Slave boson
SC	Superconductivity (or superconducting)
SDM	Spin-dependent masses
SDW	Spin-density wave
SFM	Saturated ferromagnetic
SGA	Statistically-consistent Gutzwiller approximation
SIM	Spin-independent masses

Chapter 1

Introduction

In this Chapter we review briefly different types of unconventional superconductivity and emphasize the role of strong electronic correlations in formation of those unconventional phases. Next, we concentrate on the Fulde-Ferrell-Larkin-Ovchinnikov (FFLO) phase, which is the central topic of the Thesis. We review the experimental systems in which the FFLO phase has been indicated, concentrating on the heavy fermion superconductor $CeCoIn_5$ - the most likely candidate as the host for the FFLO phase. Finally, we substantiate why strong correlations should be a key ingredient in theories of the FFLO state, and we set the aim of the Thesis as to provide such a formulation.

1.1 Unconventional superconductivity

Unconventional superconductivity is recently a very hot topic in the condensed-matter physics. It is studied almost as frequently as high-temperature superconductivity and comprises a number of heavy-fermion [1] and organic metallic [2] systems. Among the novel states observed and discussed intensively recently is the superconductivity in the systems without space-inversion [3, 4], and time-reversal [5, 6] symmetry, the states in which superconductivity coexists with antiferromagnetic [7–9] or ferromagnetic [10, 11] order, as well as the FFLO state [12–14] coexisting with the incommensurate spin-density wave order [15–17].

Since all the systems of interest have narrow bands, the *role of electronic correlations is crucial* in formation of exotic phases. To support this point of view let us quote a few authors:

- *Strong electron-electron correlation is one of the central issues of the current condensed-matter physics. The so-called heavy-fermion materials represent a typical example of systems in which strong correlation effects are essential in determining their physical properties.*, Tsunetsugu *et al.* 1997, Ref. 18.

- *A systematic search for novel forms of superconductive pairing interactions and pairing symmetries hence requires a systematic quantitative determination of the quasiparticle interactions in the presence of strong electronic correlations.*, Pfleiderer 2009, Ref. 1.

- *The relationship between large-moment magnetism and superconductivity (...) cannot be explained by conventional models (...). Electronic duality manifested in $CeRhIn_5$ requires a new conceptual framework that poses a challenge to theory. An appropriate description of strong electronic correlations must be a key ingredient of this framework.*, Park *et al.* 2008, Ref. 19.

In brief, by unconventional superconductivity we understand the superconductivity, which is not described by the BCS theory and the superconducting state under consideration involves usually (strongly) correlated fermions.

1.2 Fulde-Ferrell-Larkin-Ovchinnikov phase

1.2.1 Theory

The FFLO superconducting state has been proposed theoretically in the 1960s [20, 21]. In this unconventional superconducting state the Fermi surface splitting of the electrons due to the Zeeman term of the magnetic field makes it favorable for the Cooper pair to have a nonzero total momentum $\mathbf{Q}$. Consequently, the phase of the superconducting gap oscillates spatially with the wave vector $\mathbf{Q}$, i.e. $\Delta(\mathbf{r}) = \Delta_{\mathbf{Q}} e^{i\mathbf{Qr}}$. By forming such a condensate of moving Cooper pairs, the superconducting state survives to the magnetic fields higher than the *Pauli H_{c2} limit*. The simplest FFLO phase (with $\Delta(\mathbf{r}) = \Delta_{\mathbf{Q}} e^{i\mathbf{Qr}}$) is called the Fulde-Ferrell (FF) state. By forming superposition of such superconducting gaps with different directions of the Cooper pair momentum $\mathbf{Q}$, the Larkin-Ovchinnikov (LO) state is obtained. In the simplest case of LO phase, the gap is a standing wave, i.e., $\Delta(\mathbf{r}) = (\Delta_{\mathbf{Q}} e^{i\mathbf{Qr}} + \Delta_{\mathbf{Q}} e^{-i\mathbf{Qr}})/2 = \Delta_{\mathbf{Q}} \cos(\mathbf{Qr})$, but more complicated phases are possible [14, 21]. In this Thesis we will consider only FF type of FFLO state. We will sometimes call this state as FFLO, since it is a subclass of FFLO states.

For the stability of the FFLO phase the orbital effects must be strongly suppressed and the *Maki parameter* [22] high. This parameter is defined as the ratio of the upper critical fields coming from orbital effects H_{c2}^{orb} to the upper critical field coming from the Pauli paramagnetism (Zeeman term) H_{c2}^{P}, namely $\alpha = \sqrt{2} H_{c2}^{orb} / H_{c2}^{P}$. The Maki parameter expresses the relative importance of orbital and Pauli effects in destabilizing the condensed state. The required minimum value of the Maki parameter for the formation of the FFLO state is $\alpha = 1.8$ [23]. For lower Maki parameters the influence of the orbital effects becomes the dominating factor, and the FFLO state is not stable.

1.2.2 Experimental realization

The FFLO state has suddenly gained renewed interest recently (for a review see Ref. 14) because of its possible realization in the heavy fermion superconductor $CeCoIn_5$ [12, 13, 17, 24–26] (for details see Section 1.2.3), although the nature of the high-field low-temperature (HFLT) phase observed in this system is still under hot debate after incommensurate spin-density wave order has been observed in the vicinity of this phase [15–17, 27–30].

The FFLO state has also been proposed for the organic superconductor κ-(BEDT-TTF)$_2$Cu(NCS)$_2$ [31, 32], β''-(ET)$_2$SF$_5$CH$_2$CF$_2$SO$_3$ [33], and other layered organic superconductors (see References in Ref. 32). Also, the FFLO state has been indicated in other heavy-fermion systems: PuRhGa$_5$ [34], Ce$_2$PdIn$_8$ [35] (see Ref. 1, Sec. V.B.1 for a more detailed account), as well as in the pnictide superconductor LiFeAs [36]. The FFLO state is also investigated in high density quark and nuclear matter [37], as well as in optical lattices [38–40].

1.2.3 The case of CeCoIn$_5$

CeCoIn$_5$ is a member of the Ce-based '115' heavy-fermion compounds - the family of CeMIn$_5$ (with $M = Co, Rh, Ir$) [41–43]. Superconductivity in CeCoIn$_5$ has been reported by Petrovic *et al.* [44]. It has the highest critical temperature ($T_c = 2.25$ K) of all the heavy fermion compounds and superconductivity is believed to be magnetically mediated. The relevant energy scale for such superconductivity is T_{sf}, the characteristic spin-fluctuation temperature. In CeCoIn$_5$, $T_{sf} = 10$ K [44], which gives $T_c/T_{sf} = 0.2$, quite close to the maximum theoretically predicted value of $20 - 40\%$ [45] (in Ref. 46, the authors claim that in zero field $T_{sf} \approx 5$ K, what yields the ratio $T_c/T_{sf} = 0.4$). The electronic structure of the normal phase of CeCoIn$_5$ is quasi-2D [44, 47–49] and the superconducting gap exhibits a d-wave symmetry [50–52]. The band structure calculations for CeCoIn$_5$ have also been performed [53–55], but they are not directly relevant to the topics tackled in this Thesis.

A novel HFLT superconducting phase has been indicated in CeCoIn$_5$ for the first time by Murphy *et al.* [56] by magnetization measurements. This state has been further investigated by specific heat measurements by Bianchi *et al.* [24] (see Figure 1.2a for the obtained phase diagram). Radovan *et al.* [57] performed heat capacity and magnetization measurements, and interpreted their data as indicative of regions of superconductivity alternating with walls of spin-polarized unpaired electrons as expected in the FFLO phase but this interpretation has been contested [58]. Kakuyanagi *et al.* [12] performed the first Nuclear Magnetic Resonance (NMR) study of the HFLT phase (for a review of application of the NMR technique to probing the superconducting state of heavy fermions see Ref. 59). This analysis has also been contested [60] and defended [61]. Similar NMR measurements for the parallel field orientation (with respect to the ab plane) were performed in Ref. 13 (see Figure 1.2b for the phase diagrams obtained for both field orientations).

The first indication of an intricate interplay of magnetism and superconductivity as origin of the HFLT phase has been provided by Mitrovic *et al.* [27]. The authors observed an increased spin susceptibility in the HFLT phase as compared to the uniform SC state. Magnetic order in the vicinity of the HFLT phase has been investigated by Young *et al.* [15]. The authors interpreted NMR spectra as indicative of ordered static spin moments in the vortex cores. Kenzelmann *et al.* [16, 30] investigated the HFLT phase by high-field neutron diffraction to search for magnetic Bragg peaks within HFLT phase. The authors found that this phase simultaneously carries cooperating superconducting and magnetic orders and the

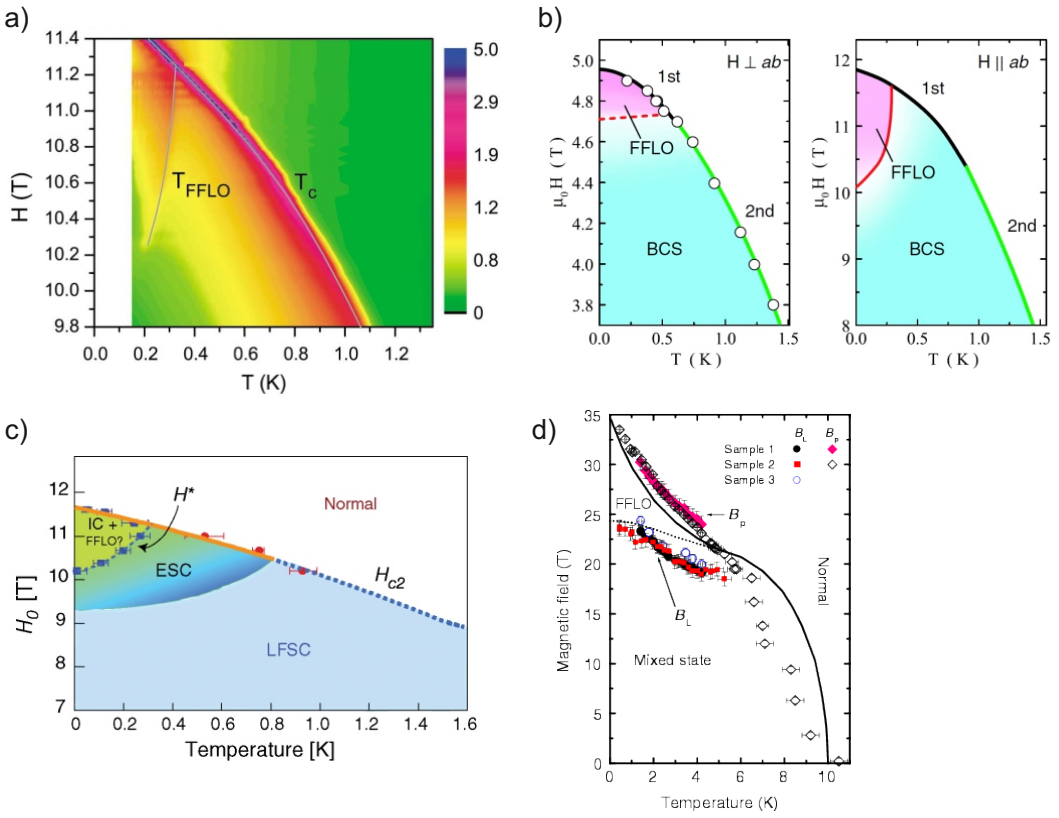

Figure 1.1: Experimental phase diagrams of $CeCoIn_5$ determined by: (a) electronic specific heat measurements, after Ref. 24, (b) NMR experiments for both parallel (right) and perpendicular (left) field orientations, after Ref. 13, and (c) the revised phase diagram proposed in Ref. 17. The phases in (c) are labeled as follows: LFSC - low field superconducting, ESC - exotic superconducting, IC+FFLO - a phase with incommensurate spin density wave and FFLO modulation of the superconducting gap. In (d) the phase diagram for the organic superconductor κ-$(BEDT\text{-}TTF)_2Cu(NCS)_2$ has been added for comparison, after Ref. 31.

latter exists only in the vicinity of the HFLT phase. Moreover, the magnetic order extends over a length scale much larger than the diameter of the vortex cores. The Cooper pair momentum $|\mathbf{Q}|$ has been found to be field-independent in $CeCoIn_5$, contrary to the FFLO picture.

Meanwhile, the FFLO scenario has been supported by pressure [25] and doping [62–64] studies (for a theoretical interpretation see Ref. 65). Namely, the HFLT phase expands with applying pressure, i.e. with lowering the influence of antiferromagnetic fluctuations [25]. Moreover, the HFLT phase turns out to be sensitive to a minute amount of impurities [62], what indicates that it is not magnetically-driven but fundamentally superconducting.

Koutroulakis *et al.* [17] performed NMR measurements and proposed an alternative phase diagram with a region dominated by strong spin fluctuations but without static magnetic long-range order, referred to as "exotic" SC, ESC (see Figure 1.2c for the phase diagram), which could be an FFLO phase without the magnetic long-range order. They also deduced that the long-range magnetic order appearing in the vicinity of the HFLT phase is an incommensurate Spin Density Wave (SDW) with moments oriented along the c axis, independent of the in-plane field orientation. Kenzelmann *et al.* [30] interpreted this independence (seen also in their neutron-scattering measurements) as evidence for modulation of AF order along the lines of nodes of the d-wave superconducting order parameter. They suggested that the SDW order may hence have its origin in the local magnetism inside the vortex cores observed in Refs. 15 and 66.

Very recently, Kumagai *et al.* [26] (using the NMR technique) provided direct evidence of the normal quasiparticles appearing in the HFLT phase, what speaks in favor of the FFLO scenario. Also, it has been shown theoretically that paramagnetic pair breaking induces not only the FFLO state but also an incommensurate SDW order [67, 68].

Therefore, one clearly sees, that there is no consensus on the true nature of the HFLT phase in $CeCoIn_5$, and no existing theory explains all experimental findings. As yet, no measurements have provided direct evidence for the spatial modulation of the order parameter, what would unambiguously prove the FFLO scenario. A candidate technique for such measurements is the Andreev reflection spectroscopy, as it is a probe sensitive to both the phase and amplitude modulation of the superconducting order parameter [69, 70].

1.3 Aim and scope of the Thesis

All the systems suggested to be a host to the FFLO phase have a *reduced dimensionality*, what is crucial for the FFLO phase stability, as then the orbital effects are suppressed and the Pauli effect (Zeeman splitting) may become the dominant factor. Another feature, which suppresses the orbital effects is the *heavy quasiparticle mass*. These characteristics of possible FFLO hosts indicate that these systems are *likely to have strong electron (fermion) correlations*.

The role of strong correlations in the most likely candidate for the FFLO state, $CeCoIn_5$ is essential not only because this system is a heavy fermion supercon-

ductor, with a narrow band originating from $4f$ electrons and large Hubbard U. Additionally, spin-dependent masses (SDM) of quasiparticles have been observed in this system [47] by means of the de Haas-van Alphen oscillations in strong applied magnetic field. SDM are a hallmark of strong correlations, as they appear naturally in theories incorporating correlations (Gutzwiller [71], slave-bosons [72–74], Dynamical Mean Field Theory, DMFT [75], fluctuation-exchange approximation, FLEX [76]) when the system is spin-polarized.[1]

In effect, since $CeCoIn_5$ is clearly a strongly-correlated superconductor, it is important to *provide a theory of the superconducting state in an applied Zeeman field, which would account for strong correlations among the paired quasiparticles.* This is the principal aim of the present Thesis. This goal has not yet been achieved in the context of the FFLO phase. All theories relating to $CeCoIn_5$, although providing important results (i.e. the correct orders of phase transitions, similar phase diagram, coexistence with antiferromagnetism), are uncorrelated [68, 79, 80]. For example the Hubbard U assumed [79] is about two orders of magnitude smaller than the value coming from e.g. band structure calculations. These theories also contain phenomenological terms in the starting Hamiltonian (are not microscopic). Note also, that superconductivity with the spin-asymmetric bandwidths (on the technical level similar to spin-dependent masses) has been investigated in Ref. 81. There, the bandwidths were assumed as free parameters (not determined by e.g. the Gutzwiller scheme). Moreover, that study reflects a different physical situation, i.e. the coexistence of strong pairing correlations and itinerant electron ferromagnetism, although the authors have also made a reference to $CeCoIn_5$.

Additional motivation for the research described in this Thesis has been provided by results of the M. Sc. Thesis of the author [82]. Therein, the single Cooper pair has been investigated in the case of a strongly-correlated system and in applied field. The single Cooper pair is a precursor of the condensed state of pairs. In low magnetic fields the Cooper pair has a zero momentum and is in the spin-singlet state, whereas for the increasing magnetic field the transition to a moving-Cooper-pair state takes place. The moving Cooper pair is in the spin-specific state, which can be viewed as a superposition of the singlet and the triplet components (see Figure 1.2 and Ref. 83).

1.4 A brief summary

In the present Thesis we intend to describe superconductivity in a system with strong correlations and in an applied Zeeman field. The need for such study is provided by the observation of high-field low-temperature phase (possibly FFLO) in the heavy-fermion superconductor $CeCoIn_5$, in which strong correlations undoubtedly play important role.[2]

[1] SDM have also been observed in other heavy-fermion systems [77, 78].

[2] Although the motivation for our study is material-related, we perform calculations for a model situation, as already such analysis leads to quite interesting and universal physical conclusions.

Therefore, the basic questions we pose at the beginning of this Thesis are:

1. *What is the role of strong correlations in stabilization of the FFLO phase and other high-field low-temperature unconventional superconducting phases?*

2. *How do the correlations manifest themselves experimentally in a superconducting state?*

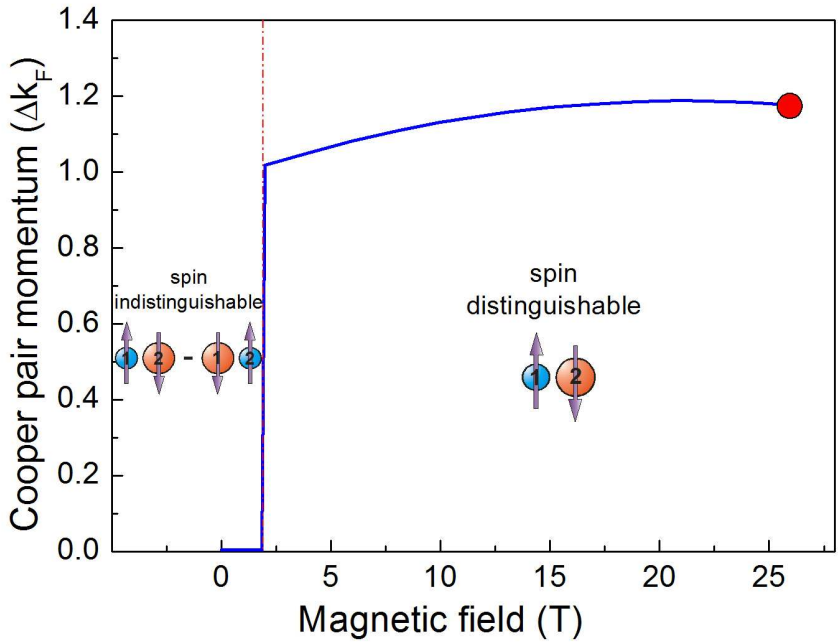

Figure 1.2: Optimal Cooper pair center-of-mass momentum versus magnetic field. For high enough fields $|\mathbf{Q}| \simeq \Delta k_F$, where $\Delta k_F \equiv k_{F2} - k_{F1}$ is the Fermi-wave vectors splitting. The regimes with the full spin-singlet and the specific-spin wave functions are also shown. The solid circle at the end marks the Pauli limiting critical field, at which the pair binding energy vanishes. The different sizes of circles corresponding to different spin orientations and express unequal, spin-dependent masses.

Chapter 2

Theoretical framework

In this Chapter we set the theoretical framework of a theory of strongly-correlated superconductors. The strong correlations among quasiparticles are discussed and taken into account first by means of the Gutzwiller method. We review this method in the simplest formulation (still used in the literature, mostly in the context of high-Tc superconductors under the name of Renormalized Mean-Field Theory, RMFT). Next, we explain, why this formulation turns out insufficient, and we provide an improved formalism (called Statistically-consistent Gutzwiller Approximation, SGA [84]). This version is equivalent with the slave-boson formalism (for a formal proof see Ref. 84) and will be used throughout the Thesis. Finally, we comment on how to obtain both Gutzwiller band narrowing factors and the pairing term in the model Hamiltonian. The resulting Hamiltonian is a one-band effective Hamiltonian which accounts for both *strong correlations* and the *pairing*, and will be used in the following Chapters.

2.1 Gutzwiller Approximation

To introduce Gutzwiller Approximation (GA) we start from the simplest Hamiltonian in which electron correlations play an important role, namely the single-band Hubbard Hamiltonian, which has the form

$$\hat{\mathcal{H}} = \sum_{ij\sigma} t_{ij} c^{\dagger}_{i\sigma} c_{j\sigma} + U \sum_{i} \hat{n}_{i\uparrow} \hat{n}_{i\downarrow} + \sum_{i\sigma} \sigma h c^{\dagger}_{i\sigma} c_{i\sigma}, \tag{2.1}$$

where the first term expresses particle hopping between the sites i and j (with the hopping amplitude t_{ij}), the second describes the intra-atomic repulsive interaction characterized by the Hubbard parameter U, and the third is the Zeeman term with the reduced field $h = g\mu_B H$. In the following Λ, $N_{\uparrow}$, ($N_{\downarrow}$), and D denote the number of lattice sites, of spin up (down) electrons, and of double occupied sites, respectively. Also, $n_{\sigma} \equiv N_{\sigma}/\Lambda$ for $\sigma = \uparrow, \downarrow$ and $D/\Lambda \equiv d^2$ (this quantity is identical with the quantity d of Ref. 85 and d^2 of Ref. 86).

We summarize here the standard[1] GA [87] following the notation of Ref. 85. The Gutzwiller trial state $|\psi\rangle$ is derived from an uncorrelated, normalized single-

[1]The word "standard" refers to e.g. expressions for the approximate ground-state energy. The

particle state $|\psi_0\rangle$ by suppressing the weight of those components of the latter, which correspond to doubly occupied sites. In the simplest case, $|\psi\rangle$ depends on a single variational parameter g, i.e. the many-body trial wave function is postulated of the form

$$|\psi\rangle = \prod_i [1-(1-g)\hat{n}_{i\uparrow}\hat{n}_{i\downarrow}]|\psi_0\rangle \equiv \hat{P}_G|\psi_0\rangle. \tag{2.2}$$

In the present case $|\psi_0\rangle$ represents an ordinary Fermi sea, although it may be magnetically polarized (more complicated uncorrelated states exhibiting e.g. antiferromagnetic and/or superconducting order, can also be considered [88], cf. also Chapter 6). Using the projection (2.2), one may try to evaluate the expectation value of the Hamiltonian (2.1), i.e. $\langle\psi|\hat{\mathcal{H}}|\psi\rangle/\langle\psi|\psi\rangle$. However, this is a nontrivial task and to deal with it we have to introduce further approximations, which will not be discussed in detail here [85, 87]. In result, following Gutzwiller [87], we obtain a relatively simple formula for the ground-state energy E_g, which for the translationally invariant state reads

$$\frac{1}{\Lambda}\frac{\langle\psi|\hat{\mathcal{H}}|\psi\rangle}{\langle\psi|\psi\rangle} \approx E_g/\Lambda = q_\uparrow(d,n_\uparrow,n_\downarrow)\bar{\epsilon}_\uparrow + q_\downarrow(d,n_\uparrow,n_\downarrow)\bar{\epsilon}_\downarrow + Ud^2. \tag{2.3}$$

In the above, the quantity

$$q_\sigma(d,n_\uparrow,n_\downarrow) = \frac{\{[(n_\sigma-d^2)(1-n_\sigma-n_{\bar{\sigma}}+d^2)]^{1/2} + d[(n_{\bar{\sigma}}-d^2)]^{1/2}\}^2}{n_\sigma(1-n_\sigma)}, \tag{2.4}$$

has an interpretation of the band narrowing (renormalization) factor and

$$\bar{\epsilon}_\sigma = \Lambda^{-1}\langle\psi_0|\sum_{ij} t_{ij}c^\dagger_{i\sigma}c_{j\sigma}|\psi_0\rangle = \Lambda^{-1}\sum_{\mathbf{k}}\epsilon_{\mathbf{k}}, \tag{2.5}$$

where the $\mathbf{k}$-summation is taken over the filled part of the bare band with spin σ and $\bar{\epsilon}_\sigma$ is an average bare band energy per site for particles of spin $\sigma = \pm 1$. It is also convenient to change variables from n_σ to $n \equiv \sum_\sigma n_\sigma$ and $m \equiv \sum_\sigma \sigma n_\sigma$ representing the band filling and magnetic moment (spin-polarization) per site, respectively. It is important to note, that due to the approximate evaluation of the l.h.s. of Eq. (2.3) it is not guaranteed that E_g is higher then the exact ground-state energy of the Hubbard model. Eq. (2.3) may be interpreted as an expectation value of an effective single-particle Hamiltonian, $\hat{\mathcal{H}}_{GA}$, evaluated with respect to $|\psi_0\rangle$, e.g.

$$E_g = \langle\psi_0|\hat{\mathcal{H}}_{GA}|\psi_0\rangle. \tag{2.6}$$

From Eqs. (2.3)-(2.5) it follows directly that

$$\begin{aligned}\hat{\mathcal{H}}_{GA}(d,n,m) &= \sum_{ij\sigma} q_\sigma(d,n,m)t_{ij}c^\dagger_{i\sigma}c_{j\sigma} - \sum_{i\sigma}\sigma h c^\dagger_{i\sigma}c_{i\sigma} + \Lambda U d^2 \\ &= \sum_{\mathbf{k}\sigma}(q_\sigma(d,n,m)\epsilon_{\mathbf{k}} - \sigma h)c^\dagger_{\mathbf{k}\sigma}c_{\mathbf{k}\sigma} + \Lambda U d^2. \end{aligned}\tag{2.7}$$

method of solution presented here is the simplest one, but it cannot be called standard, as in the literature there are many different ways of solving the mean-field (MF) model resulting from GA.

Furthermore, $|\psi_0\rangle$ is chosen to be the ground state of $\hat{\mathcal{H}}_{GA}$, $\hat{\mathcal{H}}_{GA}|\psi_0\rangle = E_g|\psi_0\rangle$. Thus, the Gutzwiller approximation can be alternatively introduced as based on the effective quasiparticle Hamiltonian (2.7) (for an intuitive formulation of the description see Refs. 89 and 90). This type of approach is termed the *renormalized mean-field theory* (RMFT) [88, 91], as the Hamiltonian (2.7) contains renormalized (by q_σ) *bare* hopping integral t_{ij} (or single-particle energy $\epsilon_{\mathbf{k}}$). In its essence, the original Hamiltonian (2.1) has been brought to a single-particle form (2.7), with extra parameters to be evaluated either self-consistently or variationally.

Namely, Hamiltonian $\hat{\mathcal{H}}_{GA}$ depends in a non-Hartree-Fock manner on the parameters n, m, and d, the values of which are not determined as yet. The first two of them have the meaning of expectation values of single particle operators, i.e. $n = N/\Lambda$ and $m = M/\Lambda$, where

$$N \equiv \langle \hat{N} \rangle = \sum_{\mathbf{k}\sigma} \langle c^\dagger_{\mathbf{k}\sigma} c_{\mathbf{k}\sigma} \rangle, \qquad M \equiv \langle \hat{M} \rangle = \sum_{\mathbf{k}\sigma} \sigma \langle c^\dagger_{\mathbf{k}\sigma} c_{\mathbf{k}\sigma} \rangle. \tag{2.8}$$

Although the Gutzwiller approach was devised for zero temperature, we may still construct (from $\hat{\mathcal{H}}_{GA} - \mu\hat{N}$) the partition function and the (generalized) grand-potential functional $\mathcal{F}^{(GA)}$

$$\mathcal{F}^{(GA)} = -\frac{1}{\beta} \sum_{\mathbf{k}\sigma} \ln[1 + e^{-\beta E^{(GA)}_{\mathbf{k}\sigma}}] + \Lambda U d^2, \tag{2.9}$$

where $\beta = 1/(k_B T)$ is the inverse temperature and the quasiparticle energies are given by

$$E^{(GA)}_{\mathbf{k}\sigma} = q_\sigma \epsilon_{\mathbf{k}} - \sigma h - \mu. \tag{2.10}$$

Explicitly, within GA procedure one minimizes the "Landau functional" (2.9) with respect to the variational parameter d, which leads to the condition

$$\frac{\partial \mathcal{F}^{(GA)}}{\partial d} = 2\Lambda U d + \sum_{\mathbf{k}\sigma} \frac{\partial q_\sigma}{\partial d} f(E^{(GA)}_{\mathbf{k}\sigma}) \epsilon_{\mathbf{k}} = 0, \tag{2.11}$$

with $f(E)$ being the Fermi-Dirac distribution function. This equation is supplemented with the self-consistent equations coming from Eq. (2.8), namely

$$n = \frac{1}{\Lambda} \sum_{\mathbf{k}\sigma} f(E^{(GA)}_{\mathbf{k}\sigma}), \qquad m = \frac{1}{\Lambda} \sum_{\mathbf{k}\sigma} \sigma f(E^{(GA)}_{\mathbf{k}\sigma}). \tag{2.12}$$

Thus we see, the GA solution contains a mixture of self-consistent equations for m and μ and a variational minimization of d. Eqs. (2.11)-(2.12) form a complete set for d, m, and μ (for a fixed n), which is solved numerically. Strictly speaking, the above equations express the way of solving the Gutzwiller approximation (GA) which is used frequently e.g. in the context of the t-J model [92–94]. This formulation differs from that of Ref. 85.

Note, that the nonzero temperature formalism presented here, in the $\beta \to \infty$ limit, is fully equivalent to the original Gutzwiller approach devised for $T = 0$.

Also, the appearance of spin-dependent **k**-independent band-narrowing factor q_σ in Eqs. (2.7) and (2.10) leads to the spin-dependent masses (SDM) of quasiparticles. From comparison of these Eqs. with the dispersion relation of a free electron gas $\epsilon_{\mathbf{k}}^{(gas)} = \hbar^2\mathbf{k}^2/(2m^*)$ one can deduce that the quasiparticle mass m^* is inversely proportional to the band narrowing factor q_σ. As a consequence, m^* is spin dependent in the spin-polarized situation (i.e. when $m \neq 0$, what implies $q_\uparrow \neq q_\downarrow$). In the investigation of strong correlations we will always work in the $U \to \infty$ limit, in which $d \to 0$, and then the expression for the masses becomes

$$m_\sigma \propto \frac{1}{q_\sigma(n,m)} = \frac{1-n_\sigma}{1-n}, \qquad \frac{m_\sigma}{m_B} \equiv \frac{1}{q_\sigma}, \tag{2.13}$$

where m_B represents uncorrelated (band) mass of bare particles.

2.2 Statistically-consistent Gutzwiller Approximation - SGA

In this Section we start with explaining deficiencies of the scheme presented in the previous Section. Next, we provide a corrected version, which will be called Statistically-consistent Gutzwiller Approximation (SGA) [84]. Finally, we present the minimal version of this formulation, which will be used in the following part of the Thesis.

2.2.1 Motivation for the approach: Deficiency of the Gutzwiller approximation

To demonstrate directly that the basic method of solving GA summarized in Section 2.1 represents not fully-optimized approach, we analyze the ground state in the general case, i.e. when q_σ depends on the spin polarization m. Then, it is straightforward to show that the derivative $\partial\mathcal{F}^{(GA)}/\partial m = \sum_{\mathbf{k}\sigma} \frac{\partial q_\sigma(d,n,m)}{\partial m}\epsilon_{\mathbf{k}} f(E_{\mathbf{k}\sigma}) \neq 0$, which physically means that by transferring a small number of particles from one spin-subband to the other (i.e. by changing spin polarization m), we observe a decrease in the total energy of the system (see Figure 2.1 for illustration). We may understand this decrease intuitively by noting that the spin transfer process between the subbands leads not only to a change in the energy level occupation (as would be for bare particles), but also to an alteration of the renormalization factor $q_\sigma(d,n,m)$ for *all* the single particle energy levels. Such instability is present only if the Gutzwiller factors depend explicitly on the spin polarization m.[2]

Within the method to be introduced next, we treat m and other mean-fields as variational parameters, with respect to which the appropriate grand-potential

[2]This deficiency of GA may, or may still not cause problems depending on the model studied. For example, when studying properties of a strongly-correlated paired gas of quasiparticles (Chapter 4, Ref. 83) analysis within GA lead to nonphysical results: jump of free energy at the BCS-FFLO phase transition. On the other hand, analysis of the same problem within tight-binding approximation is free of such a jump [95].

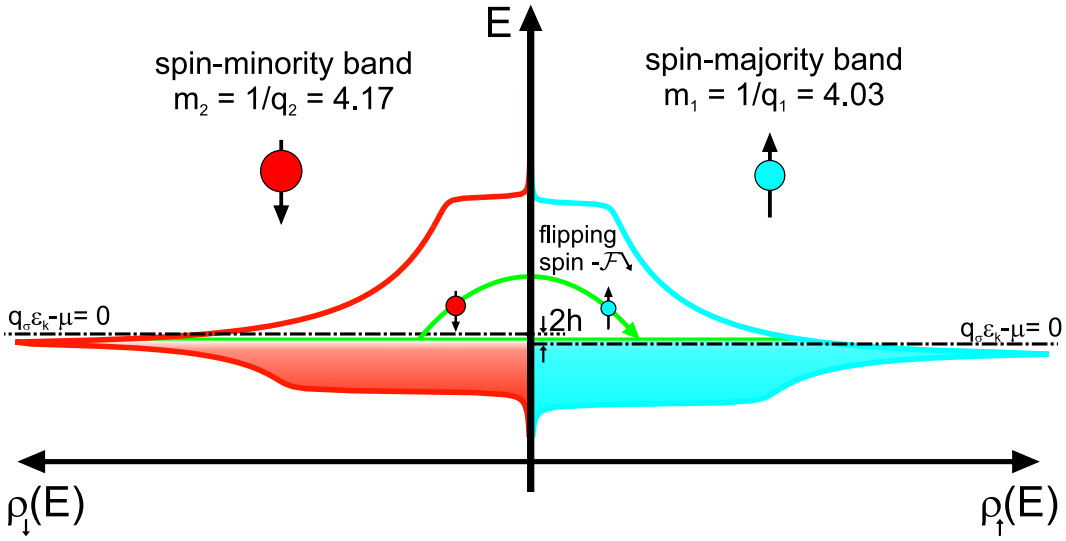

Figure 2.1: Spin-resolved density of states for the spin-majority ($\sigma =\uparrow$) and the spin-minority ($\sigma =\downarrow$) subbands calculated in the standard Gutzwiller approximation. The dot-dashed lines show the reference energy (defined by $q_\sigma \epsilon_{\mathbf{k}} - \mu = 0$). Those points of the subbands are shifted by the Zeeman spin splitting $2h$. The calculations were performed for $U = 12$ and $h = 0.05$ (in units of t) for a two-dimensional band on a grid of size $\Lambda = 512 \times 512$ (also the nearest- and next-nearest-neighbor hoppings were assumed as $t = 1$ and $t' = 0.25$, respectively). The quantities m_1 and m_2 are the corresponding spin-dependent mass-enhancement factors in units of m_B.

(Landau) functional is minimized. To carry out the procedure, we introduce constraints as discussed next.

2.2.2 Formal structure of SGA

On the technical level, a direct minimization of $\mathcal{F}^{(GA)}$ with respect to m would lead to violation of the self-consistency equation (2.8). Therefore, in order to preserve the self-consistency, additional constraint on m has to be imposed by means of the Lagrange-multiplier method. Analogously, we introduce the constraint on n. In general, there should be a constraint for each mean field appearing explicitly in a non-Hartree-Fock manner in the effective MF Hamiltonian (also, for e.g. not included here the staggered magnetization and the pairing amplitude, cf. Chapter 6). Here, m and n appear in $\hat{\mathcal{H}}_{GA}$ via $q_\sigma(d, n, m)$. The presence of those constraints leads to a redefinition of the Hamiltonian (2.7), according to the prescription

$$\hat{\mathcal{H}}_\lambda \equiv \hat{\mathcal{H}}_{GA} - \lambda_m(\hat{M} - M) - \lambda_n(\hat{N} - N). \tag{2.14}$$

The Lagrange multipliers λ_m and λ_n play the role of (spatially homogenous) molecular fields, which are coupled to the spin polarization and the total charge, respectively (the general, inhomogeneous case can be treated analogously). Similar terms are present in some papers [96–98] and absent in others (for the latter cf. treatment in Ref. 85 and in those on application of RMFT to the t-J model [88, 92–94]). On the contrary, the variational parameter d is not an average value of any operator appearing in $\hat{\mathcal{H}}_{GA} - \mu\hat{N}$, and as such, does not require any self-consistency-preserving constraint.

Next, we construct the generalized grand-potential functional $\mathcal{F}$ for the effective Hamiltonian (2.14),

$$\mathcal{F}^{(SGA)} \equiv -\beta^{-1} \ln \mathcal{Z}_\lambda, \qquad \mathcal{Z}_\lambda \equiv \mathrm{Tr}[\exp(-\beta(\hat{\mathcal{H}}_\lambda - \mu\hat{N}))]. \tag{2.15}$$

Explicitly, we have now the generalized grand potential functional (of the Landau type), which takes the form

$$\mathcal{F}^{(SGA)} = -\frac{1}{\beta}\sum_{\mathbf{k}\sigma} \ln[1 + e^{-\beta E^{(SGA)}_{\mathbf{k}\sigma}}] + \Lambda(\lambda_n n + \lambda_m m + U d^2). \tag{2.16}$$

Note that the definition of $\mathcal{F}^{(SGA)}$ is based on $\hat{\mathcal{H}}_\lambda$, not on $\hat{\mathcal{H}}_{GA}$. The quasiparticle energies are thus defined now in the form

$$E^{(SGA)}_{\mathbf{k}\sigma} = q_\sigma \epsilon_{\mathbf{k}} - \sigma(h + \lambda_m) - \tilde{\mu}, \tag{2.17}$$

with $\tilde{\mu} \equiv \mu + \lambda_n$ as shifted chemical potential and $h + \lambda_m$ as an effective field. All the averages appearing above are defined with the help of the following density operator

$$\hat{\rho}_\lambda = \mathcal{Z}_\lambda^{-1} \exp(-\beta(\hat{\mathcal{H}}_\lambda - \mu\hat{N})) \tag{2.18}$$

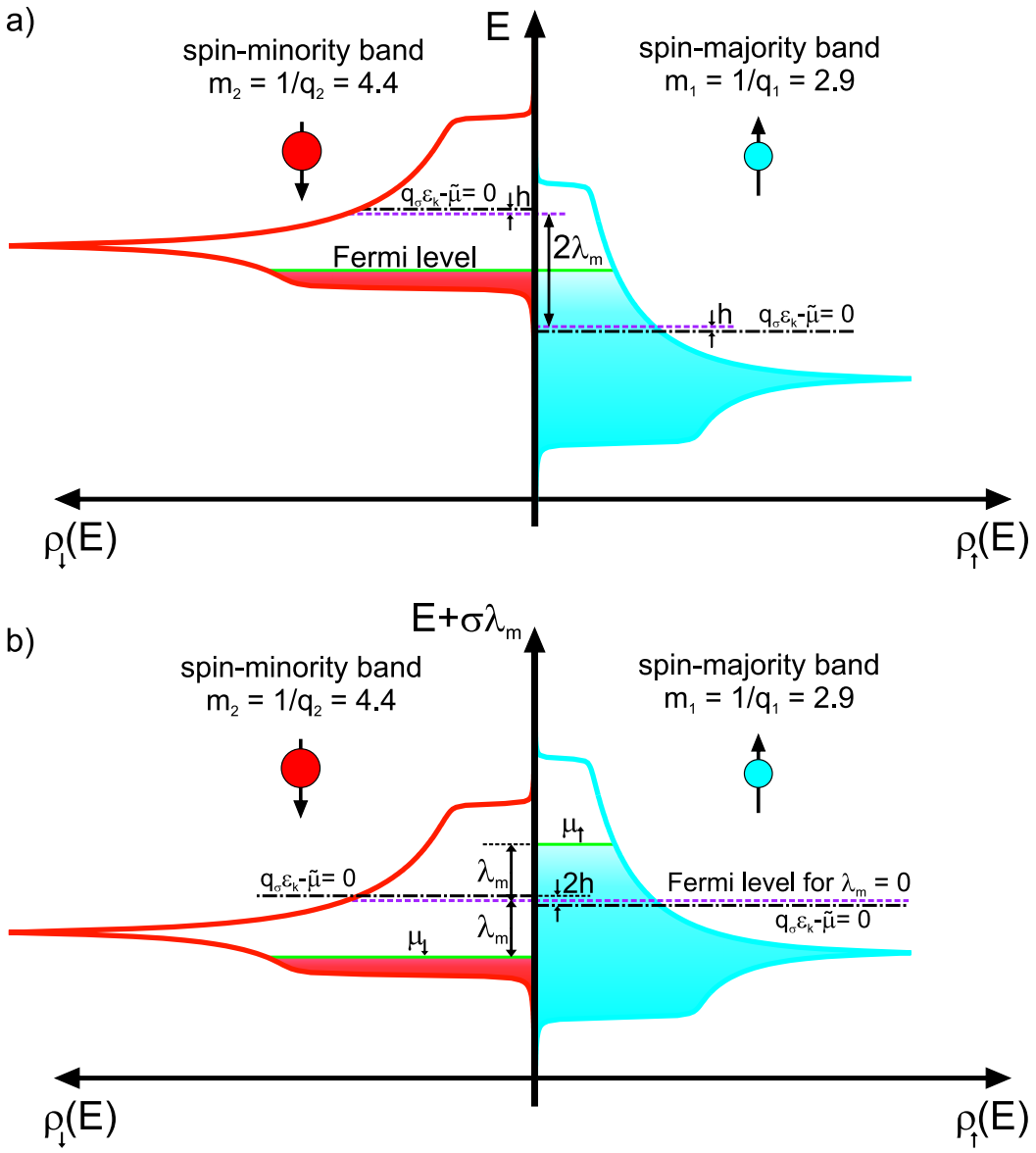

Figure 2.2: Density of states for the spin-majority ($\sigma =\uparrow$) and spin-minority ($\sigma =\downarrow$) subbands obtained within SGA. The Fermi liquid can be viewed equivalently as either (a) with a single chemical potential or (b) with different effective chemical potentials $\mu_\sigma \equiv \tilde{\mu} + \sigma\lambda_m$. The dashed line in (b) marks the Fermi-level position if we put $\lambda_m = 0$. The dot-dashed lines show the reference energy (defined by $q_\sigma\epsilon_{\mathbf{k}} - \tilde{\mu} = 0$). Those points are now shifted not only by $2h$ as previously, but by $2h + 2\lambda_m$, which leads to the much greater mass-splitting than in the standard Gutzwiller case (cf. Figure 2.1). The calculations were performed for the same parameter values as in Figure 2.1. The masses are in units of m_B.

in a standard manner, i.e. $A \equiv \langle \hat{A} \rangle = \mathrm{Tr}[\hat{A}\hat{\rho}_\lambda]$. The equilibrium values of the mean fields and the Lagrange multipliers are obtained from the necessary conditions for $\mathcal{F}$ to have a minimum subject to the constraints, i.e.

$$\frac{\partial \mathcal{F}}{\partial \vec{A}} = 0, \qquad \frac{\partial \mathcal{F}}{\partial \vec{\lambda}} = 0, \qquad \frac{\partial \mathcal{F}}{\partial d} = 0. \tag{2.19}$$

In the above equations: $\partial \mathcal{F}/\partial \vec{A} \equiv \nabla_A \mathcal{F}$, etc., and by $\vec{A}$, $\vec{\lambda}$ we denote respectively the sets of the mean fields and of Lagrange multipliers; explicitly: $\vec{A} = (n, m)$ and $\vec{\lambda} = (\lambda_n, \lambda_m)$. Needless to say, that the conditions $\partial \mathcal{F}/\partial \vec{\lambda} = 0$ guarantee the realization of the self-consistent equations automatically. Explicitly, in the present case, Eqs. (2.19) yield

$$\lambda_n = -\frac{1}{\Lambda} \sum_{\mathbf{k}\sigma} \frac{\partial q_\sigma}{\partial n} f(E^{(SGA)}_{\mathbf{k}\sigma}) \epsilon_{\mathbf{k}}, \tag{2.20}$$

$$\lambda_m = -\frac{1}{\Lambda} \sum_{\mathbf{k}\sigma} \frac{\partial q_\sigma}{\partial m} f(E^{(SGA)}_{\mathbf{k}\sigma}) \epsilon_{\mathbf{k}}, \tag{2.21}$$

$$n = \frac{1}{\Lambda} \sum_{\mathbf{k}\sigma} f(E^{(SGA)}_{\mathbf{k}\sigma}), \tag{2.22}$$

$$m = \frac{1}{\Lambda} \sum_{\mathbf{k}\sigma} \sigma f(E^{(SGA)}_{\mathbf{k}\sigma}), \tag{2.23}$$

$$2Ud = -\frac{1}{\Lambda} \sum_{\mathbf{k}\sigma} \frac{\partial q_\sigma}{\partial d} f(E^{(SGA)}_{\mathbf{k}\sigma}) \epsilon_{\mathbf{k}}. \tag{2.24}$$

In effect, the following variables are to be determined from the variational minimization procedure: d, m, λ_m, λ_n, and μ, for fixed n. The reason behind the presence of both λ_n and μ is the following: the former ensures a self-consistent way of evaluating n, whereas the latter fixes n at a desired value. The physical meaning of λ_m is illustrated in Figure 2.2. Namely, λ_m optimizes the free energy by allowing for the Fermi-level mismatch between the spin-subbands to readjust. The MF thermodynamics is constructed by defining the grand potential $\Omega(T, h, \mu)$ from the generalized grand-potential functional $\mathcal{F}$, evaluated for the optimal values of all parameters (i.e. the solutions of Eqs. (2.19)), and has the form

$$\Omega(T, h, \mu) = \mathcal{F}(T, h, \mu; \vec{A}_0(T, h, \mu), \vec{\lambda}_0(T, h, \mu), d_0(T, h, \mu)). \tag{2.25}$$

In the above formula $\vec{A}_0(T, h, \mu)$, $\vec{\lambda}_0(T, h, \mu)$, and $d_0(T, h, \mu)$ denote the equilibrium values of the mean-fields, the Lagrange multipliers, and the double occupancy, respectively. Consequently, the free energy is defined as $F = \Omega + \mu N$. Note that μ, not $\tilde{\mu} \equiv \mu + \lambda_n$ is present in the above formulas. The (equilibrium) thermodynamic potentials depend neither on the mean-fields, nor on the molecular fields, as they are calculated explicitly in the process of the corresponding functional minimization. Therefore, the quantity μ plays the role of the thermodynamic chemical potential entering in the relations

$$\frac{\partial \Omega}{\partial \mu} = -N, \qquad \frac{\partial F}{\partial N} = \mu. \tag{2.26}$$

2.2.3 Formulation without the constraint on $\hat{N}$

If we disregarded λ_n (putting $\lambda_n = 0$), then the condition $\partial\mathcal{F}/\partial n = 0$ should not be used. In such scheme (labeled in the following as SGA'), the values of the quantities m, λ_m, d^2 would be the same, but the relations (2.26) would not be fulfilled. Then, for fixing n the self-consistency condition (Eqs. (2.8) and (2.12)) should be used and the value of μ in this scheme would correspond to $\mu + \lambda_n$ from the full formulation. This is the scheme we utilize in Chapters 3-5, and therefore we provide below a proof of its "equivalency" with the full SGA formulation.

Explicitly, in this scheme we define the Hamiltonian $\hat{\mathcal{H}}_\lambda$ similarly as in Eq. (2.14) but without the constraint on $\hat{N}$

$$\hat{\mathcal{H}}_\lambda \equiv \hat{\mathcal{H}}_{GA} - \lambda_m(\hat{M} - M). \tag{2.27}$$

Then, we use the generalized free-energy functional, and not the grand-potential functional, namely

$$\mathcal{F}_{FE}^{(SGA')} = -\frac{1}{\beta}\sum_{\mathbf{k}\sigma} \ln[1 + e^{-\beta E_{\mathbf{k}\sigma}^{(SGA')}}] + \Lambda(\lambda_m m + Ud^2) + \Lambda\mu n, \tag{2.28}$$

with the quasiparticle energies differing from those in Eq. (2.17) by the absence of λ_n

$$E_{\mathbf{k}\sigma}^{(SGA')} = q_\sigma \epsilon_{\mathbf{k}} - \sigma(h + \lambda_m) - \mu. \tag{2.29}$$

In the solution procedure we minimize $\mathcal{F}_{FE}^{(SGA')}$ with respect to m, λ_m, and d as previously, but for fixing n we use the self-consistency condition (2.8). Explicitly, we obtain the following equations

$$\lambda_m = -\frac{1}{\Lambda}\sum_{\mathbf{k}\sigma} \frac{\partial q_\sigma}{\partial m} f(E_{\mathbf{k}\sigma}^{(SGA')})\epsilon_{\mathbf{k}}, \tag{2.30}$$

$$n = \frac{1}{\Lambda}\sum_{\mathbf{k}\sigma} f(E_{\mathbf{k}\sigma}^{(SGA')}), \tag{2.31}$$

$$m = \frac{1}{\Lambda}\sum_{\mathbf{k}\sigma} \sigma f(E_{\mathbf{k}\sigma}^{(SGA')}), \tag{2.32}$$

$$2Ud = -\frac{1}{\Lambda}\sum_{\mathbf{k}\sigma} \frac{\partial q_\sigma}{\partial d} f(E_{\mathbf{k}\sigma}^{(SGA')})\epsilon_{\mathbf{k}}. \tag{2.33}$$

It can be seen that the present set of equations is equivalent to Eqs. (2.21)-(2.24) with the only difference being the presence of μ (in Eqs. (2.30)-(2.33) and dispersion (2.29)) instead of $\mu + \lambda_n$ (in Eq. (2.21)-(2.24) and dispersion (2.17)) with λ_n set by the "additional" Eq. (2.20). Therefore, the parameters (μ_0, m_0, λ_{n0}, λ_{m0}, d_0) are solution of Eqs. (2.20)-(2.24), if and only if the parameters ($\mu_0' = \mu_0 + \lambda_{n0}$, m_0, λ_{m0}, d_0) are solution of Eqs. (2.30)-(2.33).

The free energy of the system is the quantity which, in the case of a fixed number of particles N (or equivalently, of a fixed band filling n), determines the stable phase from a choice of *a priori* possible phases. Obviously the stable phase is the one

with the lowest free energy. In our two schemes of approach (SGA and SGA'), the free energy is obtained from the grand-potential functional (2.16) or free-energy functional (2.28) by evaluating them for the values of parameters obtained from the solution of either, Eqs. (2.20)-(2.24) or Eqs. (2.30)-(2.33), respectively, and according to the prescription

$$\begin{aligned} F^{(SGA)} &= \mathcal{F}_0^{(SGA)} + \mu_0 N = -\frac{1}{\beta}\sum_{\mathbf{k}\sigma} \ln[1 + e^{-\beta E_{\mathbf{k}\sigma}^{(SGA)}}] \\ &\quad +\Lambda(\lambda_{m0} m_0 + U d_0^2 + (\lambda_{n0} + \mu_0) n_0), \end{aligned} \tag{2.34}$$

$$\begin{aligned} F^{(SGA')} &= \mathcal{F}_{FE\ 0}^{(SGA')} = -\frac{1}{\beta}\sum_{\mathbf{k}\sigma} \ln[1 + e^{-\beta E_{\mathbf{k}\sigma}^{(SGA')}}] \\ &\quad +\Lambda(\lambda_{m0} m_0 + U d_0^2 + \mu_0' n_0). \end{aligned} \tag{2.35}$$

After noting that $\mu_0' = \mu_0 + \lambda_{n0}$, we see that these two free energies are indeed the same. Therefore, the above scheme, without the explicit constraint for $\hat{N}$ ($\sim \lambda_n$), is sufficient to analyze the system properties in a statistically-consistent manner. The only disadvantage of such simplification is that the chemical potential μ it provides is not the physical chemical potential, which enters e.g. in the thermodynamic relations, Eq. (2.26). Since we do not use such relations, this scheme is sufficient for our analysis of the strongly-correlated condensed state and we use it in Chapters 3-5. There, it has been additionally adjusted to the quasiparticle gas case (we have N/n instead of Λ, since $\sum_{\mathbf{k}} 1 = \Lambda = (\sum_{\mathbf{k}} n)/n = N/n$) and to the $U \to \infty$ limit (in this limit $d = 0$ and hence, there is no expression corresponding to Eq. (2.33)). In Chapter 6 we utilize the full SGA approach.

2.2.4 The concept of an Almost Localized Fermi Liquid (ALFL)

The concepts of **k**-independent, spin-dependent band narrowing factor (or of spin-dependent mass) and of the correlation field renormalizing both the applied field[3] and the chemical potential [cf. Eqs. (2.29) and (2.17)] extend the concept of the Landau quasiparticle in an essential manner. Moreover, those renormalizations are strong when the band filling $n \to 1$, i.e., the system is close to the Mott-Hubbard localization (i.e. the Hubbard-interaction magnitude U is comparable or larger than the bare bandwidth W). In that situation the liquid composed of such quasiparticles exhibits metamagnetism [72, 85], a phenomenon absent in the Fermi liquid. Furthermore, in distinction to Landau Fermi liquid, in the present situation the chemical potential is readjusted (recalculated) in each phase (normal, magnetic, superconducting), as the interaction is neither small (as compared to the Fermi energy), nor its effects limited to the vicinity of the Fermi surface (as $\hbar\omega_C/\epsilon_F \approx 0.13$). Therefore, it is proper to call this Fermi liquid as an *Almost*

[3]The presence of h_{cor} can be regarded as an applied-field dependent renormalization of the Lande' g factor (as e.g. in magnetic semiconductors), but the present interpretation is better, as it allows to see clearly its physical influence on the system properties.

Localized Fermi Liquid (ALFL) [71, 99]. Within this paradigm, the unconventional superconductivity, as it is understood here, concerns the paired superfluid states of ALFL.

2.3 The pairing Hamiltonian

In the following investigation of the superconductivity in the situation with strong correlations we will use as a starting point a BCS-like Hamiltonian with Gutzwiller band narrowing factors already included, namely

$$\hat{\mathcal{H}}_0 = \sum_{\mathbf{k}\sigma}(q_\sigma \epsilon_{\mathbf{k}} - \sigma h) c^\dagger_{\mathbf{k}\sigma} c_{\mathbf{k}\sigma} + \frac{1}{N}\sum_{\mathbf{k}\mathbf{k}'\mathbf{Q}} V_{\mathbf{k}\mathbf{k}'} c^\dagger_{\mathbf{k}+\mathbf{Q}/2\uparrow} c^\dagger_{-\mathbf{k}+\mathbf{Q}/2\downarrow} c_{-\mathbf{k}'+\mathbf{Q}/2\downarrow} c_{\mathbf{k}'+\mathbf{Q}/2\uparrow}, \quad (2.36)$$

where $\epsilon_{\mathbf{k}}$ is the bare dispersion relation, N is the total number of electrons, (for a lattice case $\Lambda = N/n$ gives the number of sites). After introduction of the constraint on magnetization with the Lagrange multiplier $h_{cor} \equiv \lambda_m$ [4] and subtraction of the chemical potential term, we obtain

$$\begin{aligned} \hat{\mathcal{H}} &= \hat{\mathcal{H}}_0 - h_{cor}\sum_{\mathbf{k}}(\hat{m}_{\mathbf{k}} - m) - \mu \sum_{\mathbf{k}\sigma} \hat{n}_{\mathbf{k}\sigma} = \\ &= \sum_{\mathbf{k}\sigma}(q_\sigma \epsilon_{\mathbf{k}} - \sigma h - \sigma h_{cor} - \mu) c^\dagger_{\mathbf{k}\sigma} c_{\mathbf{k}\sigma} \\ &\quad + \frac{1}{N}\sum_{\mathbf{k}\mathbf{k}'\mathbf{Q}} V_{\mathbf{k}\mathbf{k}'} c^\dagger_{\mathbf{k}+\mathbf{Q}/2\uparrow} c^\dagger_{-\mathbf{k}+\mathbf{Q}/2\downarrow} c_{-\mathbf{k}'+\mathbf{Q}/2\downarrow} c_{\mathbf{k}'+\mathbf{Q}/2\uparrow} + \frac{N}{n} m h_{cor}, \quad (2.37) \end{aligned}$$

where $\hat{m}_{\mathbf{k}} \equiv n_{\mathbf{k}\uparrow} - n_{\mathbf{k}\downarrow}$ and we have used the relation $\sum_{\mathbf{k}} 1 = \Lambda = N/n$.

The Hamiltonian (2.36) can also be justified microscopically starting from the Periodic Anderson Model. This procedure has been introduced in Ref. 100, and the way it leads to our starting Hamiltonian has been summarized in Ref. 95, Appendix A.

Note that we do not perform calculations for a realistic band with a full microscopic Hamiltonian, because we intend to single out novel features of a strongly-correlated superconductivity in a model situation, as it already leads to very interesting conclusions.

2.4 Concluding remarks

- We use an improved GA scheme - the SGA scheme - proposed recently in our group [84]. This scheme introduces additional constraints for the magnetic moment and the total number of particles to the standard GA approach.

[4] We have renamed the Lagrange multiplier λ_m as h_{cor}, and will call it *correlation field* in the following in order to underline that this quantity enters into the formulation because of correlations, and in a similar manner to the magnetic field h.

- The introduction of Lagrange multipliers makes the SGA scheme equivalent to the slave-boson approach [86], but the present formulation contains no auxiliary (slave) Bose fields. For a formal proof of the equivalence (at least in the analysis of the normal state) see Ref. 84.

- We disregard the constraint on the total number of particles (in Chapters 3 and 4) in the starting Hamiltonian ($-\lambda_n(\hat{N} - N)$), as it leads only to a shift of the chemical potential, which is not important in our analysis.

- We solve the mean-field model by constructing from a starting effective Hamiltonian $\hat{\mathcal{H}} - \mu\hat{N}$ the generalized free-energy functional (in Chapters 3 and 4) or generalized grand-potential functional (in Chapter 6).[5] This functional is minimized with respect to the mean-fields $\vec{A}$ (e.g. m, Δ), as well as with respect to the Lagrange multipliers $\vec{\lambda}$. The minimization procedure yields a system of integral equations, which are solved numerically to obtain the equilibrium values of mean fields $\vec{A} = \vec{A}_0$ and Lagrange multipliers $\vec{\lambda} = \vec{\lambda}_0$.

- Since we perform calculations for a fixed number of particles N (or equivalently for a fixed band filling n), we solve the equations for μ, with n being fixed.

- The system free-energy F is obtained from the free-energy functional or grand-potential functional $\mathcal{F}$, by evaluating them at the equilibrium values $\vec{A}_0$ and $\vec{\lambda}_0$. When starting from the grand-potential functional, the term μN is also added (see Eq. (6.50)).

- The stable phase from a choice of *a priori* possible phases is the one with the lowest free energy F.

[5] As in Chapter 6 we consider a different model, both functionals are labeled as $\mathcal{F}$ for clarity.

Chapter 3

Normal state properties

We summarize here the normal-state properties resulting from the Hamiltonian (2.37), but without the pairing part (i.e. for $V_{\mathbf{k}\mathbf{k}'} \equiv 0$), namely

$$\hat{\mathcal{H}}_{NS} = \sum_{\mathbf{k}\sigma} \xi_{\mathbf{k}\sigma} c^{\dagger}_{\mathbf{k}\sigma} c_{\mathbf{k}\sigma} + \frac{N}{n} \overline{m} h_{cor}, \tag{3.1}$$

where we have renamed the spin polarization as $\overline{m}$ to distinguish it from the quasiparticle mass m_σ, and the dispersion relation is given by

$$\xi_{\mathbf{k}\sigma} = q_\sigma \epsilon_{\mathbf{k}} - \sigma h - \sigma h_{cor} - \mu. \tag{3.2}$$

We underline once again that in the spin-polarized situation presence of the Gutzwiller band narrowing factors q_σ leads to emergence of spin-dependent masses (SDM) [71–76] of quasiparticles, with $m^*_\sigma \propto 1/q_\sigma = (1-n_\sigma)/(1-n)$ (the last equation holds in the $U \to \infty$ limit).

3.1 Quasiparticle gas

We analyze first the normal state properties of a three-dimensional quasiparticle gas with the spin-direction ($\sigma = \pm 1$) dependent masses $m^*_\sigma \equiv m_\sigma$ and the effective field induced by correlations h_{cor}. Quasiparticle energies in the applied field $h \equiv g\mu_B H$ have the form

$$\xi_{\mathbf{k}\sigma} = \frac{\hbar^2 k^2}{2m_\sigma} - \sigma h - \sigma h_{cor} - \mu, \tag{3.3}$$

where we have taken the simple parabolic dispersion relation ($\epsilon_{\mathbf{k}} = \hbar^2 k^2/(2m_B)$) and have defined from the start the energy with respect to the chemical potential μ. The spin dependence of the masses is taken in the simplest form corresponding to the narrow-band or the Kondo-lattice limits with the Hubbard interaction $U \to \infty$, i.e.

$$\frac{m_\sigma}{m_B} = \frac{1}{q_\sigma} = \frac{1-n_\sigma}{1-n} = \frac{1-n/2}{1-n} - \sigma \frac{\overline{m}}{2(1-n)} \equiv \frac{1}{m_B}(m_{av} - \sigma \Delta m/2), \tag{3.4}$$

where $\sigma = \pm 1$ is the spin quantum number, m_B is the bare band mass, $\overline{m} \equiv n_\uparrow - n_\downarrow$ is the system spin polarization and n is the band filling ($n = n_\uparrow + n_\downarrow$). Also,

$\Delta m \equiv m_2 - m_1$ is the mass difference and $m_{av} \equiv (m_1 + m_2)/2$ is the average mass (where $m_1 \equiv m_\uparrow$ and $m_2 \equiv m_\downarrow$). Note that in the magnetic saturation limit $(n_\uparrow - n_\downarrow)/(n_\uparrow + n_\downarrow) = 1$ we recover the band limit with $m_\uparrow/m_B = 1$, whereas the heavy quasiparticles in the spin-minority band disappear ($n_\downarrow = 0$). Note also, that the convention is such that the state with $\sigma = +1$ is regarded as that with magnetic moment along the applied field direction.

The system of self-consistent equations determining thermodynamic properties of the normal state starting from the free-energy functional[1] $\mathcal{F}$, is as follows

$$\mathcal{F} = -k_B T \sum_{\mathbf{k}\sigma} \ln(1 + e^{-\beta\xi_{\mathbf{k}\sigma}}) + \mu N + \frac{N}{n}\overline{m}h_{cor}, \tag{3.5}$$

$$h_{cor} = -\frac{n}{N}\sum_{\mathbf{k}\sigma} f(\xi_{\mathbf{k}\sigma})\frac{\partial\xi_{\mathbf{k}\sigma}}{\partial\overline{m}}, \tag{3.6}$$

$$\overline{m} = \frac{n}{N}\sum_{\mathbf{k}\sigma} \sigma f(\xi_{\mathbf{k}\sigma}), \tag{3.7}$$

$$n = n_\uparrow + n_\downarrow = \frac{n}{N}\sum_{\mathbf{k}\sigma} f(\xi_{\mathbf{k}\sigma}), \tag{3.8}$$

where $f(\xi_{\mathbf{k}\sigma})$ is the Fermi-Dirac distribution, and $\beta = 1/(k_B T)$ is the inverse temperature. The free energy functional $\mathcal{F}(T, H, \mu; h_{cor}, \overline{m}, n)$ given by (3.5) describes a Fermi sea with the spin-dependent masses m_σ and the correlation field h_{cor}. The equations (3.6) and (3.7) are derived from the conditions $\partial\mathcal{F}/\partial\overline{m} = 0$ and $\partial\mathcal{F}/\partial h_{cor} = 0$ respectively, and the last equation (3.8) is the self-consistency equation (2.8) on the band filling (defined by $n/V_{elem} = N/V$, where V_{elem} is the elementary cell volume). The normal-state properties determined via Eqs. (3.5) - (3.8) are to be compared with those for the paired state obtained in the next Chapter.

To compare our results with those for the non-correlated case, we assume heavy, but equal masses of quasiparticles[2] (in other words we assume that q_σ does not depend on $\overline{m}$). In such situation (which will be referred to as the case with spin-independent masses, SIM), the dispersion relation takes the form

$$\xi_{\mathbf{k}\sigma}^{(SIM)} = \frac{\hbar^2 k^2}{2m_{av}} - \sigma h - \mu, \tag{3.9}$$

and obviously $h_{cor} = 0$ (because the corresponding Hamiltonian does not depend on the spin-polarization via q_σ as in the SDM case). In the SIM case we solve only Eqs. (3.7)-(3.8).

[1]This free-energy functional is equivalent to $\mathcal{F}_{FE}^{(SGA')}$ from Eq. (2.28) and has been adjusted to the quasiparticle gas case. Namely, instead of Λ we use N/n, and as we work in the $U \to \infty$ limit, the $\Lambda U d^2$ term is absent.

[2]One may argue, that we should have assumed light masses of quasiparticles in the non-correlated case, but then (to study superconductivity) we would have to use different pairing potentials V_0 and energy cutoffs $\hbar\omega_C$. In such situation direct comparison of the results in the SIM and SDM cases would be obscured. Additionally, in the SIM case, the results for lighter quasiparticles are qualitatively similar (provided V_0 and $\hbar\omega_C$ are readjusted to obtain a stable condensed state).

Even in the more involved SDM case, the equations describing the Fermi sea characteristics can be easily solved numerically by their reduction to a single equation for n_σ of the following form

$$\frac{n\, n_1^{2/3}}{(n-n_1)(2m_{av}-m_B)+m_B n_1} = \frac{n(n-n_1)^{2/3}}{n_1(2m_{av}-m_B)+m_B(n-n_1)} + \frac{4(h+h_{cor})}{\hbar^2}\left(\frac{V_{elem}}{6\pi^2}\right)^{2/3}, \tag{3.10}$$

with $n_1 \equiv n_\uparrow$. The Fermi sea characteristics obtained for such a gas are summa-

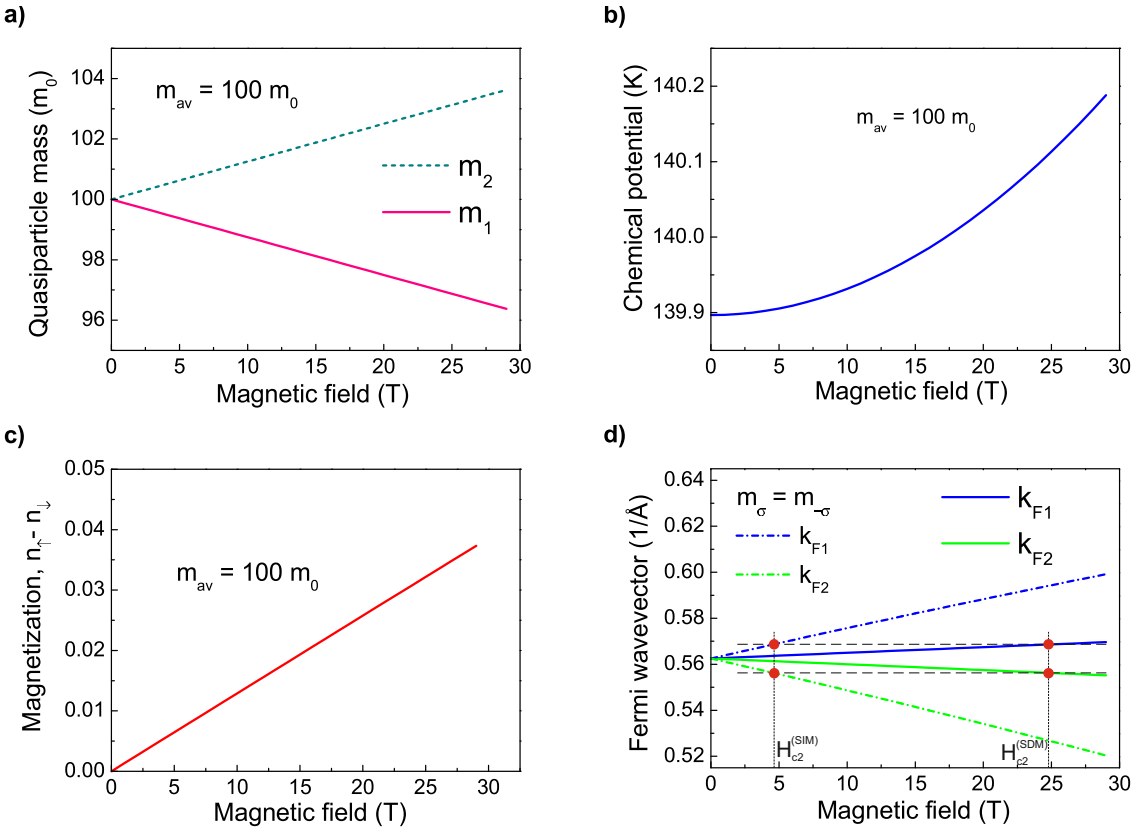

Figure 3.1: Panel with the three-dimensional Fermi sea characteristics of correlated gas in the normal state as a function of applied magnetic field (for $T = 0.05$ K). Dashed line in (a) represents the mass in the spin-minority subband, whereas the solid line characterizes that in the spin-majority subband. The dotted-dashed lines in (d) represent the results for subband Fermi wave vector in the case with spin-independent masses (SIM) with $m_\sigma = m_{av}$. Note much greater Fermi wave vector splitting in the SIM case; this is important for understanding of the results for superconducting state. The red circles in (d) mark the Fermi wavevectors at the critical field to superconductivity (H_{c2}), as determined in Chapter 4. The thin dashed black lines are guide to the eye. For details see main text.

rized in Figure 3.1. The mass difference, the Fermi vector splitting and magnetization increase linearly with the increasing field. Although we analyze a model

situation of the heavy electron gas, we take the values of parameters emulating the heavy-fermion systems: $n = 0.97$, $V_{elem} = 161$ Å^3 (data for $CeCoIn_5$) and the $h = 0$ value of the quasiparticle mass $m_{av} \equiv m_B \frac{1-n/2}{1-n} = 100\,\mathrm{m_0}$ (heaviest band of $CeCoIn_5$ [47]). The assumed mass enhancement magnitude corresponds to the moderate heavy fermions, with the value of γ in the range $100 - 200$ mJ/mol K^2. Also, the value of $n = 0.97$ corresponds to the effective valence of the Ce ions $+4 - n_f = 3.03$, a typical value. Note that the mass splitting is only about 7% in the field of $H = 30$ T, but more important is the Fermi wave vector splitting $\Delta k_F \equiv k_{F\uparrow} - k_{F\downarrow}$, displayed in Figure 3.1d. The Fermi wave vector is calculated according to the relation $k_{F\sigma} = (6\pi^2 n_\sigma / V_{elem})^{1/3}$. Most of the characteristics are indeed linear in H, as stated above.

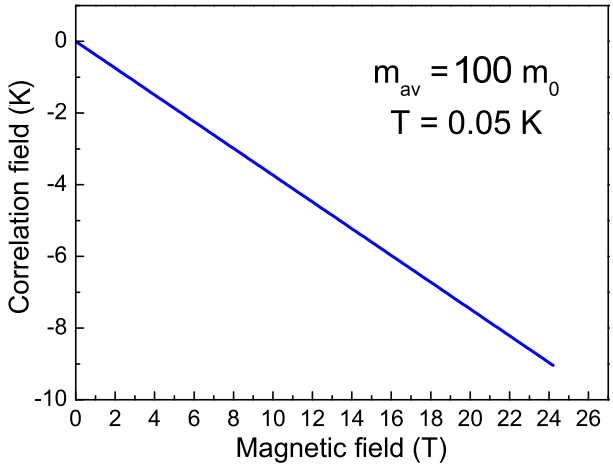

Figure 3.2: Correlation field h_{cor} as a function of the applied magnetic field for the normal state. The linear dependence is $h_{cor} = -0.6\,h$ and hence, the presence of the correlation field reduces strongly the applied field.

In Figure 3.2 we display the h dependence of the effective field h_{cor}. It is linear in h and typical values are $h_{cor} \approx -0.6\,h$. More importantly, it is always antiparallel to the applied field, and hence partly compensates it in the sense that it reduces the Zeeman contribution to the quasiparticle energy. Also, the external field induces the effective-mass splitting and this factor, together with the presence of h_{cor}, drastically decreases the difference Δk_F. In other words, correlated electrons experience a lower effective Zeeman field and hence, one can expect that the superconducting state survives to much higher fields. We return to this question in later Chapters when discussing FFLO state stability on expense of the BCS state.

3.2 Square-lattice case in the tight-binding approximation

Here we present the analysis of the situation with electrons in a two-dimensional square lattice treated within the tight-binding approximation. We utilize both

the GA and the SGA approaches. [3] We start from the Hamiltonian (3.1) with dispersion relation of the form

$$\epsilon_{\mathbf{k}} = -2t(\cos k_x + \cos k_y) + 4t' \cos k_x \cos k_y, \tag{3.11}$$

$$\xi_{\mathbf{k}\sigma} = q_\sigma \epsilon_{\mathbf{k}} - \sigma h - \sigma h_{cor} - \mu. \tag{3.12}$$

We assume $t = 1$ and $t' = 0.25$ and perform the minimization procedure analogically to that of the preceding Section (in the present case we solve the model on a lattice of size $\Lambda = 512 \times 512$). It turns out that in the $U \to \infty$ limit the saturated ferromagnetic solution ($\overline{m} = n$) is the ground state for the SGA method even at $h = 0$, whereas the GA approach provides a paramagnetic ground state ($\overline{m} = 0$) for $h = 0$ and ferromagnetic ground state ($0 < \overline{m} < n$) in the applied field $h > 0$. The density of states for both methods is exhibited in Figure 3.3. The starting mass enhancement for $h = 0$ was $q^{-1} = 17.2$

To understand the reason behind the saturated ferromagnetic ground state in the SGA method it is useful to recall the physical meaning of $\lambda_m \equiv h_{cor}$. Namely, this parameter optimizes the free energy by allowing for a mismatch between chemical potentials of the spin-subbands (cf. Figure 2.2b). It turns out that in the limit of $d = 0$ it is beneficial for one subband to be completely empty, while all electrons occupy the other one. This is easy to understand as in such situation one of the bands becomes very broad (acquires the bare bandwidth value as $q_\uparrow = 1$). Such broad band is favorable, as then its "center-of-gravity" shifts to negative energies. This ferromagnetic behavior is present even in zero Zeeman field h. The tendency in the present method of approach towards ferromagnetism makes it inappropriate to study the FFLO phase.

Parenthetically, in the t-J and t-J-U models ferromagnetism is strongly suppressed by the $J \sum_{<ij>} \mathbf{S_i} \cdot \mathbf{S_j}$ term, which favors antiferromagnetism (on the other hand, ferromagnetism can be still present in the t-J model, even at $h = 0$, see Chapter 6). The presence of the saturated ferromagnetism in the extreme limit $n \to 1$ is in agreement with the Nagaoka theorem [101] (cf. also [102–105]).

[3] We do not use the SGA approach for square lattice to study superconductivity, as it turns out that in this scheme the results show a very strong tendency towards ferromagnetism and this feature makes the interesting us FFLO phase unstable. We return to the full SGA treatment for square lattice in Chapter 6, where we include also the antiferromagnetic order.

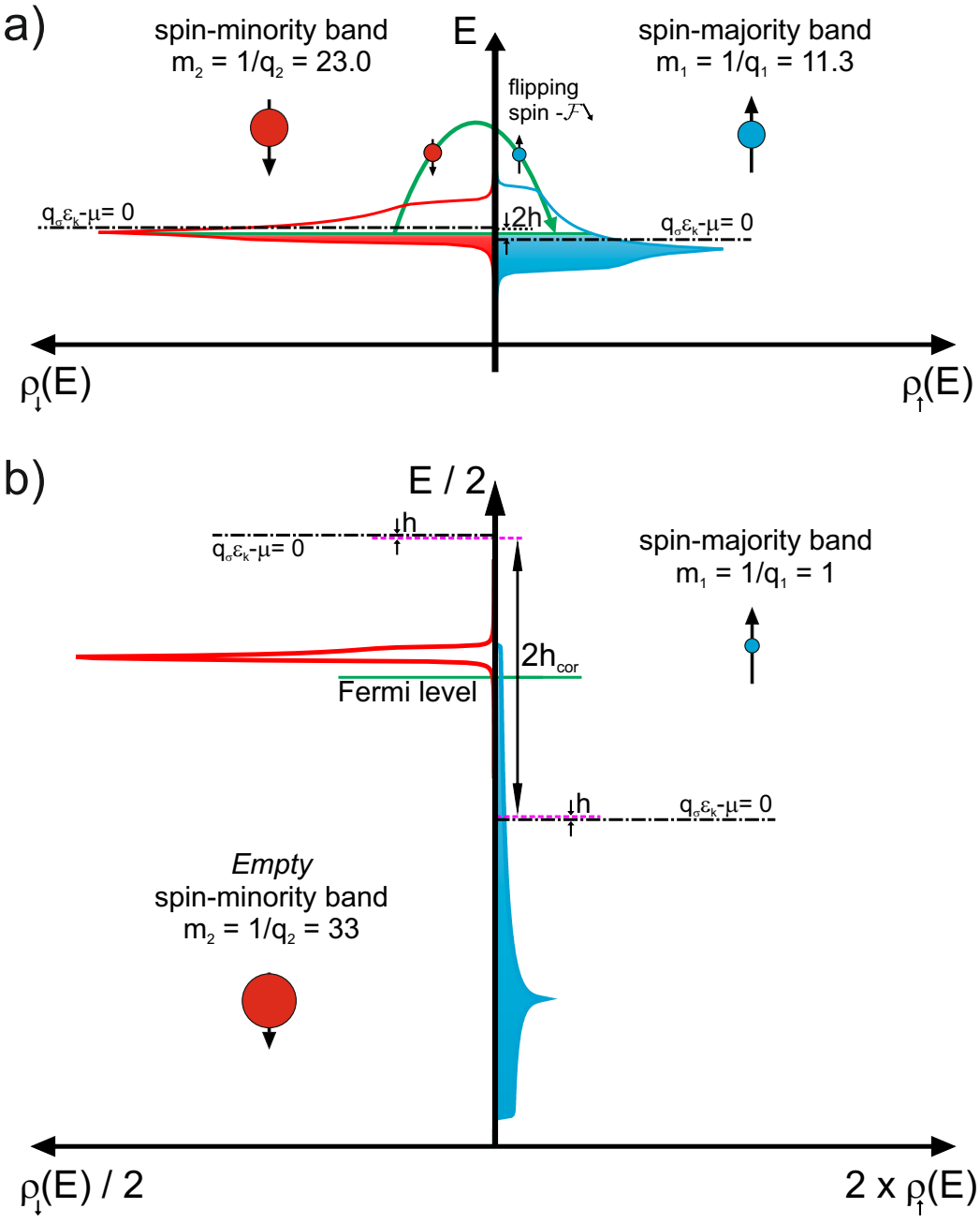

Figure 3.3: Density of states in the limit of $U \to \infty$ ($d = 0$) for the spin-majority ($\sigma =\uparrow$) and the spin-minority ($\sigma =\downarrow$) subbands, for both GA (a) and SGA (b). The dot-dashed lines show the reference energy (defined by $q_\sigma \epsilon_{\mathbf{k}} - \mu = 0$). Note that the coordinate axes in (b) are scaled for clarity. The calculations were performed for $h = 0.05$. The ground state in b) is that of a saturated ferromagnet ($\overline{m} = n$). The masses are in units of m_B.

Chapter 4

Fulde-Ferrell-Larkin-Ovchinnikov state in a correlated gas of quasiparticles

In this Chapter we start discussing the main part of the Thesis, namely we consider a paired state of correlated quasiparticles (SDM case) in the Zeeman field within the SGA scheme introduced in Chapter 2 and compare our results with those obtained in the uncorrelated situation (SIM case). The Chapter is organized as follows. In Section 4.1 we formulate the problem and provide expressions for the system free energy, as well as the set of equations determining the system properties. Next, in Section 4.2 we discuss the results: phase diagrams on the temperature - applied field plane, superconducting gaps, magnetization curves, and other properties for a choice of situations: (i) for a three-dimensional (3D) gas with s-wave gap symmetry, (ii) for a two-dimensional (2D) gas with s-wave symmetry, and (iii) for a 2D gas with d-wave gap symmetry. We observe, that in all the cases studied the FFLO state is more robust in the SDM case than in the SIM case. We conclude that the correlations stabilize the FFLO phase and possibly other high-field low-temperature (HFLT) phases. We explain the stabilization mechanism in relation to the three cases studied. In Section 4.3 we mention the results obtained within the tight-binding approximation in the GA scheme. Finally, in Section 4.4 we provide a summary and relate our results to experiment.

4.1 Model

We start from the BCS-like Hamiltonian (2.37), in which the possibility of a nonzero center-of-mass momentum $\mathbf{Q}$ of a Cooper pair is allowed

$$\begin{aligned}\hat{\mathcal{H}} &= \sum_{\mathbf{k}\sigma} \xi_{\mathbf{k}\sigma} c^{\dagger}_{\mathbf{k}\sigma} c_{\mathbf{k}\sigma} \\ &+ \frac{1}{N} \sum_{\mathbf{k}\mathbf{k}'\mathbf{Q}} V_{\mathbf{k}\mathbf{k}'} c^{\dagger}_{\mathbf{k}+\mathbf{Q}/2\uparrow} c^{\dagger}_{-\mathbf{k}+\mathbf{Q}/2\downarrow} c_{-\mathbf{k}'+\mathbf{Q}/2\downarrow} c_{\mathbf{k}'+\mathbf{Q}/2\uparrow} + \frac{N}{n} \overline{m} h_{cor}. \end{aligned} \tag{4.1}$$

The dispersion relations for the cases with SDM and SIM are chosen, respectively, in the forms

$$\xi_{\mathbf{k}\sigma} = \frac{\hbar^2 k^2}{2m_\sigma} - \sigma(h + h_{cor}) - \mu, \tag{4.2}$$

$$\xi^{(SIM)}_{\mathbf{k}\sigma} = \frac{\hbar^2 k^2}{2m_{av}} - \sigma h - \mu. \tag{4.3}$$

The magnetic field is accounted for only via the Zeeman term, as the Maki parameter [22] (cf. discussion in Section 1.2) in the systems of interest is high (Pauli limiting case). For example, in $CeCoIn_5$ the Maki parameters for $H \parallel ab$ and $H \perp ab$ are estimated to be $\alpha_\parallel = 4.6$ and $\alpha_\perp = 5.0$ [13, 106]. Note also that the required minimum value of the Maki parameter for the formation of the FFLO state is $\alpha = 1.8$ [23]. As in the BCS theory, we assume a separable pairing potential in a small region around the Fermi surface. Namely, the interaction is assumed to exist only in region $\pm\hbar\omega_C$ around the Fermi surface, more precisely in the region

$$\overline{W} = \Big[\frac{k_{b\uparrow} + k_{b\downarrow}}{2}, \frac{k_{a\uparrow} + k_{a\downarrow}}{2}\Big], \tag{4.4}$$

where $k_{b\sigma}$ is defined by $\xi_{k_{b\sigma},\sigma} = -\hbar\omega_C$, and $k_{a\sigma}$, by $\xi_{k_{a\sigma},\sigma} = \hbar\omega_C$.[1] Explicitly, the pairing potential is given by

$$V_{\mathbf{k},\mathbf{k}'} = \begin{cases} -V_0\eta_{\mathbf{k}}\eta_{\mathbf{k}'}, & \text{for } \mathbf{k}, \mathbf{k}' \in \overline{W}, \\ 0, & \text{in other cases,} \end{cases} \tag{4.5}$$

where $\eta_{\mathbf{k}} \equiv \cos(ak_x) - \cos(ak_y)$ for the d-wave case (with $a = 4.62$ Å being the lattice constant) and $\eta_{\mathbf{k}} \equiv 1$ for the s-wave case.[2] Under these assumptions, the $\mathbf{Q}$-dependent superconducting gap parameter can be expressed as

$$\Delta_{\mathbf{k},\mathbf{Q}} \equiv \frac{1}{N}\sum_{\mathbf{k}} V_{\mathbf{k}\mathbf{k}'}\langle c_{-\mathbf{k}+\mathbf{Q}/2\downarrow} c_{\mathbf{k}+\mathbf{Q}/2\uparrow}\rangle = \Delta_{\mathbf{Q}}\eta_{\mathbf{k}}. \tag{4.6}$$

Nonzero $\mathbf{Q}$ leads to spatial oscillations of the superconducting gap, namely the gap in real space can be expressed as

$$\Delta(\mathbf{r}) = \Delta_{\mathbf{Q}} e^{i\mathbf{Q}\mathbf{r}} \tag{4.7}$$

Hamiltonian (4.1) is diagonalized within the standard mean-field procedure [108] followed by the Bogolyubov-de Gennes [109] transformation of the form

$$\begin{cases} \alpha_{\mathbf{k}\uparrow} = u_{\mathbf{k}} c_{\mathbf{k}+\mathbf{Q}/2\uparrow} - v_{\mathbf{k}} c^\dagger_{-\mathbf{k}+\mathbf{Q}/2\downarrow}, \\ \alpha^\dagger_{\mathbf{k}\downarrow} = v_{\mathbf{k}} c_{\mathbf{k}+\mathbf{Q}/2\uparrow} + u_{\mathbf{k}} c^\dagger_{-\mathbf{k}+\mathbf{Q}/2\downarrow}, \end{cases} \tag{4.8}$$

[1] Such interaction region has been chosen because its width does not change significantly with the magnetic field h. We performed also calculations by selecting the interaction regime differently (namely, by choosing $\overline{W} = [k_{b\downarrow}, k_{a\uparrow}]$ and $\overline{W} = [k_{b\uparrow}, k_{a\downarrow}]$) and have obtained almost the same results.

[2] Note that the pairing potential is chosen of a separable form, i.e., the $\mathbf{k}$ and $\mathbf{k}'$ dependencies are factorized as in the case with real-space pairing for correlated electrons e.g. in the t-J model [90, 107].

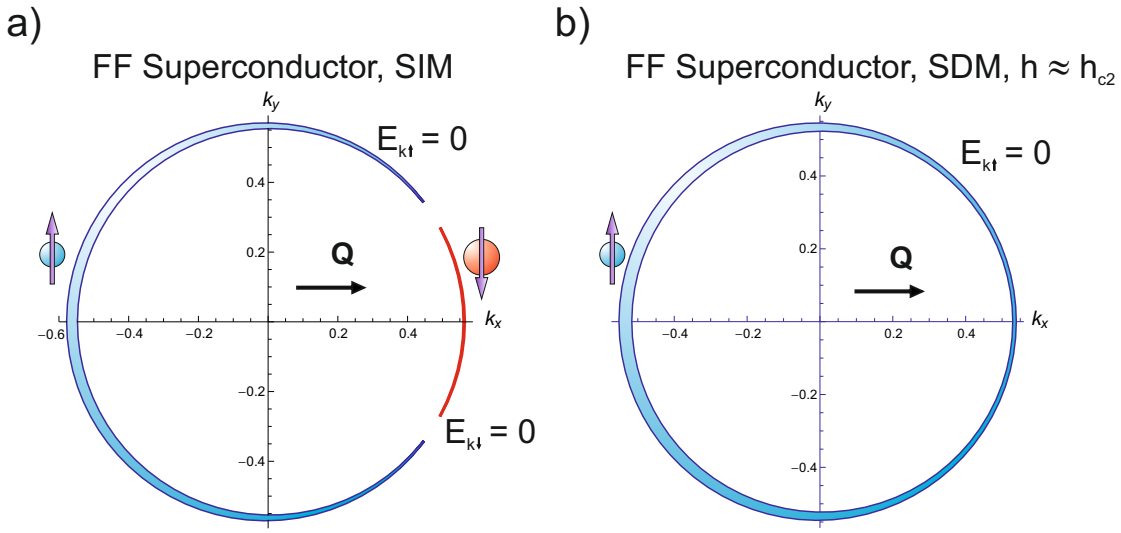

Figure 4.1: Unpaired regions in the reciprocal space for the SIM (a) and SDM (b) situations and for the field close to the critical value h_{c2}. The boundaries of these regions, are given by the $E_{\mathbf{k}\sigma} = 0$ lines, as marked in the figure. These regions are populated by $\sigma =\uparrow$ unpaired quasiparticles (blue) and $\sigma =\downarrow$ unpaired quasiparticles (red), the latter only in the SIM case. These regions are obtained from the self-consistent calculations detailed below.

which leads to the diagonal form

$$\hat{\mathcal{H}} = \sum_{\mathbf{k}\sigma} E_{\mathbf{k}\sigma}\alpha^{\dagger}_{\mathbf{k}\sigma}\alpha_{\mathbf{k}\sigma} + \sum_{\mathbf{k}}(\xi^{(s)}_{\mathbf{k}} - E_{\mathbf{k}}) + N\frac{\Delta^2_{\mathbf{Q}}}{V_0} + \frac{N}{n}\overline{m}h_{cor}, \tag{4.9}$$

and the quasiparticle spectrum characterized by energies [110]

$$E_{\mathbf{k}\sigma} = E_{\mathbf{k}} + \sigma\xi^{(a)}_{\mathbf{k}}, \qquad E_{\mathbf{k}} = \sqrt{\xi^{(s)2}_{\mathbf{k}} + \Delta^2_{\mathbf{Q}}\eta^2_{\mathbf{k}}}, \tag{4.10}$$

$$\xi^{(s)}_{\mathbf{k}} \equiv \frac{1}{2}(\xi_{\mathbf{k}+\mathbf{Q}/2\uparrow} + \xi_{-\mathbf{k}+\mathbf{Q}/2\downarrow}), \quad \xi^{(a)}_{\mathbf{k}} \equiv \frac{1}{2}(\xi_{\mathbf{k}+\mathbf{Q}/2\uparrow} - \xi_{-\mathbf{k}+\mathbf{Q}/2\downarrow}). \tag{4.11}$$

In the form (4.8) of the Bogolyubov-de Gennes transformation the quasiparticle operators $\alpha_{\mathbf{k}\uparrow}$ and $\alpha_{\mathbf{k}\downarrow}$ are distinguished by the spin label $\uparrow$ and $\downarrow$. Note also that because of the presence of $\xi^{(a)}_{\mathbf{k}}$ in Eq. (4.10), there are regions of reciprocal space with $E_{\mathbf{k}\sigma} \leq 0$, which represent nongapped excitations. In other words, these regions are populated by unpaired quasiparticles of spin σ (see Figure 4.1). This amounts to a substantial spin polarization $\overline{m} > 0$ in high fields and in the FFLO state (cf. Figure 4.1, where the $E_{\mathbf{k}\pm} = 0$ lines are shown - the contour given by these lines encircles the unpaired region of the reciprocal space). The Bogolyubov transformation coherence factors in (4.8) are given by

$$u_{\mathbf{k}} = \left[\frac{1}{2}\left(1 + \frac{\xi^{(s)}_{\mathbf{k}}}{E_{\mathbf{k}}}\right)\right]^{1/2}, \quad v_{\mathbf{k}} = \left[\frac{1}{2}\left(1 - \frac{\xi^{(s)}_{\mathbf{k}}}{E_{\mathbf{k}}}\right)\right]^{1/2}. \tag{4.12}$$

Finally, the complete set of equations determining the superconducting state properties is as follows,

$$\begin{aligned}
\mathcal{F} &= -k_B T \sum_{\mathbf{k}\sigma} \ln(1+e^{-\beta E_{\mathbf{k}\sigma}}) + \sum_{\mathbf{k}} (\xi_{\mathbf{k}}^{(s)} - E_{\mathbf{k}}) + N\frac{\Delta_{\mathbf{Q}}^2}{V_0} + \mu N \\
&\quad + \frac{N}{n}\overline{m} h_{cor}, \qquad (4.13)\\
h_{cor} &= -\frac{n}{N}\sum_{\mathbf{k}\sigma} f(E_{\mathbf{k}\sigma})\frac{\partial E_{\mathbf{k}\sigma}}{\partial \overline{m}} + \frac{n}{N}\sum_{\mathbf{k}} \frac{\partial \xi_{\mathbf{k}}^{(s)}}{\partial \overline{m}}\Big(1 - \frac{\xi_{\mathbf{k}}^{(s)}}{E_{\mathbf{k}}}\Big), \qquad (4.14)\\
\overline{m} &= \frac{n}{N}\sum_{\mathbf{k}\sigma} \sigma f(E_{\mathbf{k}\sigma}), \qquad (4.15)\\
\Delta_{\mathbf{Q}} &= \frac{V_0}{N}\sum_{\mathbf{k}} \eta_{\mathbf{k}}^2 \frac{1 - f(E_{\mathbf{k}\uparrow}) - f(E_{\mathbf{k}\downarrow})}{2E_{\mathbf{k}}}\Delta_{\mathbf{Q}}, \qquad (4.16)\\
n &= n_\uparrow + n_\downarrow = \frac{n}{N}\sum_{\mathbf{k}\sigma}\{u_{\mathbf{k}}^2 f(E_{\mathbf{k}\sigma}) + v_{\mathbf{k}}^2[1 - f(E_{\mathbf{k},-\sigma})]\}, \qquad (4.17)
\end{aligned}$$

where $\mathcal{F}(T, H, \mu; h_{cor}, \overline{m}, n, \Delta_{\mathbf{Q}})$ is the system free-energy functional for the case of a fixed number of particles [40]. Similarly as for the unpaired Fermi sea (Chapter 3), the equations (4.14), (4.15) and (4.16) are equivalent with $\partial\mathcal{F}/\partial\overline{m} = 0$, $\partial\mathcal{F}/\partial h_{cor} = 0$, and $\partial\mathcal{F}/\partial\Delta_{\mathbf{Q}} = 0$, respectively. In effect, the numerical analysis involves solving the system of four integral equations. Let us note once again the presence of the two different effective chemical potentials, $\mu_\sigma \equiv \mu + \sigma h_{cor}$, for particles with spin up and down in the spin-polarized situation. This is an unavoidable consequence of the SGA scheme [84] (or equivalently slave-boson formalism, cf. Refs. 72–74, 86) used to derive expression for the masses (3.4), and the dispersion relation (3.3). Parenthetically, we have also performed calculations by disregarding the different effective chemical potentials (i.e. we have utilized the GA scheme of Section 2.1, by putting $h_{cor} = 0$, and disregarding Eq. (4.14)) and the results obtained were nonphysical (a free-energy jump occurred at the BCS-FFLO phase transition).

The final solution within our approximation is that with a particular $\mathbf{Q}$ which minimizes the free energy F obtained from the free-energy functional (4.13) at the values of parameters being solution to Eqs. (4.14)-(4.17). The state with $\mathbf{Q} = 0$ is called *the BCS state* (or simply, BCS), and that with $|\mathbf{Q}| \neq 0$ - *the FFLO state* (or simply, FFLO). More precisely, the latter is of the Fulde-Ferrell (FF) type of the FFLO state (see Section 1.2 for details).

4.2 Numerical analysis and discussion

4.2.1 Numerical methods

The solution procedure consists of two principal tasks. First is the solution of Eqs. (4.14)-(4.17) (in the SDM case) or Eqs. (4.15)-(4.17) (in the SIM case, in which

$h_{cor} = 0$ and the dispersion relation is given by Eq. (4.3)). The second task is the minimization of F with respect to $|\mathbf{Q}|$.

In the procedure of solving the appropriate set of equations we use the hybrids algorithm (solver: `gsl_multiroot_fsolver_hybrids`) from the GNU Scientific Library (GSL). We typically use the precision $epsabs = 10^{-10}$, that is, the procedure converges when the relation $\sum_i |f_i| < epsabs$ is fulfilled (where the sum is taken over all equations, which have been brought to the form $f_i = 0$). Next, the minimization procedure with respect to $\mathbf{Q}$ is carried out with the help of GSL (we use the `gsl_min_fminimizer_brent` minimizer). In search of the minimum free energy, we use the accuracy 0.004. Namely, the procedure converges, when the Cooper pair momentum $|\mathbf{Q}|/\Delta k_F$ is determined with accuracy 0.004.

The sums in Eqs. (4.14)-(4.17) are calculated by integration over the density of states in the $\mathbf{k}$-space. The integral is computed in the radial (r, θ) or spherical (r, θ, ϕ) coordinates. This yields a two-dimensional integral in both 2D and 3D situations, as in the latter the integration over the azimuthal angle ϕ is trivial (provided the Cooper pair momentum $\mathbf{Q}$ is set along the $\theta = 0$ line). For performing the integration we use the GSL QAG adaptive integration procedure (`gsl_integration_qag`) with the precision 10^{-6}. Adaptive procedures subdivide the region of integration into subintervals, and at each iteration step, the subinterval with the largest error is bisected. This assures that the procedure concentrates on regions with local difficulties in the integral (steps, cusps, etc.), and results in quick convergence.

Additionally, as the integration procedure is time-costly, we perform the integration in parallel for the most time-consuming integrals. The parallelization is done by utilizing Win32 API Threads (note that it can be done easier with OpenMP). The integral region is subdivided into 8 subintervals and each thread performs integration over one of these subintervals.

Computing of each of the (SDM) phase diagrams shown in the following part of this Section took about one day on a machine with Quad-Core Intel Xeon E5420 processor.

In Table I the exemplary numerical values of the parameters have been provided for the situation with the d-wave form of the superconducting gap. The quantity F_{NS} is the free energy of the normal state, and therefore ΔF is the condensation energy. Also, $\Delta m \equiv m_2 - m_1$ is the mass difference and $h_{cor\,FS}$ is the correlation field value in the normal state. The free energies are calculated per elementary cell.

Table I. Equilibrium values of mean-field variables and related quantities for the d-wave solution with $H = 20.01$ T and $T = 0.1$ K.

Variable	Value	Variable	Value
$\overline{m}$	0.0271583	$\Delta m\,(m_0)$	5.27346
h_{cor} (K)	-6.47761	$h_{cor\,FS}$ (K)	-6.53133
$\Delta_{\mathbf{Q}}$ (K)	0.807311	$\lvert\mathbf{Q}\rvert$ (Å^{-1})	0.0162
μ (K)	126.424	$\lvert\mathbf{Q}\rvert/\Delta k_F$	1.05
F (K)	61.044366175	ΔF (K) $\equiv F_{NS} - F$	-0.000479434

4.2.2 Values of parameters

Although our calculations are performed for a model situation (i.e. for a gas of heavy quasiparticles) we have assumed the following values of the parameters, emulating the heavy fermion systems[3]: $n = 0.97$, $V_{elem} = 161$ Å^3 (3D case), $S_{elem} = 4.62 \times 4.62$ Å^2 (2D case), $m_{av} = 100$ m$_0$, $\hbar\omega_C = 17$ K, and $V_0/n = 90$ K (in the 3D s-wave and 2D d-wave situations) or $V_0/n = 110$ K (in the 2D s-wave case). The characteristic energy scale associated with spin-fluctuations in $CeCoIn_5$ is $T_{sf} = 10$ K [44] - a value comparable to our $\hbar\omega_C$.[4] For those parameters, the chemical potential was equal to $\mu \approx 140$ K (3D) and $\mu \approx 126$ K (2D). This means that $V_0 \lesssim \epsilon_F$ and the (weak coupling) BCS approximation can be regarded only as a proper solution on a semiquantitative level. In contrast to standard BCS formulation, the chemical potential is readjusted in the superconducting state so that n is constant. Furthermore, for the assumed values of parameters one can calculate the coupling constant $\rho(\mu)V_0 \approx 0.48$ (data for 3D case) and the coherence length at $T = 0$ K, $\xi_0 \approx 40$ Å, both already at the border of the strong-coupling limit. Also, such values have been taken to obtain the critical temperature of the order of the experimental value $T_c \simeq 2.3$ K.

We now discuss the phase diagrams for the cases of SDM and SIM in the three selected situations. See also our papers, Refs. 83, 111.

4.2.3 Three-dimensional correlated gas, s-wave gap symmetry

The phase diagram is exhibited in Figures 4.2 for the SDM and the SIM cases. Both the BCS (state with $\mathbf{Q} = 0$) and the FFLO ($\mathbf{Q} \neq 0$) phases extend to much higher fields if the masses are spin-dependent. This is a consequence of the smaller Fermi-vector splitting Δk_F for the SDM case (cf. Figure 3.1d). Note that the superconducting state in both the SDM and SIM cases survives to the field at which the splitting $\Delta k_F \approx 0.012$ Å^{-1} is the same (see Figure 3.1d). This means that indeed the Fermi-vector splitting is the factor destabilizing superconductivity.

The most interesting is the fact that in the SDM situation the FFLO state becomes much more robust compared to BCS state, especially for $T \simeq 0$. The FFLO state extends far beyond the BCS critical field H_{c2} marked by the dashed line[5] only in the SDM case. The reason for the robustness of the FFLO phase in the SDM case (the FFLO *stabilization mechanism*) is as follows: the superconductivity in the Pauli-limiting case is destroyed by the Fermi-vectors splitting Δk_F (cf. Figure 3.1d). This splitting in the case of SDM is generally smaller (in this respect SDM compensate partially the Zeeman term influence on the condensed

[3] V_{elem} and S_{elem} are elementary cell volume and area, respectively. They are taken as experimental values for $CeCoIn_5$ - see e.g. Ref. 44. The average mass m_{av} is taken for the heaviest band of $CeCoIn_5$ [47].

[4] In Ref. 46 the authors argue that $T_{sf} \sim 5$ K and is field dependent. For the modeling purposes we assume it is constant.

[5] H_{c2} is determined as the applied field in which the BCS solution becomes unstable (its free energy becomes higher than the normal-state free energy).

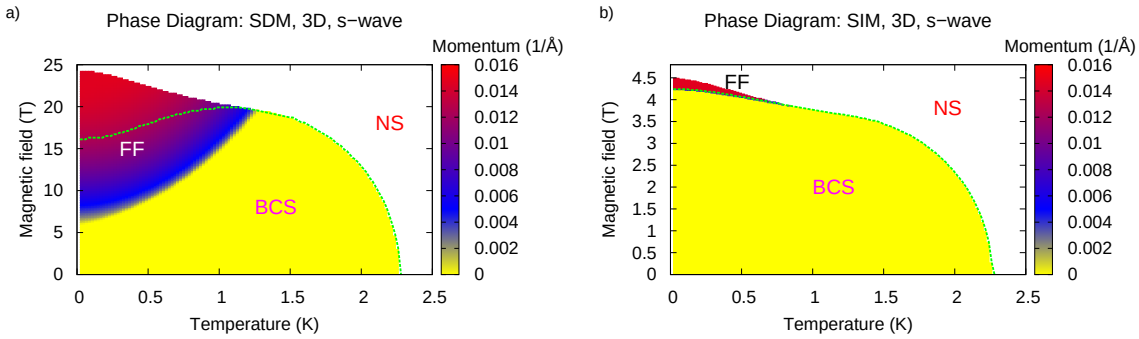

Figure 4.2: Phase diagram for the cases with the spin-dependent (a) and the spin-independent masses (b). Light (yellow) region corresponds to $\mathbf{Q} = 0$ (BCS phase), the darker (blue-red) one to $\mathbf{Q} \neq 0$ (FF phase) and the white to normal state. The dashed lines mark the BCS critical field H_{c2}. Note that with increasing temperature, the transition from BCS to FFLO state occurs at higher fields, in qualitative agreement with experimental results [12, 13, 17, 24]. The FFLO phase is stable in an extended H-T regime only in the SDM case.

state), hence the higher critical fields. However, for the masses to depend on the spin direction, the magnetic moment $\overline{m} \equiv n_\uparrow - n_\downarrow$ has to be non-zero, and in the BCS state around $T \lesssim 0.5$ K the magnetization is close to zero (see Figure 4.3) what weakens the mass dependence on the spin σ, and in effect produces larger Δk_F in the BCS superconducting phase. Therefore, the BCS state is not enhanced much by the SDM influence in that temperature interval. In the FFLO state, on the other hand the magnetization is nonzero even at $T = 0$ K. This is because in the FFLO state there are regions with unpaired quasiparticles in the reciprocal space (cf. Figure 4.1). The FFLO state becomes stable in an extended regime of field h then, as a result of a smaller Fermi-vectors splitting in that case. This stabilization mechanism should also hold for other HFLT phases, as they have higher spin polarization than the BCS phase (see e.g. Refs. 112 and 27).

Another interesting feature is the fact that with the increasing temperature, the transition from the BCS to the FFLO state occurs at high fields (cf. Figure 4.2a) consistent with experimental results [12, 13, 17, 24]. It can also be easily explained. Namely, as temperature increases, the magnetization in the BCS state increases (see Figure 4.3), allowing a substantial mass difference, and decreasing the Fermi wave vectors splitting, sustaining the BCS superconductivity. In brief, the BCS state benefits from the smaller Δk_F for SDM at higher temperatures ($T \gtrsim 0.5$ K) and becomes more stable in this regime.

Systematic evolution of the spin polarization in the condensed state is shown in Figure 4.3 (the orbital part is obviously not included). It increases at the BCS-FFLO border at lower T, as one would expect.

In the panel composing Figure 4.4 we plot the gap magnitude $\Delta_\mathbf{Q}$ and the magnitude of the wave vector $\mathbf{Q}$ for the SDM and SIM cases. The behavior of the order parameter $\Delta_\mathbf{Q}$ differs substantially in these two cases. Namely, there is no jump of $\Delta_\mathbf{Q}$ at BCS-FFLO transition for SDM, whereas for SIM this transition

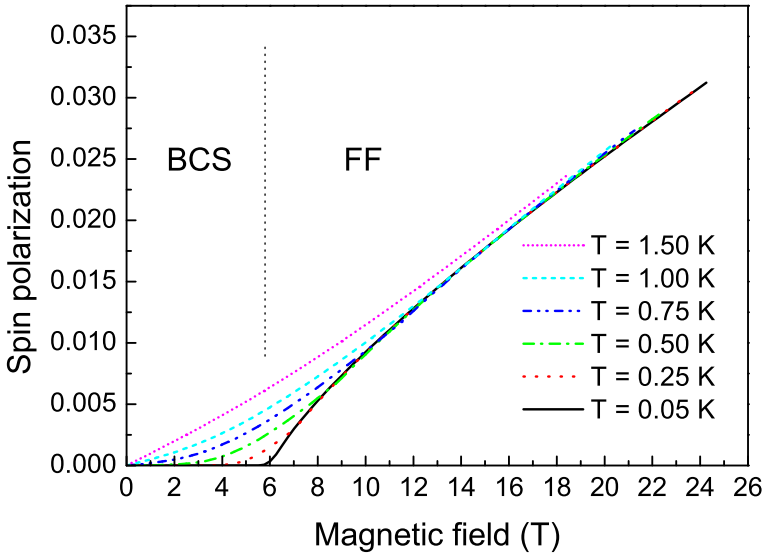

Figure 4.3: Spin polarization, $\overline{m}$ as a function of applied magnetic field for selected values of temperature. For $T = 0 - 0.5$ K, the magnetization in the BCS state is small, than it increases with applied field after the continuous BCS to FFLO transition. For higher temperatures magnetization in the BCS state becomes substantial and this produces a higher critical field for the BCS-FFLO transition at $T \gtrsim 0.5$ K.

is always discontinuous. Transitions from superconducting to normal state are continuous for the case of SDM in disagreement with the experimental results [12, 13, 17, 24]. The reasons for this discrepancy are discussed in the following Section.

Finally in Figure 4.5 we show the correlation-field dependencies on field and temperature. It can be seen that for BCS and around $T = 0$ K this field is close to zero, then increases and approaches for $H \to H_{c2}$, the value for the unpaired Fermi sea (i.e. that from Section 3.1), denoted here as h_{corFS}.

4.2.4 Two-dimensional correlated gas, s-wave gap symmetry

This case is presented for the sake of completeness, and is relevant to the subsequent analysis of normal metal-superconductor junction conductance (cf. Chapter 5). We present here only the phase diagrams for the SDM and SIM cases (see Figure 4.6). It can be seen that in the SDM case the FFLO state fills comparable portion of the superconducting regime as in the 3D case. On the other hand, in the SIM case the FFLO state is stable in much wider field range than in the 3D case. This is obviously because of geometrical reasons (better nesting conditions for the $\mathbf{Q}$ vector in 2D case).

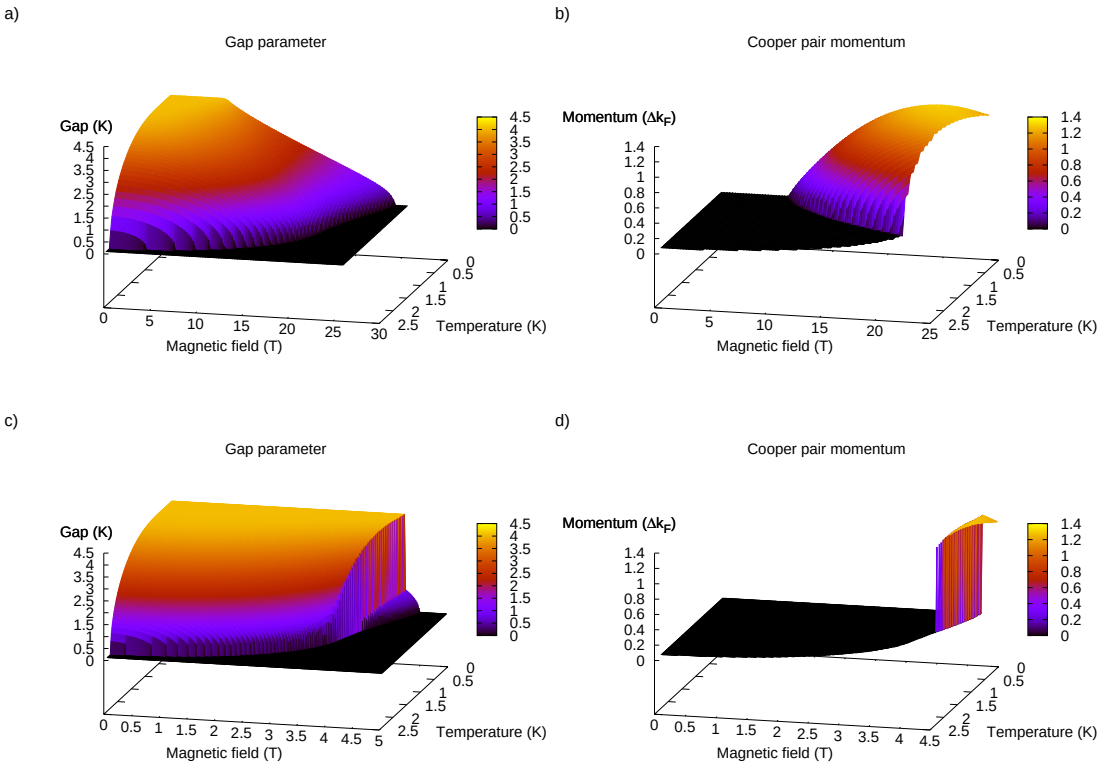

Figure 4.4: Left (a, c): gap parameter $\Delta_{\mathbf{Q}}$ as a function of temperature and magnetic field for SDM (top) and SIM (bottom). All transitions in the SDM case are continuous. Right (b, d): Cooper pair momentum in the FFLO state in units of Fermi wave vector splitting Δk_F for SDM (top) and SIM (bottom). The FFLO phase momentum $|\mathbf{Q}|$ changes continuously in the SDM case (at the transition BCS-FFLO), contrary to the case for SIM. Typical value of the momentum is $|\mathbf{Q}| \approx \Delta k_F$.

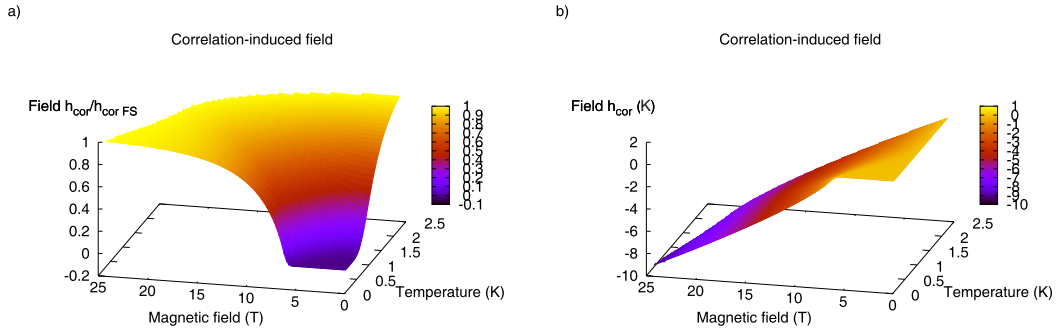

Figure 4.5: Left: Correlation field for the 3D s-wave state in units of the field obtained for the unpaired Fermi sea (h_{corFS}). Note that as $H \to H_{c2}$, the correlation-field value approaches the one for the unpaired Fermi sea. Right: Correlation field in absolute units. It is negative, i.e. it acts opposite to the applied magnetic field, partly compensating the Zeeman term.

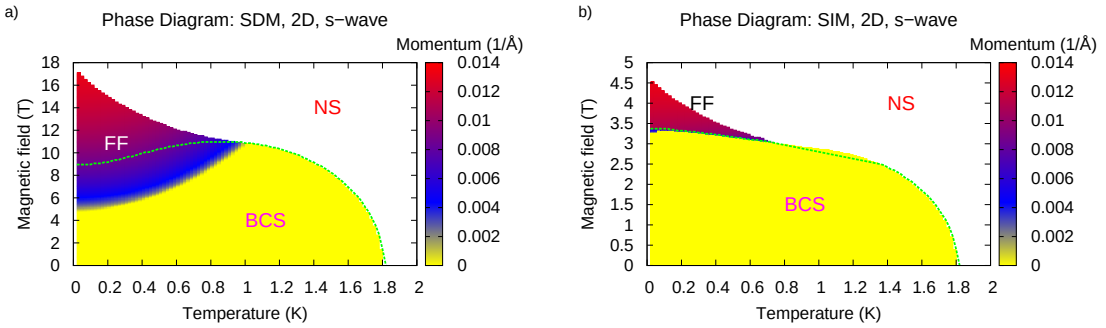

Figure 4.6: Phase diagram for the two-dimensional correlated gas with s-wave gap symmetry in the SDM (a) and SIM (b) cases. Light (yellow) region corresponds to $\mathbf{Q} = 0$ (BCS phase), the darker to the state with $\mathbf{Q} \neq 0$ (FF phase) and the white to the normal state (NS). Note the greater difference between SDM and SIM cases than for d-wave gap symmetry (see Figure 4.7 below).

4.2.5 Two-dimensional correlated gas, d-wave gap symmetry

The overall phase diagrams in 2D case with d-wave pairing are exhibited in Figure 4.7 for the cases with the spin-dependent (SDM) (a) and the spin-independent (SIM) (b) effective masses. The FFLO phase is robust only in the former case, as for the s-wave solution (discussed earlier), although the difference is greater in the s-wave case. The specific difference is that in the present case two distinct phase-boundary lines appear inside the FFLO state, as detailed in Figure 4.7: the topmost and the lowest parts (red color) have the Cooper-pair momentum $\mathbf{Q}$ oriented along the k_x (or k_y) direction, whereas the middle phase (blue color) has $\mathbf{Q}$ along the diagonal ($k_x = k_y$). Also, superconductivity of the FFLO type exists up to the field of 36 T in the SDM case, i.e. to the field about 4 times larger than that for the SIM case. Hence, the former system *indeed* belongs to the class of *high-field low-temperature superconductors*. Note also that the FFLO states exist far beyond the second critical field for BCS state, marked by the dashed line.

To visualize the detailed nature of the transition to the FFLO phase we have plotted in Figure 4.8 profiles of the gap magnitude $\Delta_{\mathbf{Q}}$ and the Cooper pair momentum $|\mathbf{Q}|$, both on the H - T plane. In the low-T limit the observed gap jumps meaning that the transitions BCS $\rightarrow$ FF1 ($\mathbf{Q} \parallel k_x$ axis), as well as the transition FF1 $\rightarrow$ FF2 ($\mathbf{Q} \parallel (k_x, k_y)$ diagonal) and FF2 $\rightarrow$ FF1' ($\mathbf{Q} \parallel k_x$ axis) are discontinuous, whereas the transition to the normal state is continuous. As the temperature increases, all the transitions (except that from FF2 to FF1') become continuous, but the exact position of the terminal bicritical point will not be discussed in detail here. The phase FF1' illustrates a reentrant high-field behavior for FF1 phase.

The above phase transitions can be connected with the magnetization changes. This is because the FFLO phase encompasses regions of $\mathbf{k}$-space with gapless quasiparticle excitations in the superconducting phase (see Figure 4.1, where these regions are exhibited for the s-wave case, in the d-wave situation these regions are similar). This means that the magnetization curve will show a nontypical behav-

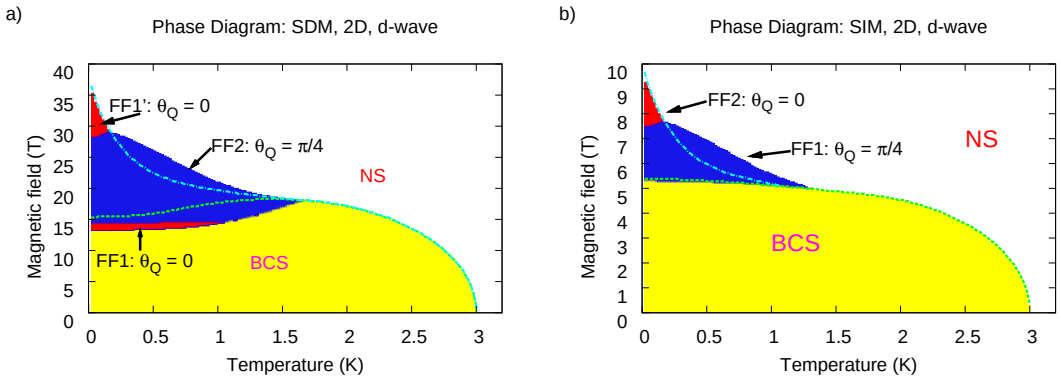

Figure 4.7: Phase diagram for 2D correlated gas on temperature-applied field plane with the d-wave gap symmetry and for the cases with SDM, (a), and SIM, (b). Light (yellow) regions correspond to $\mathbf{Q} = 0$ (BCS phase), the darker (blue, red) to the state with $\mathbf{Q} \neq 0$ (FF phase) and the white to normal state (NS). The red region corresponds to the Cooper-pair momentum $\mathbf{Q}$ in the k_x direction ($\theta_{\mathbf{Q}} = 0$), whereas the blue one to the momentum along the diagonal ($k_x = k_y$, $\theta_{\mathbf{Q}} = \pi/4$). Note that this anisotropy results solely from the d-wave gap symmetry, as the unpaired gas is isotropic. The dashed lines mark the BCS critical field H_{c2}, and the dot-dashed lines mark H_{c2} for the solution with $\theta_{\mathbf{Q}} = 0$. Note that for the SDM case with the increasing temperature, the transition from BCS to FF state occurs at higher fields, in a qualitative agreement with experimental results [12, 13, 17, 24].

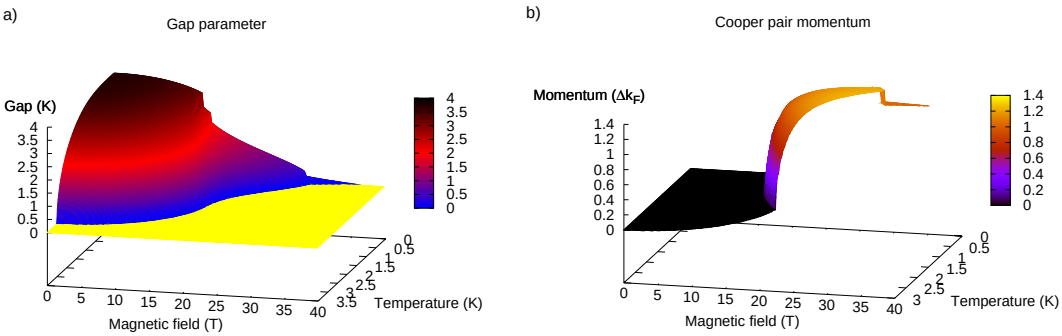

Figure 4.8: (a) Gap parameter $\Delta_{\mathbf{Q}}$ (in units of K) and (b) Cooper pair momentum $\mathbf{Q}$ in units of the Fermi momentum difference $\Delta k_F \equiv k_{F\uparrow} - k_{F\downarrow}$, both for the SDM case on the H - T plane for the d-wave SC state. Transitions between various phases are seen as a change of gap magnitude: the lower-field transition are first-order, whereas the transition to the normal state is continuous.

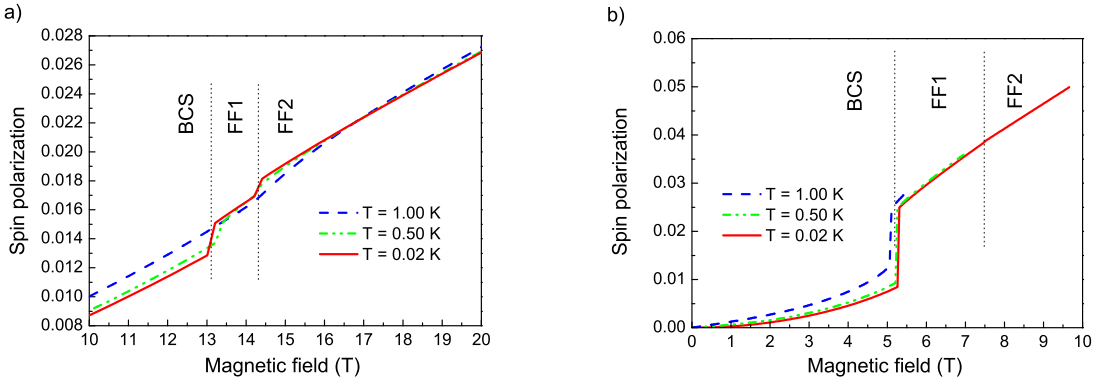

Figure 4.9: Spin polarization $\overline{m} \equiv n_\uparrow - n_\downarrow$ as a function of applied field. Note the weak jumps corresponding to the discontinuous transitions at $T = 0.02$ K and $T = 0.50$ K for SDM case (a) and much larger in the SIM case (b). For the SDM case all transitions at $T = 1$ K are already continuous.

ior, particularly in the vicinity of the transition to FFLO state, as displayed in Figure 4.9. Namely, $\overline{m}(H)$ exhibits a weak metamagnetic behavior accompanied by a weak jump at the two lower-field transition points. It is surprising at first look that the corresponding jump is much larger in the SIM case. However, one must remember that in the SDM case the field h_{cor} compensates largely the applied field (see Figure 4.10 for details).

To compare our results with those for the s-wave pairing symmetry we recall here the mechanism behind the FFLO stabilization by SDM presented in Section 4.2.3. Namely, SDM compensate the Zeeman effect influence by reducing the Fermi wave vectors splitting. Therefore, superconducting state with SDM has higher critical fields (here $H_{c2} = 10$ T for SIM, and $H_{c2} = 36$ T for the SDM case, cf. Figure 4.7). The FFLO state benefits from SDM by a greater extent than BCS because spin polarization $\overline{m}$ in the latter is smaller (cf. Figure 4.9), and from (3.4) the mass difference $\Delta m \propto \overline{m}$. Therefore, in BCS the mass difference is smaller, and the Fermi wave vectors splitting larger than in FFLO (the Zeeman term influence is compensated less effectively). Hence, at $T = 0$ the FFLO fills about 1/2 of the phase-diagram area for SIM, and about 2/3 for SDM. On the other hand, as temperature T increases, the spin polarization increases in the BCS state (see Figure 4.9) allowing larger mass difference Δm and reducing Fermi wave vectors splitting enhancing superconductivity. This is why the transition line between BCS and FFLO is curved upwards in the SDM case (and so is H_{c2} for the BCS phase). In the d-wave situation, the BCS state can have a substantial spin-polarization already at $T = 0$ (unlike in the s-wave case). Therefore, the BCS state can benefit from SDM already at $T = 0$ and the FFLO state is not stabilized so spectacularly in that situation, as it was in the s-wave case (where in the BCS phase $\overline{m} \approx 0$ at $T = 0$).

For the sake of completeness, we draw in Figure 4.10 the effective field induced by the correlations. The jumps reflect the discontinuous transitions discussed above. The field h_{cor} (in units of h_{corFS} for the unpaired Fermi sea) increases both

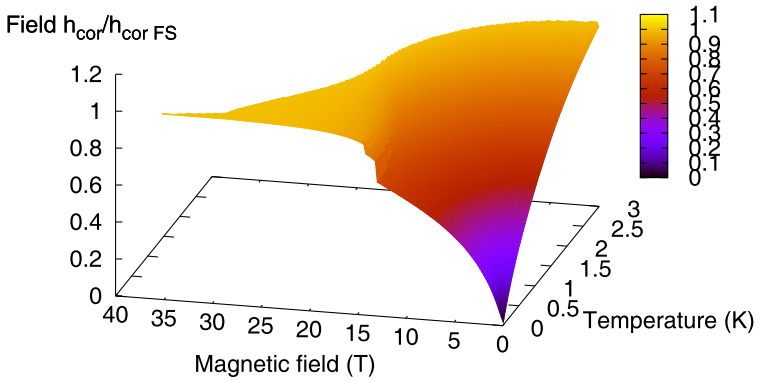

Figure 4.10: Correlation field h_{cor} in the d-wave superconducting state on $H-T$ plane relative to that in the normal state h_{corFS}, which is typically equal to $-0.5h$, and therefore the field h_{cor} compensates partly the applied field H.

with the increasing temperature and the applied field.

4.3 Superconducting states within the tight-binding approximation for electrons in square lattice

We have performed also analysis of the strongly correlated superconductivity using the SGA scheme and within the tight-binding approximation by assuming dispersion relation in the form of (3.11)-(3.12). Unfortunately, in the $U \to \infty$ limit the saturated ferromagnetic phase is the ground state (see Section 3.2), and superconductivity cannot compete with it (at least for reasonable values of the pairing potential). On the other hand, for finite U (and nonzero double occupancy probability d), the tendency towards ferromagnetism is still quite strong (see Ref. 84), with positive and strong $h_{cor} \approx 5-8h$. For such situation the FFLO state turned out unstable against the BCS state.

Analysis within the GA scheme has been performed by us in cooperation with Prof. M. Maśka and Prof. M. Mierzejewski from the University of Silesia [95]. The results obtained lead to the similar conclusions, as in the gas case. Namely the FFLO phase is more robust in the strongly-correlated case (see Figure 4.11 for the obtained phase diagram), what indicates that correlations stabilize the FFLO phase.

4.4 Conclusions, relation to experiment

We have analyzed superconducting states of a strongly-correlated gas of heavy quasiparticles (SDM case). To distinguish the novel features coming from the interparticle correlations we have studied also the case without correlations (SIM case). Despite the simplicity of our model (parabolic dispersion relation, separable and simple pairing potential, single narrow-band model), qualitative results obtained are very meaningful for the FFLO phase detectability and could hold for more

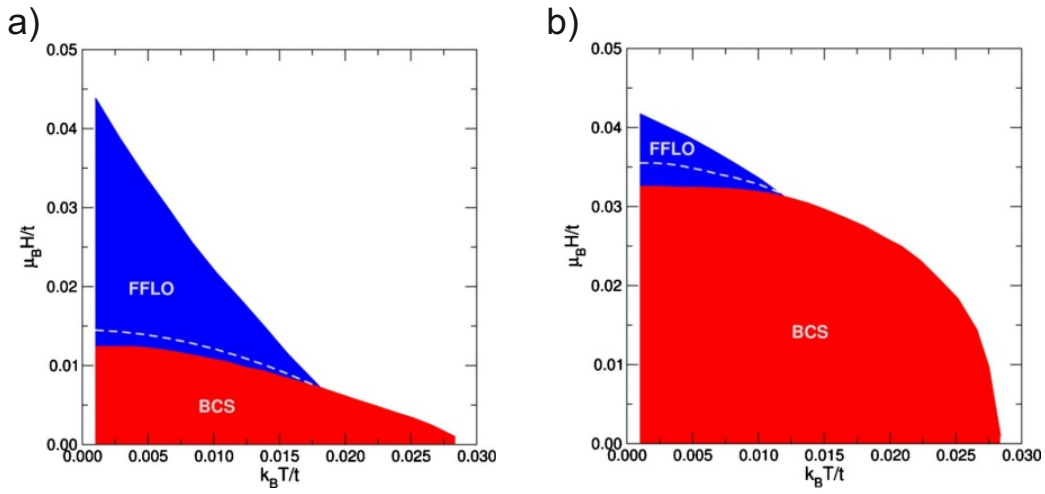

Figure 4.11: Phase diagram for the paired quasiparticles in a two-dimensional square lattice with d-wave gap symmetry and in the SDM (a) and SIM (b) cases, after Ref. 95. Red region corresponds to $\mathbf{Q} = 0$ (BCS phase), the blue to the state with $\mathbf{Q} \neq 0$ (FFLO phase) and the white to the normal state.

general and realistic models and other high-field low-temperature (HFLT) phases. This is because the spin-dependent factor renormalizing mass is $\mathbf{k}$-independent, as is h_{cor}, and they are obtained in a self-consistent manner from global equations, integrated over $\mathbf{k}$.

The most striking result is the fact that for the case of SDM the FFLO state becomes stable in much wider range of applied field and temperature. We believe that the mechanism of stabilization of the FFLO state by SDM is universal. Therefore, it should also apply to other unconventional HFLT phases such as for example the mixed staggered π-triplet SC + d-wave singlet SC + SDW phase proposed recently [80] as possible ground state of $CeCoIn_5$. This is because in such field-induced phases the spin-polarization is always higher than that for the conventional BCS (s-wave or d-wave) state [27, 112]. Those phases will benefit, from the compensation of Zeeman effect by SDM, on the expense of the BCS phase, as discussed earlier.

The detailed application of our results to concrete systems is rather limited. This is because three topics require still a conjoined analysis from the theoretical side. This is the inclusion of *magnetism* (incommensurate SDW) appearing in the vicinity of the FFLO phase. Associated with it is the *singlet-triplet mixing* [80, 113–115] (cf. also Chapter 6). Inclusion of those factors introduces additional self-consistent integral equations making the whole approach much more complex from the numerical side. Then, one has also to carry out the whole procedure for a *realistic electronic structure*. The inclusion of magnetism should result in the first-order nature of the BCS-FFLO phase boundary [79, 80].

The nature of the HFLT unconventional phase in the heavy - fermion system $CeCoIn_5$ is still unclear. Some studies suggest FFLO character, others reject it (see

discussion in Section 1.2.3). We claim that whatever this state really is, it may be stabilized by SDM due to its higher spin-susceptibility [27]. So far the observation of FFLO phase in organic metals has been indicated (see Ref. 32 and References therein), but no spin-dependence of the effective mass has been investigated for those systems.

To conclude, the simultaneous observation of the spin-dependent masses and of an unconventional HFLT superconducting phase in the same system should not be regarded as coincidental. Hence, other unconventional HFLT phases may be searched for in the systems in which spin-split masses have been observed [77] and *vice versa*.

Chapter 5

Andreev reflection spectroscopy for a strongly-correlated superconductor with FFLO phase

5.1 Introduction

In the present Chapter we concentrate on providing experimentally accessible characteristics of a superconducting state with strong correlations. Namely, we study conductance of a normal metal - superconductor junction (NSJ) with the strongly-correlated superconductor in either the Fulde-Ferrell (FF) type of the FFLO state, or in the Bardeen-Cooper-Schrieffer (BCS) state (the latter in lower fields). The properties of the superconductors are taken as those obtained in the previous Chapter. Conductance spectroscopy of a NSJ is a phase sensitive experiment and, as such, it can reveal the spatial oscillations of the order parameter. A crucial role in the conductance spectrum is played by the Andreev reflection (AR) processes [116]. In the simplest view of the Andreev reflection, an incident electron entering from normal metal into superconductor is converted at the NSJ interface into a hole moving in the opposite direction and Cooper pair inside SC (cf. Figure 5.2). Such processes increase conductance of the junction, which is analyzed in the framework provided by Blonder, Tinkham, and Klapwijk [117].

The conductance characteristics for a NSJ, with superconductor in the FFLO state, has already been investigated for both the cases of FF (with $\Delta(\mathbf{r}) = \Delta_{\mathbf{Q}} e^{i\mathbf{Q}\mathbf{r}}$) [69, 118, 119] and LO ($\Delta(\mathbf{r}) = \Delta_{\mathbf{Q}} \cos(\mathbf{Q}\mathbf{r})$) [70] types of the FFLO state, as well as for the case of superconductor with supercurrent [120, 121] (i.e. the situation similar from formal point of view). See also Refs. 122–125 for the case of NSJ with superconductor being in the BCS state of d-wave symmetry. Let us note that none of these papers takes into account strong electron correlations.

Here we consider a two-dimensional strongly-correlated superconductor in magnetic field in a Pauli-limiting situation. We perform the analysis for both s-wave and d-wave gap symmetry, and as parameters of the superconductor we take the values obtained in Sections 4.2.4 and 4.2.5, respectively. Let us remind that the strong correlations are taken into account by assuming spin-dependent masses

(SDM) of quasiparticles and the correlation field h_{cor}, as given e.g. by the Gutzwiller approximation [71], or slave-boson theory [72]. The case without strong correlations (with spin-independent masses, SIM) is analyzed for comparison. In low magnetic fields the superconductor is in the BCS state, and in higher magnetic fields a transition to the FFLO state takes place. We consider here only the FF type of FFLO state (see Section 1.2.1) and set the direction of the Cooper pair momentum $\mathbf{Q}$ as either perpendicular, or parallel to the junction interface, with more attention paid to the latter case. Let us note that the analysis is performed self-consistently. Namely, in the procedure of obtaining the superconductor parameters (Chapter 4) we choose such Cooper pair momentum $\mathbf{Q}$, which minimizes the free energy of the system. It has been shown that such careful examination of the superconductor properties is important, and non-self-consistent calculations may lead to important alterations of the conductance spectrum [118].

As we deal with heavy quasiparticles on the superconductor side of NSJ, we should in principle take into account the Fermi-velocity-mismatch effects. Then the AR processes would be severely limited by a high effective barrier strength Z. On the other hand, AR is clearly observed in junctions with heavy-fermion superconductors [126, 127] and theoretical efforts have been made to understand why this is the case [128–130]. Based on these studies, in our analysis we neglect the Fermi-velocity mismatch by assuming equal chemical potentials and equal *average* masses of quasiparticles on both sides of the junction. Namely, we choose masses on the normal side as m_{av}, and on the superconductor side we have that $(m_\uparrow + m_\downarrow)/2 = m_{av}$, with $m_{av} = 100\ \mathrm{m_0}$, which roughly corresponds to the heaviest band of $CeCoIn_5$ [47]. The masses m_σ are determined from the superconductor parameters via Eq. (3.4). We consider here only two-dimensional NSJ.

5.2 Junction conductance - theoretical analysis

5.2.1 Bogolyubov - de Gennes equations

Kinematics of the reflection may be analyzed by means of the Bogolyubov-de Gennes (BdG) equations [109]

$$Eu_\sigma(\mathbf{x}) = \hat{\mathcal{H}}_0 u_\sigma(\mathbf{x}) + \int d\mathbf{x}' \Delta(\mathbf{s},\mathbf{r}) v_\sigma(\mathbf{x}'), \tag{5.1}$$

$$Ev_\sigma(\mathbf{x}) = -\hat{\mathcal{H}}_0 v_\sigma(\mathbf{x}) + \int d\mathbf{x}' \Delta^*(\mathbf{s},\mathbf{r}) u_\sigma(\mathbf{x}'), \tag{5.2}$$

where $\mathbf{s} = \mathbf{x} - \mathbf{x}'$, $\mathbf{r} = (\mathbf{x} + \mathbf{x}')/2$, and $\sigma = \pm 1$ is the spin quantum number of the incoming quasiparticle and $u_\sigma(\mathbf{x})$ and $v_\sigma(\mathbf{x})$ are the particle and hole components. The one-particle Hamiltonian is given by

$$\hat{\mathcal{H}}_0(\mathbf{r}) = -\hat{\nabla}\frac{\hbar^2}{2\,m(\mathbf{r})}\hat{\nabla} - \sigma h - \sigma h_{cor}(\mathbf{r}) - \mu + V(\mathbf{r}), \tag{5.3}$$

where $h = g\mu_B H$ is the reduced field, the correlation field is nonzero only on the superconducting side of the junction ($h_{cor}(\mathbf{r}) = h_{cor}\Theta(x)$), and we have used the

effective mass approximation [131] to express the kinetic part as $\hat{\nabla}\frac{\hbar^2}{2\,m(\mathbf{r})}\hat{\nabla}$, with $m(\mathbf{r}) \equiv m(x) = m_{av}\Theta(-x) + m_{\sigma}\Theta(x)$,[1] similarly as in Refs. 132 and 133. Also, $\mathbf{r} = (x, y)$ and the interface scattering potential is chosen as a delta function of strength $\tilde{H}$, i.e. $V(\mathbf{r}) = \tilde{H}\,\delta(x)$. The gap function can be Fourier transformed as following

$$\Delta(\mathbf{s}, \mathbf{r}) = \int d\mathbf{k} e^{i\mathbf{k}\mathbf{s}} \tilde{\Delta}(\mathbf{k}, \mathbf{r}) = \int d\mathbf{k} e^{i\mathbf{k}\mathbf{s}} \Delta_{\mathbf{k},\mathbf{Q}}\, e^{i\mathbf{Q}\mathbf{r}}\, \Theta(x), \tag{5.4}$$

with $\Delta_{\mathbf{k},\mathbf{Q}}$ given by Eq. (4.6). We neglect the proximity effects by assuming a step-like gap function. To solve the BdG equations we make the plane-wave ansatz. Namely, we assume that the two-component pair wave function has the form

$$\psi(\mathbf{r}, \sigma) \equiv \begin{pmatrix} u_\sigma(\mathbf{r})|\sigma\rangle \\ v_\sigma(\mathbf{r})|\overline{\sigma}\rangle \end{pmatrix} = e^{i\mathbf{k}\mathbf{r}} \begin{pmatrix} \tilde{u} e^{i\mathbf{q}\mathbf{r}}\,|\sigma\rangle \\ \tilde{v} e^{-i\mathbf{q}\mathbf{r}}\,|\overline{\sigma}\rangle \end{pmatrix}, \tag{5.5}$$

with $\tilde{u}$ and $\tilde{v}$ as constants, with $\mathbf{q} = \mathbf{Q}/2$, and with $\overline{\sigma} \equiv -\sigma$ (we have also dropped the σ indices of $\tilde{u}$ and $\tilde{v}$). By substituting (5.4) and (5.5) into BdG equations (5.1), (5.2) and after some algebra we obtain the following matrix equation

$$\begin{pmatrix} -E + \xi_{\mathbf{k}+\mathbf{q},\sigma} & \Delta_{\mathbf{k},\mathbf{Q}} \\ \Delta^*_{-\mathbf{k},\mathbf{Q}} & -E - \xi_{\mathbf{k}-\mathbf{q},\overline{\sigma}} \end{pmatrix} \begin{pmatrix} \tilde{u}\,|\sigma\rangle \\ \tilde{v}\,|\overline{\sigma}\rangle \end{pmatrix} = 0, \tag{5.6}$$

where unpaired quasiparticle energies $\xi_{\mathbf{k}\sigma}$ are given by (4.2) or (4.3). Eq. (5.6) gives the dispersion relations for quasiparticles and quasiholes in the superconductor

$$E = E_{\mathbf{k}\pm} = \begin{cases} \xi^{(a)}_{\mathbf{k}} \pm \sqrt{\xi^{(s)2}_{\mathbf{k}} + \Delta_{\mathbf{k},\mathbf{Q}}\Delta^*_{-\mathbf{k},\mathbf{Q}}} & \text{for } \sigma = \uparrow, \\ -\xi^{(a)}_{-\mathbf{k}} \pm \sqrt{\xi^{(s)2}_{-\mathbf{k}} + \Delta_{\mathbf{k},\mathbf{Q}}\Delta^*_{-\mathbf{k},\mathbf{Q}}} & \text{for } \sigma = \downarrow, \end{cases} \tag{5.7}$$

where $\xi^{(s,a)}_{\mathbf{k}}$ have been defined in Eq. (4.11). One may check that the above equation is in accordance with Eq. (4.10), as $E_{\mathbf{k}+} = E_{\mathbf{k}\uparrow}$ (quasiparticle) and $E_{\mathbf{k}-} = -E_{\mathbf{k}\downarrow}$ (quasihole) for incoming particle with spin $\sigma = \uparrow$, as well as $E_{\mathbf{k}+} = E_{-\mathbf{k}\downarrow}$ (quasiparticle) and $E_{\mathbf{k}-} = -E_{-\mathbf{k}\uparrow}$ (quasihole) for incoming particle with spin $\sigma = \downarrow$. This holds as long as $\Delta^*_{-\mathbf{k},\mathbf{Q}} = \Delta^*_{\mathbf{k},\mathbf{Q}}$, which is true for any real $\mathbf{k}$. Dispersion relations $E_{\mathbf{k}\pm}$ have been presented in Figure 5.1 for a choice of situations. The situation with incident particle of energy E in Figure 5.1a (E' in (b)) leads to the Andreev reflection process (cf. also Figure 5.4). We call the corresponding range of energies as the *Andreev window* (AW) after Ref. 119 (cf. also Ref. 118).

5.2.2 Junction geometry

As already mentioned, we study the FF type of the FFLO superconducting state, in which $\Delta(\mathbf{r}) = \Delta_{\mathbf{Q}} e^{i2\mathbf{q}\mathbf{r}}$ and set the direction of the Cooper pair momentum $\mathbf{Q} = 2\mathbf{q}$ as either perpendicular ($\mathbf{Q} = (Q, 0)$), or parallel ($\mathbf{Q} = (0, Q)$) to the junction interface. The parallel configuration ($\mathbf{Q} = (0, Q)$) may lead to accommodating

[1] In the SIM case we take $m_\sigma = m_{av}$ and $h_{cor} = 0$.

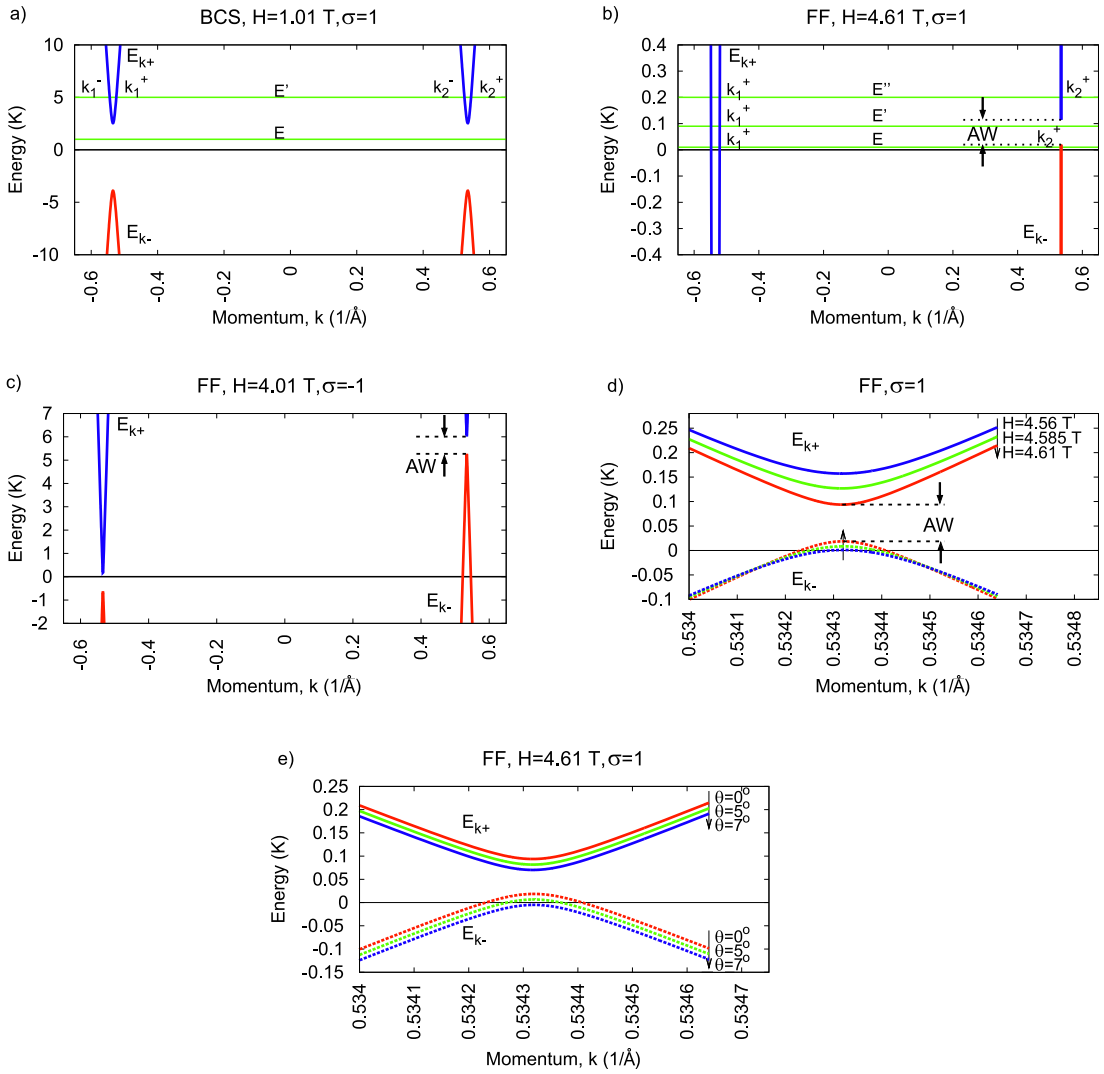

Figure 5.1: Quasiparticle and quasihole dispersion relations $E_{\mathbf{k}\pm}$ in the 2D SIM situation: (a) for BCS state at $H = 1.01$ T; (b), (c) for FF state at $H = 4.61$ T $\lesssim H_{c2}$ (b) and $H = 4.01$ T (c) for incoming electron with spin $\sigma = 1$ (b) and $\sigma = -1$ (c); (d)-(e) closer view at the region around $k \approx +k_F$ with magnetic field close to H_{c2}. (d) shows $E_{\mathbf{k}\pm}$ for a set of magnetic field H values; (e) shows $E_{\mathbf{k}\pm}$ for a choice of angle of incidence θ values. The AW region has been marked in (b)-(d). The angle of incidence is $\theta = 0$ in (a)-(d). The quasimomenta $k^{\pm}_{1,2}$ marked in (a) and (b) are solutions to the equations $E = E_{\mathbf{k}\pm}$ (Eq. (5.7)) propagating in the positive (superscript "+") and negative ("−") x direction.

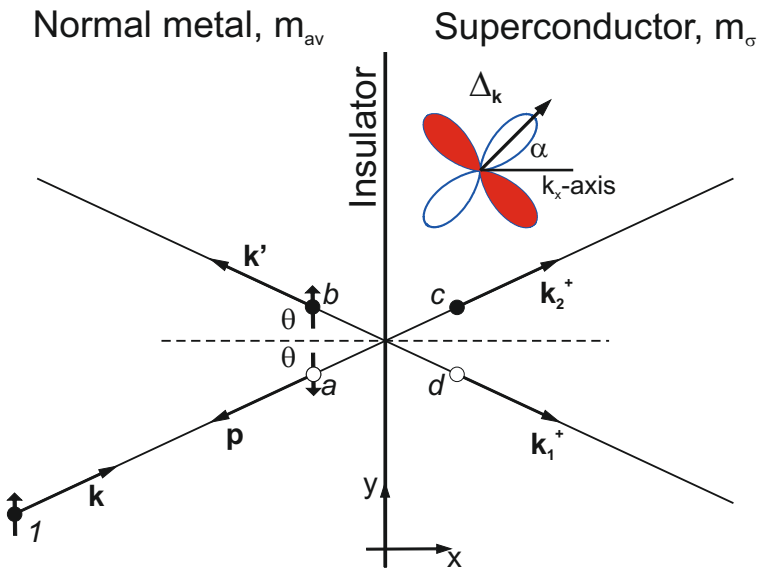

Figure 5.2: Junction geometry for incoming particle of spin $\sigma =\uparrow$. Normal-state and superconductor regions are marked. Interface lies at the $x = 0$ line. The superconducting gap is also presented: α is the angle between the k_x axis and maximum-gap (antinodal) direction. Full circles mark quasiparticles and empty ones mark quasiholes. Momentum of each of them is marked with a boldface letter, and amplitude with an italic letter. Namely, incoming particle has the momentum $\mathbf{k}$, and amplitude 1, reflected hole has $\mathbf{p}$ and a, reflected quasiparticle: $\mathbf{k}'$, b, transmitted quasiparticle: $\mathbf{k_2^+}$, c, and transmitted quasihole: $\mathbf{k_1^+}$, d. The angle of incidence is equal to θ and to the angle of reflection but other angles (of reflection of quasihole and those of transmissions) may differ (cf. also Figure 5.3).

of normal and/or supercurrent at the NSJ interface, therefore we will pay more attention to the perpendicular configuration. Note also that the accommodation processes are slow for the case of heavy quasiparticles.

As we consider electron injected from the conductor side of the junction (junction geometry is presented in Figure 5.2), the corresponding wave functions can be expressed as (we have omitted the spin part for clarity)

$$\psi_<(\mathbf{r}) = \begin{pmatrix} 1 \\ 0 \end{pmatrix} e^{i\mathbf{kr}} + a \begin{pmatrix} 0 \\ 1 \end{pmatrix} e^{i\mathbf{pr}} + b \begin{pmatrix} 1 \\ 0 \end{pmatrix} e^{i\mathbf{k'r}}, \tag{5.8}$$

$$\psi_>(\mathbf{r}) = d \begin{pmatrix} u_1 e^{iq_x x} \\ v_1 e^{-iq_x x} \end{pmatrix} e^{i\mathbf{k}_1^+\mathbf{r}} + c \begin{pmatrix} u_2 e^{iq_x x} \\ v_2 e^{-iq_x x} \end{pmatrix} e^{i\mathbf{k}_2^+\mathbf{r}}, \tag{5.9}$$

where $\psi_<(\mathbf{r})$ and $\psi_>(\mathbf{r})$ describe wave function on the normal-metal and superconductor sides, respectively. The quasimomenta $\mathbf{k}_1^+$ (for quasihole) and $\mathbf{k}_2^+$ (for quasiparticle) are solutions of Eq. (5.7) for a given incident energy E propagating in the positive x direction. From the translational symmetry of the junction along the y direction comes conservation of the y momentum component. Namely, $k_y = k'_y = p_y = k_{1y}^+ = k_{2y}^+$. All the wave vectors are presented in Figure 5.3.

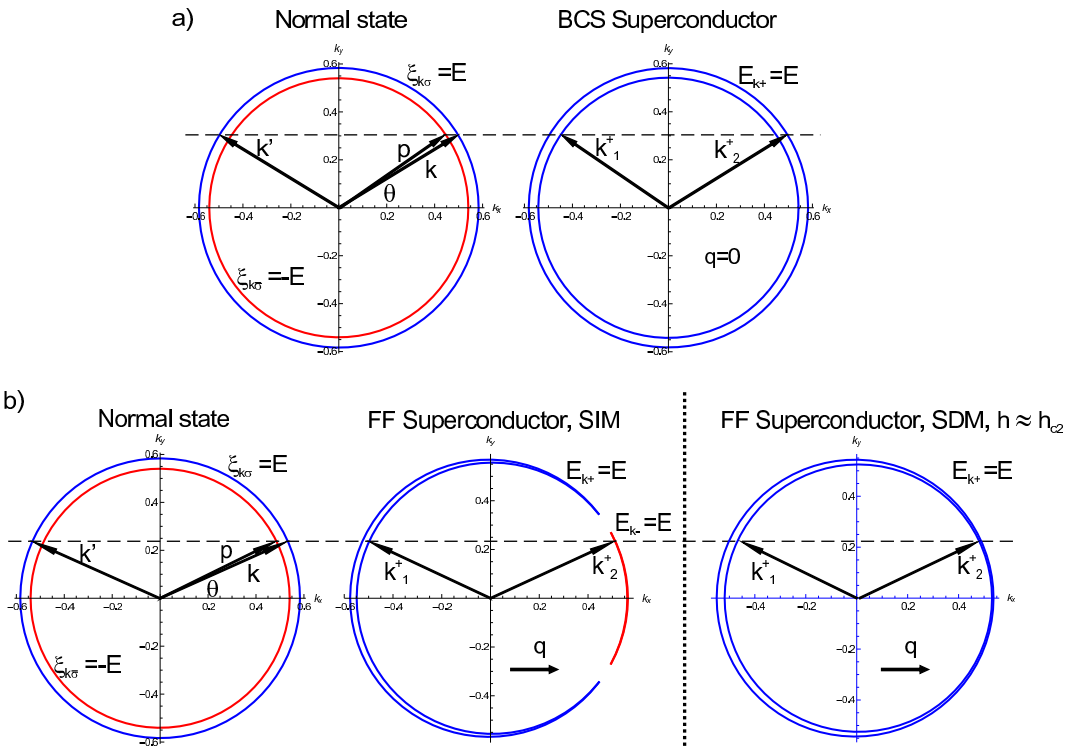

Figure 5.3: The junction geometry in the reciprocal space. All vectors are marked. It can be seen that only the incident and reflection angles are equal to θ. It can be anticipated at this point that changing θ for BCS state does not lead to drastic changes in the transmission/reflection probabilities, whereas for the FF state the situation is quite different since $\mathbf{Q} \neq 0$ induces anisotropy in the reciprocal space. The energy E value has been chosen as 10 K for all graphs except (b) "FF Superconductor" for which $E = 0.01$ K ≈ 0 (for $E > 0.5$ K there would be no $E = E_{\mathbf{k}-}$ regions in this case). The dashed lines are guide to eye and illustrate the conservation of momentum y-component.

5.2.3 System of equations and probabilities of scattering processes

We use boundary conditions with the appropriate masses[2] and the interface potential jump $\tilde{H}$; they are as follows

$$\psi_<(\mathbf{r})|_{x=0} = \psi_>(\mathbf{r})|_{x=0}, \tag{5.10}$$

$$\frac{1}{m_{av}}\frac{\partial\psi_<(\mathbf{r})}{\partial x}|_{x=0} = \frac{1}{m_\sigma}\frac{\partial\psi_>(\mathbf{r})}{\partial x}|_{x=0} - \frac{2\tilde{H}}{\hbar^2}\psi_<(\mathbf{r})|_{x=0}. \tag{5.11}$$

Those conditions lead to the following set of 4 equations[3] for the amplitudes (a, b, c, d)

$$1 + b - cu_2 - du_1 = 0, \tag{5.12}$$

$$a - cv_2 - dv_1 = 0, \tag{5.13}$$

$$\frac{ik_x(1-b)}{m_{av}} - \frac{cu_2 i(q_x + k_{2x}^+)}{m_\sigma} - \frac{du_1 i(q_x + k_{1x}^+)}{m_\sigma} + \frac{2\tilde{H}}{\hbar^2}(1+b) = 0, \tag{5.14}$$

$$\frac{aip_x}{m_{av}} - \frac{cv_2 i(k_{2x}^+ - q_x)}{m_{\overline{\sigma}}} - \frac{dv_1 i(k_{1x}^+ - q_x)}{m_{\overline{\sigma}}} + \frac{2\tilde{H}}{\hbar^2}a = 0, \tag{5.15}$$

which are similar to those in e.g. Ref. 132, but for our case vectors are replaced by their x-components: e.g. $k \leftrightarrow k_x$, $p \leftrightarrow p_x$, and also SDM are properly accounted for.[4] From the solution of Eqs. (5.12)-(5.15) one can obtain probabilities of hole reflection $p_{rh}^\sigma = |a|^2\frac{\Re[p_x]}{k_x}$, particle reflection $p_{re}^\sigma = |b|^2$, quasiparticle transmission

$$p_{te}^\sigma = |c|^2 m_{av}\frac{(\frac{|u_2|^2}{m_\sigma} - \frac{|v_2|^2}{m_{\overline{\sigma}}})\Re[k_{2x}^+] + (\frac{|u_2|^2}{m_\sigma} + \frac{|v_2|^2}{m_{\overline{\sigma}}})q_x}{k_x}, \tag{5.16}$$

and quasihole transmission

$$p_{th}^\sigma = |d|^2 m_{av}\frac{(\frac{|u_1|^2}{m_\sigma} - \frac{|v_1|^2}{m_{\overline{\sigma}}})\Re[k_{1x}^+] + (\frac{|u_1|^2}{m_\sigma} + \frac{|v_1|^2}{m_{\overline{\sigma}}})q_x}{k_x}, \tag{5.17}$$

where the σ superscript indicates the spin of the incoming electron. These probabilities are exhibited in Figure 5.4 for a choice of situations. It can be seen that in the range of energies corresponding to the AW, the probability of hole reflection is high. For example the AW is in the range of energies $0.02 - 0.1$ K in Figure 5.1b, and this yields high ρ_{rh} in the same range of energies in Figure 5.4b (upper and middle graph).

In the following we use the dimensionless barrier strength $Z \equiv 2m_{av}\tilde{H}/(k_F\hbar^2)$, where we define Fermi wave vector k_F using the zero-field value $k_F = \frac{1}{\hbar}\sqrt{2m_{av}\mu}$.

[2]Boundary conditions with unequal masses on different sides of the junction have been used before e.g. in Ref. 133.

[3]These equations are written for $y = 0$. If $y \neq 0$ additional terms $e^{\pm iq_y y}$ appear, but they do not alter the solution, so they are usually omitted for clarity.

[4]Obviously, in the SIM case we have that $m_\uparrow = m_\downarrow = m_{av}$.

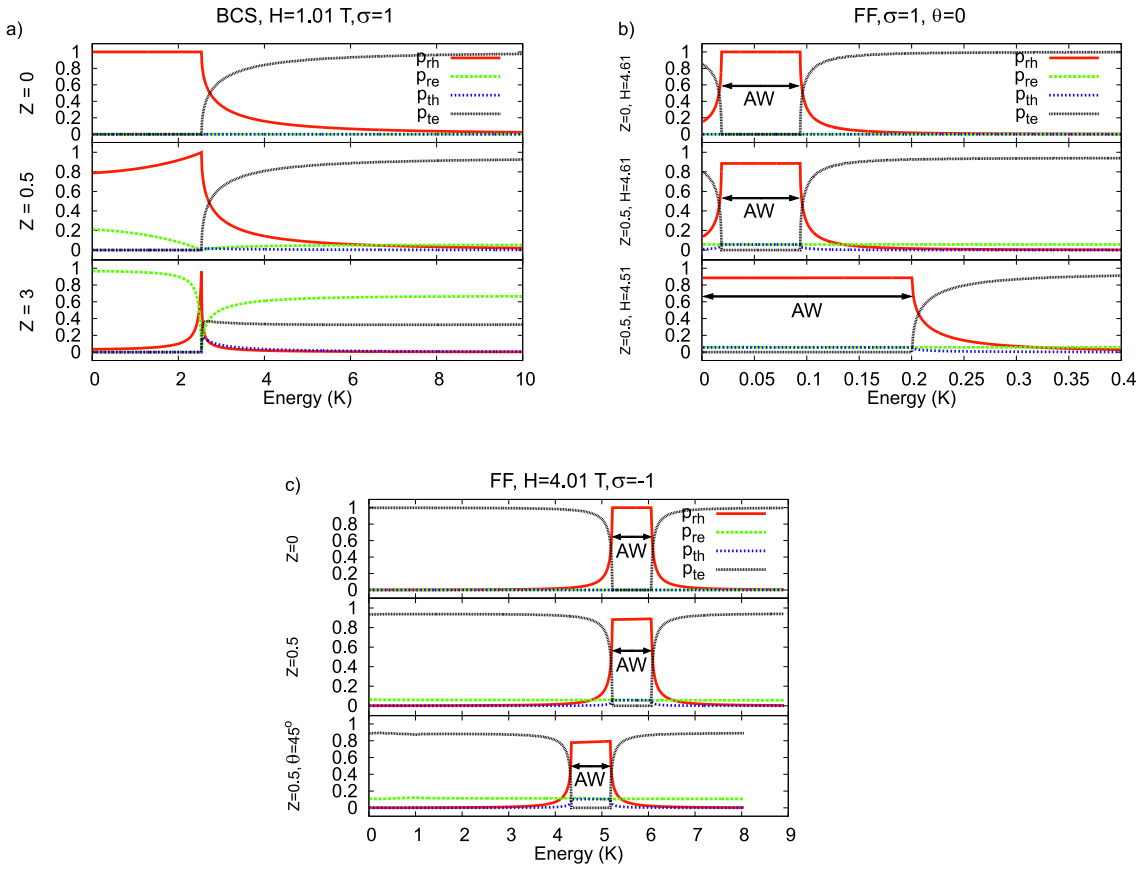

Figure 5.4: Probabilities of reflection and transmission processes in the SIM situation: (a) for BCS state and several barrier strength Z values; (b) for FF state for barrier strengths $Z = 0$ (top), $Z = 0.5$ (middle) and magnetic field $H = 4.51$ T (bottom); (c) for FF state with incoming electron of spin $\sigma = -1$ and field $H = 4.01$ T. The AW regions are shown in (b) and (c). The angle of incidence is taken as $\theta = 0$ unless stated otherwise. Note that the probabilities for BCS state (a) do not change much with θ.

Note also that we do not use the assumption $k = k' = p = k_1^+ = k_2^+ \approx k_F$ utilized at this point in majority of papers on the Andreev reflection spectroscopy, because we deal with heavy quasiparticles for which μ is of the order of 100 K. Therefore the usual assumption $\mu \gg E$ is not, strictly speaking, applicable in the present situation.

5.2.4 Differential conductance

Differential conductance ($G \equiv dI/dV$) can be obtained from the reflection and transmission probabilities [117, 134] in a straightforward manner

$$G_{ns}^{\sigma} = \frac{1}{2}\int_{-\pi/2}^{\pi/2} d\theta \cos\theta [1 - p_{re}^{\sigma}(E,\theta) + p_{rh}^{\sigma}(E,\theta)]. \tag{5.18}$$

The final result of our calculation is the conductance G averaged over spin and normalized with respect to the conductance G^{σ}_{nn} of the junction with $\Delta = 0$ but still with the same other parameters (m_{σ}, μ, h_{cor}), as the superconducting state. Namely,

$$G = \frac{G^{\uparrow}_{ns} + G^{\downarrow}_{ns}}{G^{\uparrow}_{nn} + G^{\downarrow}_{nn}}. \tag{5.19}$$

This quantity is exhibited in the following figures, sometimes with the spin-resolved conductance $G^{\sigma} \equiv G^{\sigma}_{ns}/G^{\sigma}_{nn}$. We assume the barrier strength equal to $Z = 0$ (contact limit), $Z = 0.5$ (intermediate limit), and $Z = 5$ (tunneling limit).

5.2.5 Numerical methods

The whole numerical procedure has been carried out using Mathematica 7. The most difficult part is solving of Eq. (5.7). This equation is solved for k_x at a given incident energy E (and incident angle θ). In the s-wave case this is easy, and analytically tractable, but in the d-wave situation the $\eta_{\mathbf{k}} = \cos(ak_x) - \cos(ak_y)$ factor of the superconducting gap complicates the procedure. In effect, one has to search for the solution with a numerical root-finding algorithms (we use the Newton methods implemented under the `findRoot` Mathematica procedure). In order to find the desired solution, this procedure needs to start close enough to the searched root. Ensuring this requires a lot of tweaking and a lengthy case by case analysis (note also that the solutions can be complex numbers). In order to obtain the differential conductance, Eq. (5.7) must be solved for each point appearing in the integration in Eq. (5.18), and therefore the solution procedure cannot be time consuming.

After finding the solutions of Eq. (5.7) corresponding to quasiparticles propagating in the positive-x direction, the next two steps of the numerical procedure are fairly easy (i.e. solution of a linear system of equations (5.12)-(5.15) and calculating the scattering probabilities). Finally, the integration in Eq. (5.18) is carried out (we use the `NIntegrate` Mathematica procedure[5]). This integration requires a number of recursive subdivisions to be made. Namely, we set the corresponding `MaxRecursion` parameter of `NIntegrate` to a value $20 - 40$, much larger than the standard setting. Otherwise, the precision of 10^{-5} would not be obtained.

Computation of all the conductance curves exhibited in the following Section took one hour at most (on a PC with Intel i7 processor). The computation of these curves has also been parallelized. This can be easily done by using the `Parallelize` procedure of Mathematica, with each thread calculating conductance at a different energy point.

[5]Please note that integration of complicated user-defined functions within Mathematica requires the "?NumericQ" phrase to be added after the argument of the user function. Otherwise, Mathematica tries to evaluate the integrand algebraically and returns an error. For instance, the procedure calculating conductance for a given energy E and spin σ would have a heading "G[E_?NumericQ, σ_?NumericQ]".

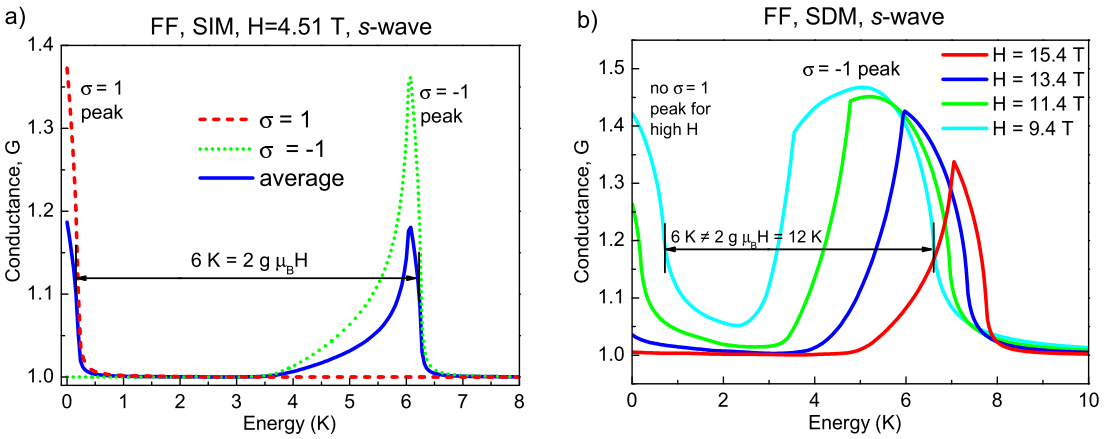

Figure 5.5: Conductance spectra for the case of s-wave FF state for SIM (a) and SDM (b) cases. The $\mathbf{Q}$ vector is oriented perpendicular to the junction and we take the intermediate barrier strength $Z = 0.5$. The distance between the peaks is twice the Zeeman energy $2h = 2g\mu_B H$ only for the SIM case. In the SDM case the correlations compensate the Zeeman splitting (by means of h_{cor} and m_σ), and the peaks are closer than $2g\mu_B H$.

5.3 Results

Our goal in the following is to identify novel, *model-independent* features of the strongly-correlated situation (SDM). Namely, these features should not depend on the assumed dispersion relation or on the pairing potential. We first discuss the results for the s-wave case with the Cooper pair momentum $\mathbf{Q}$ oriented perpendicular to the junction interface, as then the Andreev window is most clearly visible. Next, we concentrate on the results for the parallel orientation (with both s-wave and d-wave gap symmetry).

5.3.1 s-wave pairing symmetry

In Figure 5.5 the conductance for the s-wave gap symmetry and $\mathbf{Q}$ vector oriented perpendicular to the junction, is presented. It can be seen that there are peaks in the conductance originating from AR processes of quasiparticles with different spins [118]. Namely, the spin-up peak at $E \approx 0$ results from AR processes taking place when the energy E (of incoming $\sigma =\uparrow$ particle) fits into the corresponding AW - see Figure 5.4b (lower panel). The spin-down peak at $E \approx 6$ K results from analogous processes for incoming particle with $\sigma =\downarrow$, for which the AW is in much higher range of energies (cf. Figure 5.4c). Also, the broadness of the spin-down peak (the tail at lower energies: $E = 4 - 6$ K in Figure 5.5a) results from the fact that AW shifts to lower energies with the increasing θ (see Figure 5.4c, lower panel).

The conductance peaks are separated by a distance equal to twice the Zeeman energy ($2h = 2g\mu_B H$) only in the case without strong correlations (SIM, Figure 5.5a). For the SDM case the correlations compensate the Zeeman splitting

(by means of h_{cor} and m_σ, cf. Chapter 4 and Refs. 83 and 111) and as result the conductance peaks are closer than twice the Zeeman energy (Figure 5.5b). We identify this feature as a *hallmark of strong correlations in the superconducting state*. Another interesting feature differentiating the SIM and SDM cases is absence of the $\sigma =\uparrow$ peak for SDM at magnetic fields $H \gtrsim 12$ T. For such fields the junction is transparent to incoming particles with $\sigma =\uparrow$ because the AW falls below $E = 0$. In other words, the quasiparticle energy $E_{\mathbf{k}+}$ within FF superconductor is below zero around the whole Fermi surface. This leads to breaking of Cooper pairs and produces normal state region filling whole angular space around the Fermi surface (see Figure 4.1, SDM case). Since there are normal particles with $\sigma =\uparrow$ within the FF superconductor, the incoming $\sigma =\uparrow$ quasiparticle does not feel the superconducting gap presence, and the junction is transparent, what yields $G_\uparrow \approx 1$.

In all the following figures the parallel orientation of the $\mathbf{Q}$ vector has been assumed. In Figure 5.6 the NSJ conductance for the s-wave gap symmetry has been presented. Again, at high magnetic fields $H \gtrsim 12$ T the junction is transparent to incoming quasiparticles with $\sigma =\uparrow$. In the present case it is difficult to discern characteristic features of the conductance from the spin-up and spin-down channels, in such a way that the splitting of peaks would be measured. For this purpose, spin-resolved signals G_σ would have to be analyzed, as shown in Figure 5.6bd. Again, the characteristic features of spin-up and spin-down signals are separated by a distance equal to twice the Zeeman energy for SIM (Figure 5.6a) and are closer for SDM (Figure 5.6d).

5.3.2 d-wave pairing symmetry

In Figure 5.7 the conductance in the case of FF state with $\theta_{\mathbf{Q}} = 0$ is presented. Such phase is stable in the high-field regime (see Figure 4.7). Note that by fixing the direction of $\mathbf{Q}$ with respect to the NSJ interface we fix also the angle α (see Figure 5.2), as $\theta_{\mathbf{Q}}$ is determined from the results presented in Chapter 4. Namely, the parallel vector $\mathbf{Q}$ orientation with respect to the junction interface implies that $\alpha = 0$. In this case no remarkable, model-independent differences between the SDM and SIM cases are present.

The conductance spectra for the d-wave FF phase with $\theta_{\mathbf{Q}} = \pi/4$ (with $\alpha = \pi/4$) have been presented in Figure 5.8. As in the s-wave case, and for the same reasons, at high magnetic fields the junction is transparent to spin-up quasiparticles in the SDM case. Only at $H \lesssim 14.4$ T we were able to discern characteristic features of the spectra (see Figure 5.8ad for the spin-resolved spectra). These features are again split by twice the Zeeman energy for SIM, and are closer for SDM.

Finally, in Figure 5.9 we show the conductance spectra for the d-wave BCS state with (100) contact. In this case, in the tunneling limit ($Z = 5$) the peaks originating from AR of quasiparticles with different spins, are most clearly visible. As previously, these peaks are split by twice the Zeeman energy for SIM, and closer for SDM. We identify this case as the most promising for experimental verification,

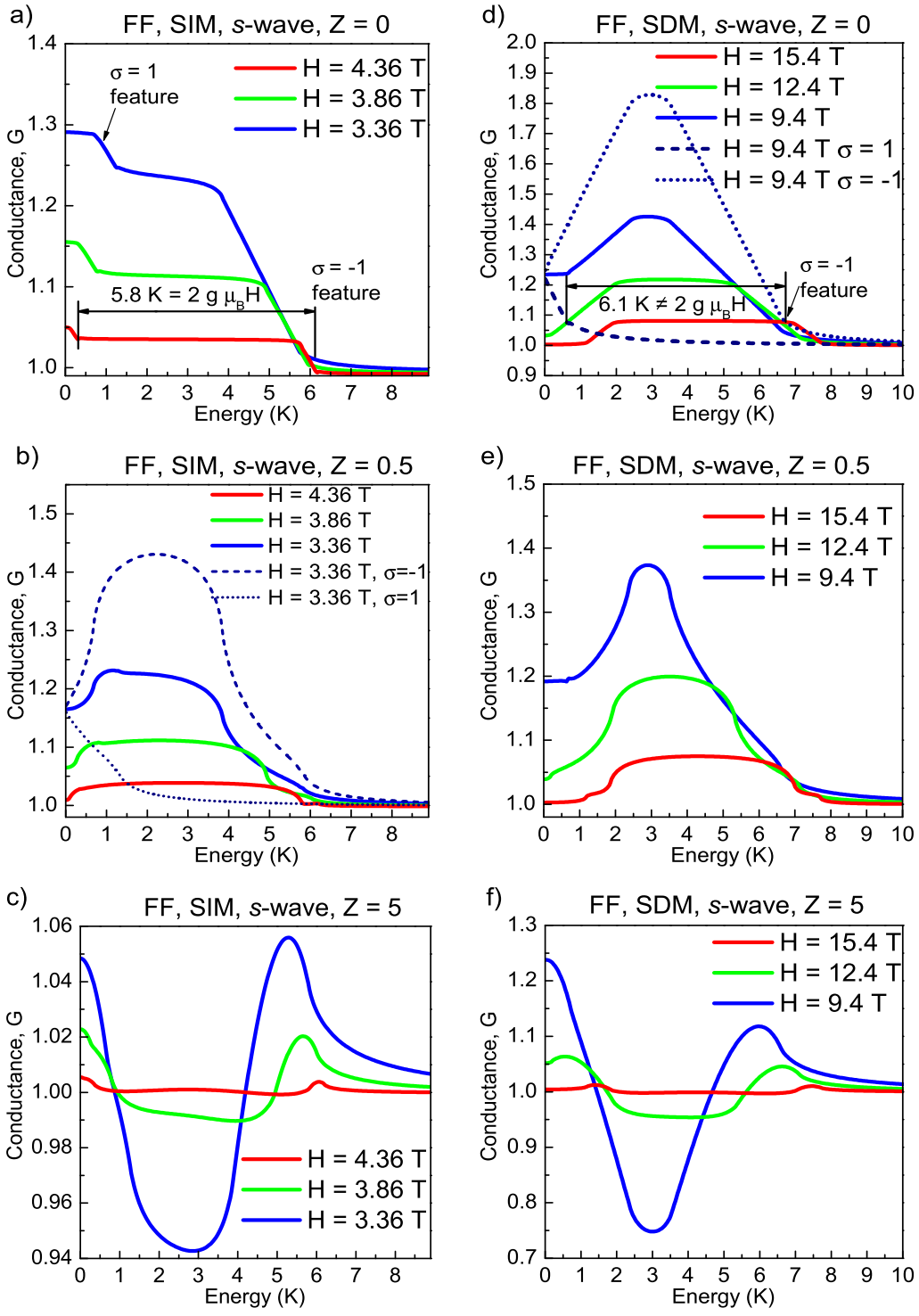

Figure 5.6: Conductance spectra for the case of s-wave FF state for SIM (a-c) and SDM (d-f), the $\mathbf{Q}$ vector oriented parallel to the junction, and different Z values. In (b) and (d) also the spin-resolved signals G_σ are presented. The distance between the characteristic features is also shown in (a) and (d). In the SDM case for $H \gtrsim 12$ T there are no features of the spin-up signal because the junction is transparent for incoming electrons with spin $\sigma =\uparrow$ (for explanation see main text).

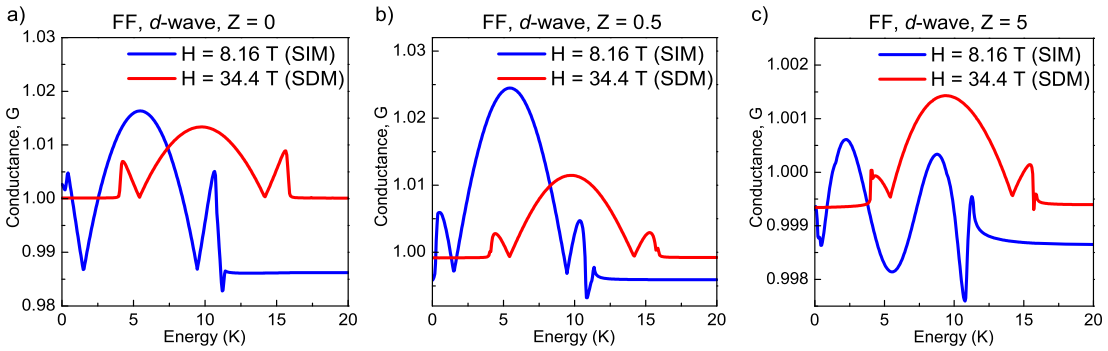

Figure 5.7: Conductance spectra for the case of d-wave FF state for different Z values, for the SIM and SDM cases. The Cooper pair momentum is oriented along the gap node (i.e. $\theta_{\mathbf{Q}} = 0$ and $\alpha = 0$; see Figures 4.7 and 5.2). The magnetic field is close to H_{c2}. There is no clear distinct feature, which differentiates between the SIM and the SDM situations for this configuration.

as discussed in the following.

5.4 Relation to experiment

Our results imply that the splitting between the spin-up and the spin-down features of the conductance spectra is equal to twice the Zeeman energy only in the non-correlated case (SIM). In the strongly-correlated case, due to the presence of spin-dependent masses (SDM) m_σ and correlation field h_{cor}, the separation of the spin-up and the spin-down features differs essentially. In the present case of a two-dimensional, correlated electron gas, this separation is smaller (because m_σ and h_{cor} compensate the Zeeman term; typically $h_{cor} \approx 0.5 \times (-h)$ - see Chapter 4), but in general it may be larger. For example in the two-dimensional Hubbard model, our recent calculations [84] yield typically $h_{cor} \approx 5 \times h$, and therefore in that model correlations *enhance* splitting of the conductance peaks.

It should be in principle possible to measure the conductance-peaks splitting experimentally. Especially the BCS case with (100) contact and high barrier strength Z (Figure 5.9cf) looks promising, as the peaks are clearly visible, and the BCS state exists in lower magnetic fields than FFLO, what should make the whole analysis simpler (the orbital effects [135], which may be essential especially on the normal metal side, are less important in that regime).

Another feature differentiating the SIM and SDM cases is the absence of the spin-up features of conductance spectra for high magnetic fields and for the FF state. It is difficult to say, if this feature is model-independent or characteristic of the model with dispersion relation of a free-electron gas with renormalized masses.

Andreev reflection spectroscopy in magnetic field has already been reported in some compounds [136–140]. For example in Mo_3Sb_7 point contact AR spectroscopy lead to identification of this compound as an unconventional superconductor [140]. Such measurements have also been performed on pure and Cd-doped $CeCoIn_5$ [138, 139]. This compound, as a heavy-fermion superconductor and possibly host

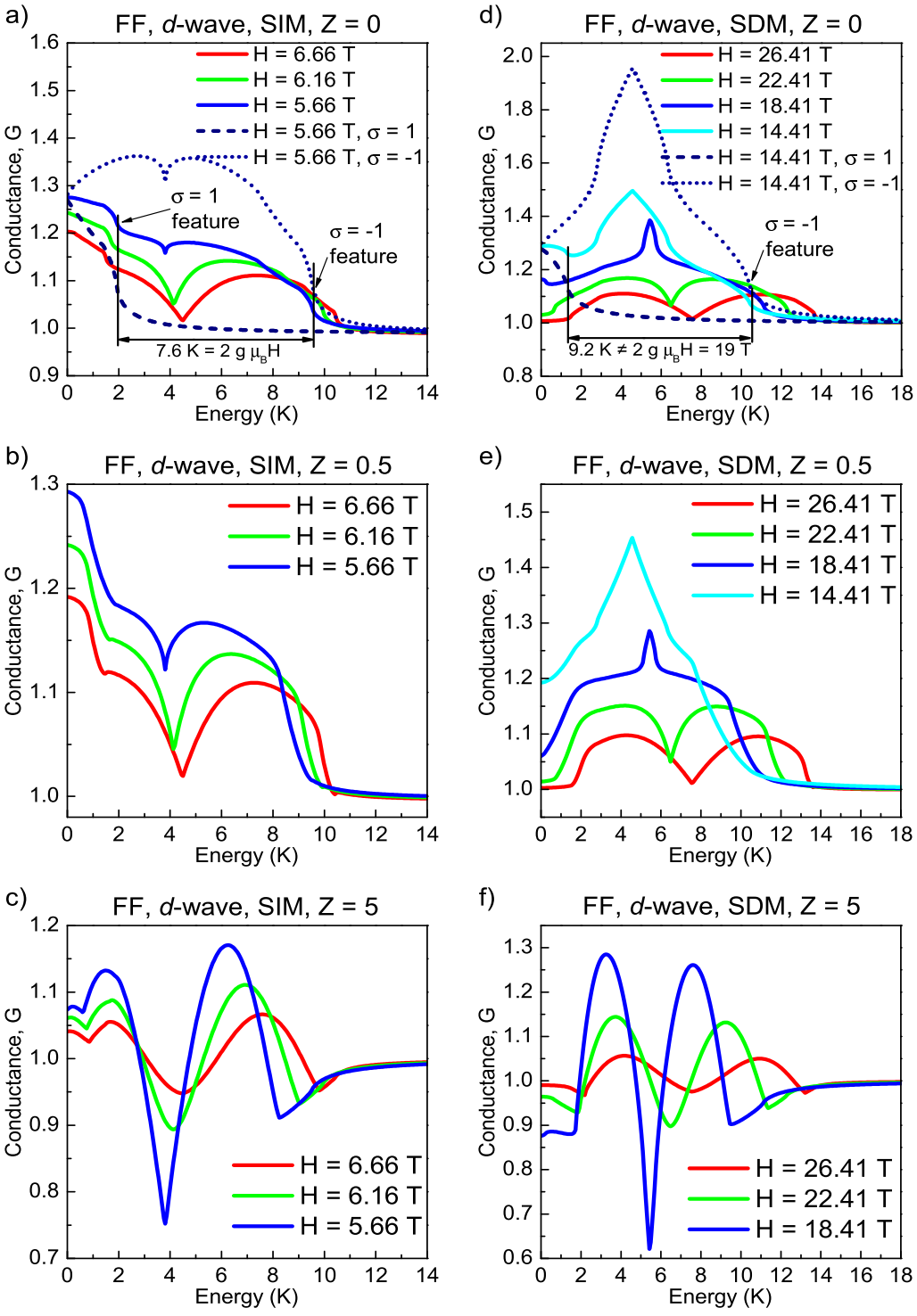

Figure 5.8: Conductance spectra for the d-wave FF state with $\theta_{\mathbf{Q}} = \pi/4$ ($\mathbf{Q}$ along the antinodal direction, $\alpha = \pi/4$) for selected barrier strengths for the SIM (a-c) and the SDM (d-f) cases. In (a) and (d) also the spin-resolved conductance G_σ has been presented to identify spectra features for both spin channels. These features are separated by twice the Zeeman energy for SIM, and are closer for SDM.

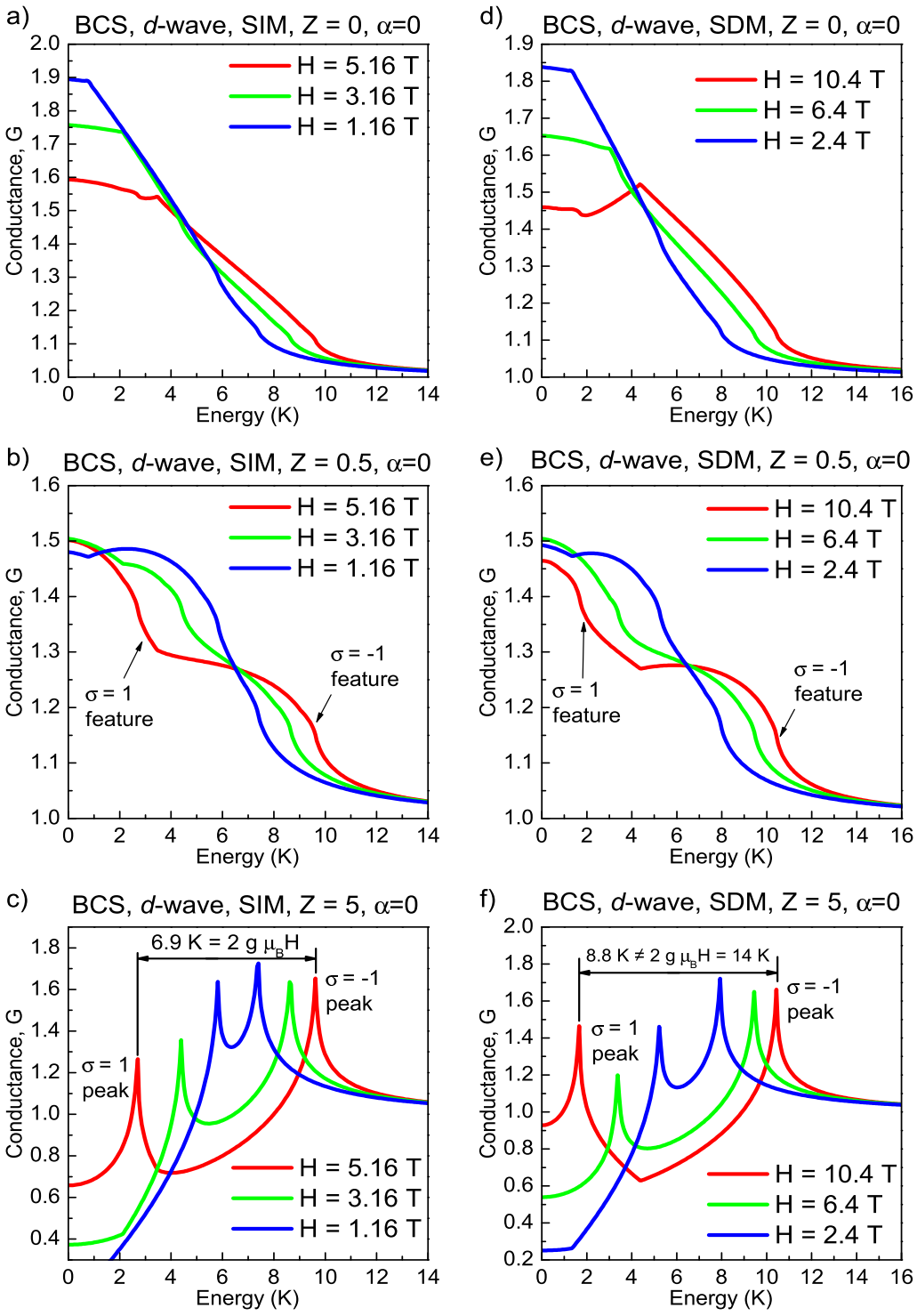

Figure 5.9: Conductance spectra for the d-wave BCS state with (100) contact ($\alpha = 0$) for selected barrier strengths for the SIM (a-c) and the SDM (d-f) cases. In (c) and (f) in the tunneling regime ($Z = 5$) conductance peaks from spin-up and spin-down channels are clearly visible already in the total conductance G. These peaks are separated by twice the Zeeman energy for SIM (c), and are closer for SDM (f).

to the FFLO phase, is a natural candidate for verification of the present results. Spectra presented in Figure 4 of Ref. 138 resemble our Figure 5.9e, with splitting between the spin-up and the spin-down features of the order of 8 T in fields of approximately 2 T. This might indicate that $h_{cor} \uparrow\uparrow h$ (h_{cor} enhances h), but in $CeCoIn_5$ the one-band model assumed in our calculations may not be sufficient [141] and therefore, our interpretation is only a speculation. On the other hand, for a two-band model with strong correlations the h_{cor} terms are also present (for both bands), and our conclusions should also hold.

Let us note that, in view of the present results, spectra of the BCS state with (100) contact and in the tunneling limit (high Z) would be most helpful in investigations of strong correlations in superconductors.

5.5 Concluding remarks

In this Chapter we have provided a detailed analysis of the conductance spectra of normal metal - strongly-correlated superconductor junction. The splitting of conductance peaks in the strongly correlated case differs from that in the uncorrelated case (it is equal to twice the Zeeman energy only in the latter case). We identify this feature as one of the *hallmarks of strong correlations in the superconducting phase*, as it should hold true for other models with different dispersion relations. It is most clearly visible in the case of BCS superconductor with (100) contact and in the tunneling regime (high Z). In other cases it is also present, but the spin-resolved conductance must be analyzed in order to identify the splitting unambiguously.

Chapter 6

Coexistence of antiferromagnetism and superconductivity

In the foregoing Chapters we have considered BCS type of pairing among strongly correlated quasiparticles. Now we consider a real-space pairing in which magnetism and superconductivity are intimately connected. Explicitly, the coexistence of antiferromagnetism with superconductivity is studied within the t-J model with the Zeeman term included. The strong electron correlations are accounted for by means of the extended Gutzwiller projection method. The phase diagram on the band filling - magnetic field plane is shown, and subsequently the system properties are analyzed for the fixed band filling $n = 0.97$. In this regime, the results resemble those observed recently in some heavy fermion systems. Namely, (i) with the increasing magnetic field the system evolves from coexisting phase, through antiferromagnetic phase, towards the normal state with nonzero spin polarization (ferromagnetic state), and (ii) the onset of superconducting order suppresses partly the staggered moment. The superconducting gap has both the spin-singlet and the staggered-triplet components, a consequence of a coexistence of the superconducting state with antiferromagnetism.

The Chapter is organized as follows. In Section 6.1 we provide an introduction. In Section 6.2 we present the theoretical formulation. Next, in Section 6.3 we characterize the details of the numerical analysis. In Section 6.4 we provide the numerical results, and finally in Section 6.5, our findings are briefly summarized.

6.1 Introduction

The interplay of antiferromegnetism (AF) with superconductivity (SC) is one of the important topics in condensed-matter physics [142], as better understanding of this subject would improve our knowledge of systems such as high-Tc [143], heavy-fermion [1], and organic [2] superconductors. In all those systems, superconductivity appears in the vicinity of magnetic phases (mostly antiferromagnetic, but also ferromagnetic [10, 11]). Moreover, magnetic interactions or fluctuations

are very frequently considered to be the pairing mechanism in unconventional superconductors [45, 144]. Typically, antiferromagnetism and superconductivity are competing quantum phenomena because of the competition between the Meissner-supercurrent screening and the internal-fields generation by magnetic ordering. This antagonism can be overcome by a spatial separation of the AF and the SC phases or by subdivision of the f electrons into more localized (resulting in AF) and more itinerant parts (participating in SC). However, especially interesting is the situation, when the same electrons are involved in both phenomena as is the case for some heavy-fermion systems. There, SC and AF can coexist easily, when the periodicity of magnetic structure $\lambda_{AF}(=2a)$ is much smaller than the coherence length ξ for the Cooper pair. In other words, when $\xi \gg a$, as then the staggered exchange field averages out to zero within the coherence volume. In this respect the Ce-based '115' heavy-fermion compounds - the family of $CeMIn_5$ (with $M = Co, Rh, Ir$) [41–43] is the most promising, as both antiferromagnetism and superconductivity are believed to arise from $4f$ electrons, and the interplay (not necessarily the competition) of the two orders can be studied by tuning the system with pressure, magnetic field, or doping.

Recently, a competitive coexistence of AF and SC has been reported in $CeRhIn_5$ [8, 19, 106, 145] and $CeCo(In_{1-x}Cd_x)_5$ [7, 146]. In the latter system, mutual influence of AF and SC has been observed, namely the onset of SC order with lowering temperature prevents any further increase of the antiferromagnetic magnetization [7]. Also, such coexistence has been observed in $CeRhSi_3$ [9].

In the heavy-fermion systems strong correlations among electrons are the reason for emergence of new interesting physics. Therefore, they should be properly accounted for when modeling those systems. In this Chapter, an investigation of the coexistence of AF with SC in an applied magnetic field is presented. To account for strong electron correlations, the Gutzwiller-projected t-J model is used with the Zeeman term included. The extended Gutzwiller scheme proposed recently [147] is utilized for calculation of operator averages.

It is commonly believed that the minimal model for investigation of heavy-fermion systems should be the two-band Periodic Anderson Model (PAM) (see e.g. Ref. 148) or the Kondo lattice model [18]. On the other hand, the one-band calculations have already proved fruitful in the analysis of AF and SC coexistence in $CeRhIn_5$ [149], as well as in investigations of the high-field low-temperature unconventional superconducting phase of $CeCoIn_5$ [79, 80]. The single-band limit of PAM has also been obtained theoretically elsewhere (see Ref. 95, Appendix A).

6.2 Model

We start from the t-J model [150] with the Zeeman term included

$$\hat{\mathcal{H}}_{tJ} = \hat{P}\Big(\sum_{ij\sigma} t_{ij} c^{\dagger}_{i\sigma} c_{j\sigma} + J \sum_{\langle ij \rangle} \mathbf{S_i S_j} - h \sum_{i\sigma} \sigma \hat{n}_{i\sigma}\Big)\hat{P}, \tag{6.1}$$

where $\langle ij \rangle$ denotes the summation over bonds, and $\sigma = \pm 1$ is the spin z-component. The advantage of using this model is that both AF and SC come from a microscopic

parameter - antiferromagnetic exchange J and therefore, there are no phenomenological terms in the Hamiltonian (as opposed to some earlier studies of AF and SC coexistence). We neglect the orbital effects, as the the Maki parameter [22] in the systems of our interest here is high [13, 106]. The Gutzwiller projector $\hat{P} \equiv \Pi_i(1 - \hat{n}_{i\uparrow}\hat{n}_{i\downarrow})$ eliminates double occupancies in real space. In the following we will use the more general correlator

$$\hat{P}_C \equiv \Pi_i \lambda_{i\uparrow}^{\hat{n}_{i\uparrow}/2} \lambda_{i\downarrow}^{\hat{n}_{i\downarrow}/2} (1 - \hat{n}_{i\uparrow}\hat{n}_{i\downarrow}), \tag{6.2}$$

where $\lambda_{i\sigma}$ are the so-called fugacity factors. Also, this correlator connects the correlated $|\Psi\rangle$ and uncorrelated $|\Psi_0\rangle$ wave functions [151], via

$$|\Psi\rangle = \hat{P}_C|\Psi_0\rangle. \tag{6.3}$$

This allows to express average of any operator $\hat{O}$ in the correlated state as

$$\langle\hat{O}\rangle \equiv \langle\Psi|\hat{O}|\Psi\rangle = \frac{\langle\hat{P}_C\hat{O}\hat{P}_C\rangle_0}{\langle\hat{P}_C\hat{P}_C\rangle_0}, \tag{6.4}$$

where $\langle ...\rangle_0 \equiv \langle\Psi_0|...|\Psi_0\rangle$. With the above equation one can in principle calculate average value of Hamiltonian (6.1), namely

$$W \equiv \langle\hat{\mathcal{H}}_{tJ}\rangle = \sum_{ij\sigma} t_{ij}\langle c_{i\sigma}^\dagger c_{j\sigma}\rangle + J\sum_{\langle ij\rangle}(\langle S_i^z S_j^z\rangle + \langle S_i^x S_j^x + S_i^y S_j^y\rangle) - h\sum_{i\sigma}\sigma\langle\hat{n}_{i\sigma}\rangle, \tag{6.5}$$

but this is a nontrivial task (because the correlator (6.2) is non-local), and one has to make some approximations at this point. There are a few ways to perform this operation, and this is still an active field of research, so one can expect new calculation schemes to appear. Here, we use the scheme proposed recently by Fukushima [147, 152] in the local-constraint version, which assumes that the average number of particles at any site and with any spin is unchanged by the projection,

$$\langle\hat{n}_{i\sigma}\rangle = \langle\hat{n}_{i\sigma}\rangle_0. \tag{6.6}$$

This formalism is known to reproduce the Variational Monte Carlo results better than the conventional Gutzwiller approximation (at least, for the projected uniform nonmagnetic d-wave BCS superconductor - see Figures 3 and 4 of Ref. 147). The local-constraint version of the formalism is quite general in the sense that it is capable of accounting for antiferromagnetism, superconductivity, and the ferromagnetic polarization. The explicit expressions for all averages appearing in Eq. (6.5) are given in Ref. 147. To express them in terms of mean-fields of our interest, we need to assume what is the character of the uncorrelated wave function $|\Psi_0\rangle$. Since our goal is the description of coexistence of AF and SC, we assume the corresponding mean-fields as nonzero at the level of $|\Psi_0\rangle$ as in the following. We start with the particle number

$$n_{i\sigma} \equiv \langle\hat{n}_{i\sigma}\rangle_0 = \frac{1}{2}\Big(n + \sigma\, m_{FM} + \sigma\, m_{AF}\, e^{i\mathbf{Q}\mathbf{r_i}}\Big), \tag{6.7}$$

where n is the band filling (assumed as constant), m_{FM} is the ferromagnetic spin polarization, and m_{AF} is the antiferromagnetic polarization. The term $e^{i\mathbf{Q}\mathbf{r_i}}$ (with $\mathbf{Q} = (\pi, \pi)$) is responsible for the appropriate change of sign of the antiferromagnetic magnetization when switching sublattices [153]. We also assume the superconducting order parameter

$$\Delta_{ij} \equiv \langle c_{j\downarrow} c_{i\uparrow} \rangle_0 = \begin{cases} \tau_{ij}\Delta_A, & \text{for } i \in A - sublattice, \\ \tau_{ij}\Delta_B, & \text{for } i \in B - sublattice, \end{cases} \tag{6.8}$$

where τ_{ij} ensures the d-wave gap symmetry by setting $\tau_{ij} = +1(-1)$ for $j = i \pm \hat{x}$ ($j = i \pm \hat{y}$), with $\hat{x}$, $\hat{y}$ being the lattice vectors. The d-wave solution is taken throughout in the following analysis. The superconducting order parameter can be expressed in terms of the singlet and the staggered π-triplet components, namely

$$\begin{aligned} \Delta_{ij} &\equiv \langle c_{j\downarrow} c_{i\uparrow} \rangle_0 \equiv \frac{1}{2}\Big(\langle c_{j\downarrow} c_{i\uparrow} + c_{j\uparrow} c_{i\downarrow} \rangle_0 + \langle c_{j\downarrow} c_{i\uparrow} - c_{j\uparrow} c_{i\downarrow} \rangle_0 \Big) = \\ &= \frac{1}{2}\Big(\langle c_{j\downarrow} c_{i\uparrow} - c_{i\downarrow} c_{j\uparrow} \rangle_0 + \langle c_{j\downarrow} c_{i\uparrow} + c_{i\downarrow} c_{j\uparrow} \rangle_0 \Big) \equiv \Delta_{ij}^{(S)} + \Delta_{ij}^{(T)}\, e^{i\mathbf{Q}\mathbf{r_i}}, \quad (6.9) \\ \Delta_{ij}^{(S)} &= \frac{1}{2}\tau_{ij}(\Delta_A + \Delta_B), \quad (6.10) \\ \Delta_{ij}^{(T)} &= \frac{1}{2}\tau_{ij}(\Delta_A - \Delta_B). \quad (6.11) \end{aligned}$$

Such superconducting order parameter is defined on a bond (n.n. pair of sites). To define the gap per site, we make use of the standard [154] d-wave relation

$$\begin{aligned} \Delta_i^{(S)} &\equiv \frac{1}{4}\sum_{j(i)} \tau_{ij}(\Delta_{i,j(i)} - \Delta_{j(i),i}) = \frac{1}{2}(\Delta_A + \Delta_B), \quad (6.12) \\ \Delta_i^{(T)} &\equiv \frac{1}{4}\sum_{j(i)} \tau_{ij}(\Delta_{i,j(i)} + \Delta_{j(i),i}) = \frac{1}{2}(\Delta_A - \Delta_B)\, e^{i\mathbf{Q}\mathbf{r_i}}, \quad (6.13) \end{aligned}$$

where $j(i)$ denotes the nearest neighbors of site i. The existence of the triplet component is inevitable even if there is no triplet channel in the pairing potential. Namely, the triplet component is dynamically induced by the singlet and antiferromagnetism [80, 154–156]. From a microscopic point of view this is also not surprising (see Figure 6.1). An interesting feature of the superconducting gap given by Eq. (6.9) is the nonzero momentum of Cooper pairs for the triplet component (it results from the $e^{i\mathbf{Q}\mathbf{r_i}}$ term, analogously as for the FFLO phase). A superconducting state with nonzero momentum has been investigated in a number of cases [20, 21, 80, 157], and even in zero external magnetic field [158]. The one presented here is analogous to that from Ref. 80.

With the above assumptions, we can express the ground-state energy W from Eq. (6.5) as a function of band filling n, magnetizations m_{FM} and m_{AF}, superconducting gaps Δ_A and Δ_B, as well as hoppings $\chi_{ij\sigma} \equiv \langle c_{i\sigma}^\dagger c_{j\sigma} \rangle_0$. We assume as nonzero first- and second-nearest-neighbor hopping integrals t and t', which leads to 6 different hopping parameters

$$\chi_{ij\sigma} \equiv \langle c_{i\sigma}^\dagger c_{j\sigma} \rangle_0 \in \{\chi_{AB\uparrow}, \chi_{AB\downarrow}, \chi_{AA\uparrow}, \chi_{AA\downarrow}, \chi_{BB\uparrow}, \chi_{BB\downarrow}\}. \tag{6.14}$$

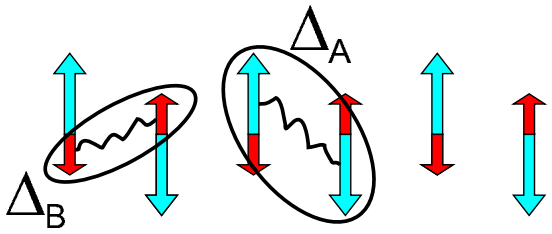

Figure 6.1: Spin-majority (blue, bigger arrows) and spin-minority (red arrows) electrons in a system with AF order and superconducting gap. Δ_A binds two spin-majority electrons, and Δ_B binds two spin-minority electrons and therefore, there is a priori no reason for these two gaps to be equal (as would be the case for no staggered π-triplet component). In other words, the two distinct gaps make effectively the $\uparrow - \downarrow$ and $\downarrow - \uparrow$ pairing components of the spin pairs distinguishable.

The resulting expression for W is quite lengthy and has been reproduced in Appendix A. Next, as in the SGA method[1] [84, 159, 160], to solve the model in a statistically-consistent way, we impose constraints on all introduced mean fields by means of the Lagrange multipliers method. Namely, we use the following energy operator

$$\begin{aligned}\hat{K} \equiv & -\sum_{ij\sigma}[\lambda^{(\chi)}_{ij\sigma}(c^{\dagger}_{i\sigma}c_{j\sigma} - \chi_{ij\sigma}) + h.c.] - \sum_{ij}[\lambda^{(\Delta)}_{ij}(c_{j\downarrow}c_{i\uparrow} - \Delta_{ij}) + h.c.] \\ & -\sum_{ij\sigma}\lambda^{(n)}_{i\sigma}(\hat{n}_{i\sigma} - n_{i\sigma}) + W(n, m_{AF}, m_{FM}, \Delta_A, \Delta_B, \chi_{ij\sigma}) \\ & -\mu\sum_{i\sigma}\hat{n}_{i\sigma}. \end{aligned} \tag{6.15}$$

This method of approach is equivalent in the $T \to \infty$ ($\beta \to 0$) limit to that presented in Refs. 161 and 162. The equivalence can be seen from the comparison of Eq. (6.15) and Eqs. (6.32)-(6.39) with the corresponding Eqs. form Refs. 161 and 162 (e.g. Eq. (13) from Ref. 161 gives a Hamiltonian with operator part equivalent to our $\hat{K}$). The Lagrange multipliers have the same symmetries, as the mean fields to which they correspond. We also assume they are homogeneous. Namely,

$$\lambda^{(n)}_{i\sigma} \equiv \lambda_n + \sigma\lambda_{m_{FM}} + \sigma\lambda_{m_{AF}}\, e^{i\mathbf{Q}\mathbf{r_i}} \tag{6.16}$$

$$\lambda^{(\Delta)}_{ij} \equiv \lambda^{(S)}_{\Delta} + \lambda^{(T)}_{\Delta} e^{i\mathbf{Q}\mathbf{r_i}}, \tag{6.17}$$

[1]There are two equivalent formulations of the SGA method. In the one used in the preceding Chapters the constraints are added to the Hamiltonian (as in Eq. (2.14), (2.27), (2.37) and in Refs. 84 and 159). In an alternative formulation, the constraints are added to the average value W of the Hamiltonian (see Eq. (6.15)). This scheme has been introduced in Ref. 160 and is used throughout this Chapter.

with

$$\lambda_{\Delta}^{(S)} = \frac{1}{2}(\lambda_{\Delta_A} + \lambda_{\Delta_B}), \tag{6.18}$$

$$\lambda_{\Delta}^{(T)} = \frac{1}{2}(\lambda_{\Delta_A} - \lambda_{\Delta_B}). \tag{6.19}$$

After performing Fourier transformation of the operator part of $\hat{K}$ we obtain

$$\begin{aligned}\hat{K} &= {\sum}_{\mathbf{k}}{}' \Psi_{\mathbf{k}}^{\dagger} \mathbf{M}_{\mathbf{k}} \Psi_{\mathbf{k}} + \Lambda(\mu + \lambda_n - \lambda_{m_{FM}}) + W(\vec{A}) \\ &+\Lambda\Big[n\lambda_n + m_{FM}\lambda_{m_{FM}} + m_{AF}\lambda_{m_{AF}} + 4(\Delta_A\lambda_{\Delta_A} + \Delta_B\lambda_{\Delta_B}) \\ &+4\sum_{\sigma}(2\chi_{AB\sigma}\lambda_{\chi_{AB\sigma}} + \chi_{AA\sigma}\lambda_{\chi_{AA\sigma}} + \chi_{BB\sigma}\lambda_{\chi_{BB\sigma}})\Big],\end{aligned} \tag{6.20}$$

where the primed sum denotes summation over the folded (magnetic) Brillouin zone, by $\vec{A}$ we denote all mean-fields, Λ is the total number of sites, and the four-component operator $\Psi_{\mathbf{k}}^{\dagger}$ has the following form

$$\Psi_{\mathbf{k}}^{\dagger} = (c_{\mathbf{k}\uparrow}^{\dagger}, c_{-\mathbf{k}\downarrow}, c_{\mathbf{k}+\mathbf{Q}\uparrow}^{\dagger}, c_{-\mathbf{k}+\mathbf{Q}\downarrow}). \tag{6.21}$$

The matrix $\mathbf{M}_{\mathbf{k}}$ is given as

$$\mathbf{M}_{\mathbf{k}} = \begin{pmatrix} \xi_{\mathbf{k}\uparrow} & -2\lambda_{\Delta}^{(S)}\eta_{\mathbf{k}} & \zeta_{\mathbf{k}+\mathbf{Q}\uparrow} & -2\lambda_{\Delta}^{(T)}\eta_{\mathbf{k}+\mathbf{Q}} \\ -2\lambda_{\Delta}^{(S)}\eta_{\mathbf{k}} & -\xi_{-\mathbf{k}\downarrow} & -2\lambda_{\Delta}^{(T)}\eta_{\mathbf{k}} & \zeta_{-\mathbf{k}\downarrow} \\ \zeta_{\mathbf{k}\uparrow} & -2\lambda_{\Delta}^{(T)}\eta_{\mathbf{k}} & \xi_{\mathbf{k}+\mathbf{Q}\uparrow} & 2\lambda_{\Delta}^{(S)}\eta_{\mathbf{k}+\mathbf{Q}} \\ -2\lambda_{\Delta}^{(T)}\eta_{\mathbf{k}+\mathbf{Q}} & \zeta_{-\mathbf{k}+\mathbf{Q}\downarrow} & 2\lambda_{\Delta}^{(S)}\eta_{\mathbf{k}+\mathbf{Q}} & -\xi_{-\mathbf{k}+\mathbf{Q}\downarrow} \end{pmatrix}, \tag{6.22}$$

where

$$\zeta_{\mathbf{k}\sigma} = -2\sigma\,\delta\lambda_{\sigma}^{(\chi)}\epsilon'_{\mathbf{k}} - \lambda_{m_{AF}}, \tag{6.23}$$

$$\xi_{\mathbf{k}\sigma} = -\mu - \lambda_n - \sigma\lambda_{m_{FM}} - 2\epsilon_{\mathbf{k}}\lambda_{\chi_{AB\sigma}} - 2\epsilon'_{\mathbf{k}}\bar{\lambda}_{\sigma}^{(\chi)}, \tag{6.24}$$

$$\epsilon_{\mathbf{k}} = 2(\cos k_x + \cos k_y), \tag{6.25}$$

$$\epsilon'_{\mathbf{k}} = 4\cos k_x \cos k_y, \tag{6.26}$$

$$\eta_{\mathbf{k}} = \cos k_x - \cos k_y, \tag{6.27}$$

and the combinations of Lagrange multipliers have been introduced for clarity, namely

$$\bar{\lambda}_{\sigma}^{(\chi)} = \frac{1}{2}(\lambda_{\chi_{AA\sigma}} + \lambda_{\chi_{BB\sigma}}), \tag{6.28}$$

$$\delta\lambda_{\sigma}^{(\chi)} = \frac{1}{2}(\lambda_{\chi_{AA\sigma}} - \lambda_{\chi_{BB\sigma}}). \tag{6.29}$$

We have also used the fact that $\sum_{\mathbf{k}}\epsilon_{\mathbf{k}} = \sum_{\mathbf{k}}\epsilon'_{\mathbf{k}} = 0$. Note that in the present formulation $\lambda_{m_{FM}}$ corresponds to both the magnetic field h, and the correlation-induced field h_{cor} [83, 111] (or equivalently the Lagrange multiplier β in the slave-boson theory [72–74, 86]). Namely, $\lambda_{m_{FM}} \equiv h + h_{cor} \equiv h + \beta$ what is evident from comparison of Eq. (6.24) with appropriate Eqs. from Refs. 72, 83, 111.

Next, we determine the eigenvalues of $\mathbf{M_k}$, as they correspond to quasiparticle excitations in the system. Unfortunately, an analytical diagonalization of $\mathbf{M_k}$ produces very long expressions, and more importantly, expressions with square roots of possibly negative numbers. For subsequent implementation, we diagonalize this matrix numerically. Having determined the eigenvalues $\{E_{\mathbf{k}i}\}_{i=1,2,3,4}$, we define the generalized grand potential functional

$$\begin{aligned}\mathcal{F} &= -\beta^{-1}\sum\nolimits'_{\mathbf{k},i=1,2,3,4}\ln(1+e^{-\beta E_{\mathbf{k}i}}) + \Lambda(\mu+\lambda_n-\lambda_{m_{FM}}) + W(\vec{A}) \\ &+\Lambda\Big[n\lambda_n + m_{FM}\lambda_{m_{FM}} + m_{AF}\lambda_{m_{AF}} + 4(\Delta_A\lambda_{\Delta_A}+\Delta_B\lambda_{\Delta_B}) \\ &+4\sum_\sigma(2\chi_{AB\sigma}\lambda_{\chi_{AB\sigma}} + \chi_{AA\sigma}\lambda_{\chi_{AA\sigma}} + \chi_{BB\sigma}\lambda_{\chi_{BB\sigma}})\Big]. \qquad (6.30)\end{aligned}$$

The physical (equilibrium) values of the mean fields and the Lagrange multipliers are obtained from the necessary conditions for $\mathcal{F}$ to have a minimum subject to the constraints, i.e.,

$$\frac{\partial\mathcal{F}}{\partial\vec{A}} = 0, \qquad \frac{\partial\mathcal{F}}{\partial\vec{\lambda}} = 0, \qquad (6.31)$$

where by $\vec{\lambda}$ we denote collectively the Lagrange multipliers. Equations $\partial\mathcal{F}/\partial\vec{A}=0$ provide the explicit analytic expressions for the Lagrange multipliers, i.e.,

$$\begin{aligned}\lambda_n &= -\Lambda^{-1}\partial_n W(\vec{A}), &(6.32)\\ \lambda_{m_{FM}} &= -\Lambda^{-1}\partial_{m_{FM}} W(\vec{A}), &(6.33)\\ \lambda_{m_{AF}} &= -\Lambda^{-1}\partial_{m_{AF}} W(\vec{A}), &(6.34)\\ \lambda_{\Delta_A} &= -\frac{1}{4}\Lambda^{-1}\partial_{\Delta_A} W(\vec{A}), &(6.35)\\ \lambda_{\Delta_B} &= -\frac{1}{4}\Lambda^{-1}\partial_{\Delta_B} W(\vec{A}), &(6.36)\\ \lambda_{\chi_{AB\sigma}} &= -\frac{1}{8}\Lambda^{-1}\partial_{\chi_{AB\sigma}} W(\vec{A}), &(6.37)\\ \lambda_{\chi_{AA\sigma}} &= -\frac{1}{4}\Lambda^{-1}\partial_{\chi_{AA\sigma}} W(\vec{A}), &(6.38)\\ \lambda_{\chi_{BB\sigma}} &= -\frac{1}{4}\Lambda^{-1}\partial_{\chi_{BB\sigma}} W(\vec{A}). &(6.39)\end{aligned}$$

The above expressions can be used to eliminate Lagrange multipliers $\vec{\lambda}$ from the solution procedure and obtain 11 equations to be solved numerically for the mean fields $\vec{A}$, instead of 22 equations for $\vec{A}$ and $\vec{\lambda}$. The equations for the mean fields (obtained from $\partial\mathcal{F}/\partial\vec{\lambda}=0$) have the following form

$$
\begin{aligned}
0 &= \beta^{-1}\partial_{\lambda_n} f_\beta(\vec{\lambda}) - \Lambda(n-1), && (6.40)\\
0 &= \beta^{-1}\partial_{\lambda_{m_{FM}}} f_\beta(\vec{\lambda}) - \Lambda(m_{FM}+1), && (6.41)\\
0 &= \beta^{-1}\partial_{\lambda_{m_{AF}}} f_\beta(\vec{\lambda}) - \Lambda m_{AM}, && (6.42)\\
0 &= \beta^{-1}\partial_{\lambda_{\Delta_A}} f_\beta(\vec{\lambda}) - 4\Lambda\Delta_A, && (6.43)\\
0 &= \beta^{-1}\partial_{\lambda_{\Delta_B}} f_\beta(\vec{\lambda}) - 4\Lambda\Delta_B, && (6.44)\\
0 &= \beta^{-1}\partial_{\lambda_{\chi_{AB\sigma}}} f_\beta(\vec{\lambda}) - 8\Lambda\chi_{AB\sigma}, && (6.45)\\
0 &= \beta^{-1}\partial_{\lambda_{\chi_{AA\sigma}}} f_\beta(\vec{\lambda}) - 4\Lambda\chi_{AA\sigma}, && (6.46)\\
0 &= \beta^{-1}\partial_{\lambda_{\chi_{BB\sigma}}} f_\beta(\vec{\lambda}) - 4\Lambda\chi_{BB\sigma}, && (6.47)
\end{aligned}
$$

where

$$
f_\beta(\vec{\lambda}) \equiv \sum_{\mathbf{k},i=1..4} \ln(1+e^{-\beta E_{\mathbf{k}i}}). \qquad (6.48)
$$

The derivative $\partial_{\lambda_n} f_\beta(\vec{\lambda})$ is computed numerically with a 5-point stencil method (as it gives two-three orders of magnitude better precision than the standard 3-point stencil). For example

$$
\begin{aligned}
\partial_{\lambda_n} f_\beta(\vec{\lambda}) &= \frac{1}{12x}\Big[- f_\beta(\lambda_n+2x, \lambda_{mFM}, \lambda_{mAF}, ...) + 8 f_\beta(\lambda_n+x, \lambda_{mFM}, \lambda_{mAF}, ...)\\
&\quad -8 f_\beta(\lambda_n-x, \lambda_{mFM}, \lambda_{mAF}, ...) + f_\beta(\lambda_n-2x, \lambda_{mFM}, \lambda_{mAF}, ...)\Big]\\
&\quad +O(x^4) \qquad (6.49)
\end{aligned}
$$

where we use the "equilibrium" values of $\vec{\lambda}$ as given by Eqs. (6.32)-(6.39). The step x is typically equal to $x = 0.0001$. Larger values of x would cause greater error in the above formula. Smaller values would result in loss of numerical precision.

6.3 Numerical methods

The equations (6.40)-(6.47) are solved numerically with the use of GNU Scientific Library (we use the `gsl_multiroot_fsolver_hybrids` solver which implements the hybrids algorithm) on a grid of size $\Lambda = 256 \times 256$. We use the precision $epsabs = 10^{-7}$. Namely, the procedure converges when the relation $\sum_i |f_i| < epsabs$ is fulfilled (where the sum is taken over all equations, which have been brought to the form $f_i = 0$ and divided by Λ to ensure lattice-independent convergence conditions).

The most time-consuming part of the computations is to carry out explicitly the summation in Eq. (6.48), which takes place when computing derivatives of $f_\beta(\vec{\lambda})$ (according to Eq. (6.49)) in Eqs. (6.40)-(6.47).

This summation is performed over the folded (magnetic) Brillouin zone. The summing procedure is parallelized with OpenMP. In Appendix B, we show a sample of the code performing the summation (in both single- and multi-thread versions).

Calculation of the phase diagram, exhibited in Figure 6.2 took about one day using a 24-thread task of "SHIVA" cluster located in our Institute. Such 24-thread task was found to perform about 5 times better than a PC with Intel i7 processor. Note that performing the code optimization described in Appendix B would result in approximately 4 times faster computation.

In Table II the exemplary numerical values of the parameters have been provided for the sake of completeness. Numerical accuracy is on the level of the last digit specified. The energy scale has been set by taking the value of the exchange integral as unit, $J = 1$.

Table II. Equilibrium values of mean-field variables, Lagrange multipliers, free energy F and grand potential functional $\mathcal{F}$ at $h = 0.3$ and $\beta = 500$.

Variable	Value	Variable	Value
μ	3.2997360	λ_n	-5.1331996
m_{FM}	0.0000000	$\lambda_{m_{FM}}$	0.3000001
m_{AF}	0.8100315	$\lambda_{m_{AF}}$	2.5817963
Δ_A	0.0922998	λ_{Δ_A}	0.2730140
Δ_B	0.0479298	λ_{Δ_B}	0.4395630
$\chi_{AB\uparrow}$	0.1218625	$\lambda_{\chi_{AB\uparrow}}$	0.4258402
$\chi_{AB\downarrow}$	0.1218625	$\lambda_{\chi_{AB\downarrow}}$	0.4258402
$\chi_{AA\uparrow}$	-0.0167505	$\lambda_{\chi_{AA\uparrow}}$	-0.1031297
$\chi_{AA\downarrow}$	0.0275895	$\lambda_{\chi_{AA\downarrow}}$	-0.0120561
$\chi_{BB\uparrow}$	0.0275895	$\lambda_{\chi_{BB\uparrow}}$	-0.0120561
$\chi_{BB\downarrow}$	-0.0167505	$\lambda_{\chi_{BB\downarrow}}$	-0.1031297
F/Λ	-1.0110048	$\mathcal{F}/\Lambda$	-4.2117488

6.4 Results

We assume the following values of parameters: $t = 3$, $t' = t/4 = 0.75$, $J = 1$, and $\beta = 500$, what yields the temperature $T = 1/\beta = 0.002 \approx 0$.

A number of stable phases emerge as solutions of the equations depending on the physical condition (n, h). As already mentioned in Chapter 2, working with a constant number of particles n implies that the stable phase is the one with the lowest free energy, defined by

$$F = \mathcal{F} + \mu n \Lambda, \tag{6.50}$$

where the equilibrium values of $\vec{A}$ and $\vec{\lambda}$ have been inserted in $\mathcal{F}$. The exemplary phase diagram on the band filling n - magnetic field h plane is exhibited in Figure 6.2. It can be seen that antiferromagnetism is the dominating phenomenon in the low-field regime above $n = 0.8$. For $n \gtrsim 0.935$ antiferromagnetism coexists with superconductivity what amounts to a phase with coexisting three order parameters (similarly as in e.g. Ref. 80). In the low-n part of the phase diagram (for $n < 0.8$) the saturated ferromagnetic (SFM) phase with $m_{FM} = n$ becomes the most favorable energetically. This phase is stable even in the $h \to 0$ limit. This is an interesting result, which adds to the discussion of ferromagnetism in the

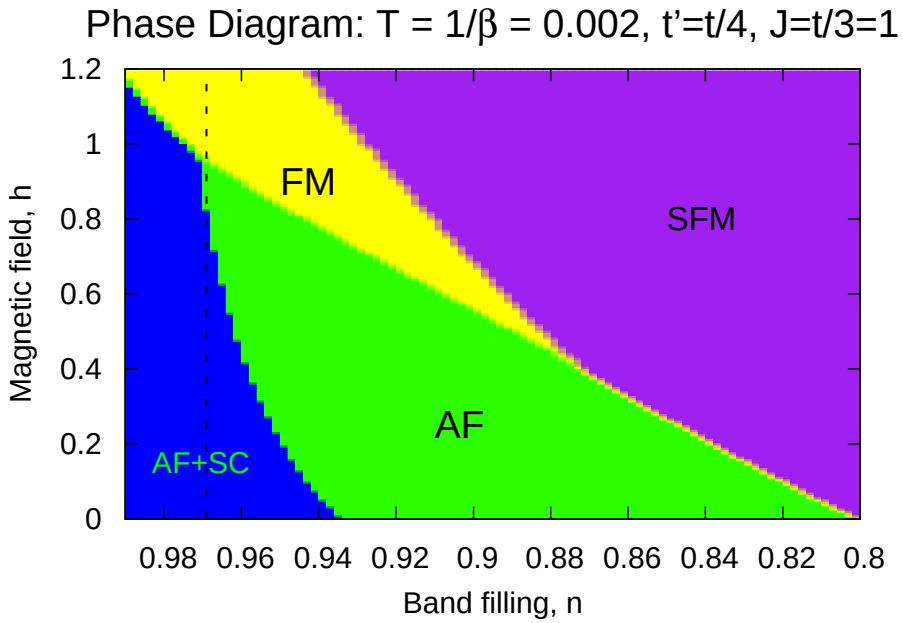

Figure 6.2: Phase diagram on the band filling - magnetic field plane. The phases are labeled as follows: AF+SC - phase with coexisting superconductivity and antiferromagnetism, AF - antiferromagnetic phase, FM - ferromagnetic phase, SFM - saturated ferromagnetic phase (with $m_{FM} = n$). For further analysis we restrict ourselves to $n = 0.97$ as marked by the dashed vertical line. No stable pure superconducting solution has been found.

t-J [163, 164] model. There is also a number of papers (see e.g. Refs. 160 and 93) analyzing the t-J model (6.1) with the Gutzwiller-type of approach with the parameters in a similar range (i.e. with $n < 0.8$ and similar values of t_{ij} and J). Some of those papers disregard completely the Zeeman-term influence, and this disregarding is justified by application of the model to high-Tc superconductors, where orbital effects dominate over the Pauli magnetism. We have shown, that even at $h = 0$ the system may be completely spin-polarized and therefore, the inclusion of ferromagnetic polarization m_{FM} is important in treatment of the t-J model.

At band filling $n = 0.97$ the phase diagram (or phase sequence as a function of field h) resembles those observed recently in the heavy-fermion compounds $CeCo(In_{1-x}Cd_x)_5$ [7] at doping $x = 0.0075$ and $CeRhSi_3$ [9] at pressure $p \approx 17$ kbar.[2] Namely, in low magnetic fields a phase with coexisting antiferromagnetic and superconducting orders (AF+SC) is stable, whereas for higher magnetic fields a continuous transition to the antiferromagnetic (AF) phase takes place, followed by a discontinuous transition to the ferromagnetic (FM) phase. The phases appearing

[2] Although in $CeRhSi_3$ the phases have only been analyzed as a function of temperature.

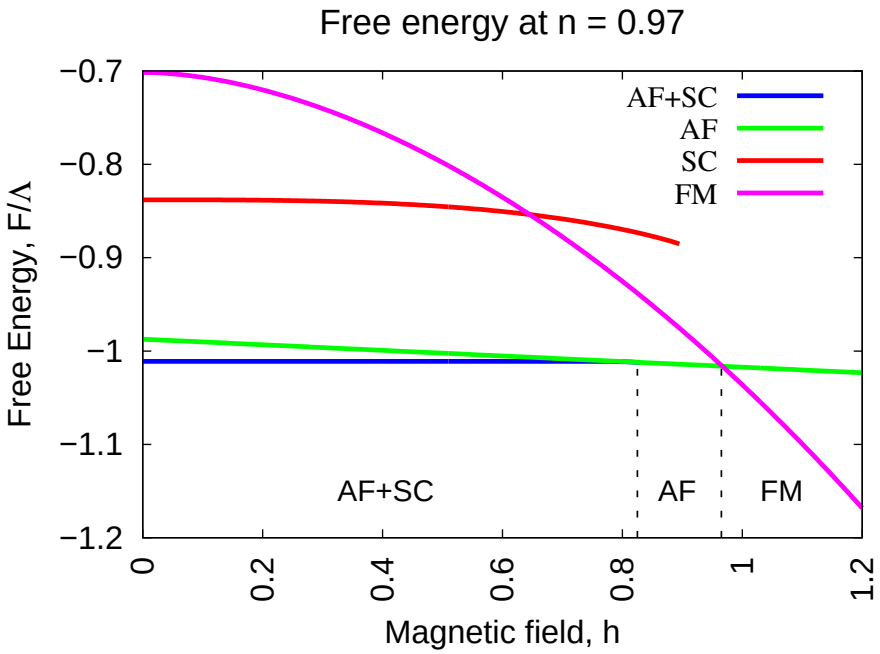

Figure 6.3: Free energy per site as a function of magnetic field for the specified choice of phases. Types of order are marked explicitly at the bottom. The "SC" phase is the pure superconducting phase (i.e. with $m_{AF} = 0$), which obviously has higher energy than other phases and hence does not appear in the phase diagram. The vertical dashed lines mark the phase boundaries: the AF+SC - AF line marks a continuous transition, whereas that for the AF - FM is discontinuous, as one can see by looking at the behavior of the slope $\partial F/\partial h$.

at this band filling ($n = 0.97$) are analyzed in detail in the following.

In Figure 6.3 we show the free energy lines for a choice of *a priori* possible phases. It can be seen (also from the following Figures) that the transition AF+SC $\rightarrow$ AF is continuous, whereas the transition AF $\rightarrow$ FM is of the first order. Also, pure superconducting (SC) solution is unstable, and this holds for other band fillings as well. It can be concluded from Figure 6.3 that antiferromagnetism is the "dominating" phenomenon, since the energy gain from developing antiferromagnetic order (which can be seen from closer look at the difference $(F_{FM} - F_{AF})$) is much higher than the gain from developing superconducting order $(F_{FM} - F_{SC})$. Moreover, the energy gain from developing AF order within SC phase $(F_{SC} - F_{AF+SC})$ is much higher than that from developing SC order within the AF phase $(F_{AF} - F_{AF+SC})$.

In Figure 6.4 we exhibit the magnetic moment per site of the system for different phases. Namely, we plot the staggered magnetization m_{AF} and the ferromagnetic magnetization m_{FM} (spin-polarization). The staggered magnetization is close to the limiting value of $m_{AF} = n = 0.97$. The spin-polarization of the pure AF phase is equal to $m_{FM} = 1-n$ at all magnetic fields. Also, it can be seen that development of SC order within the AF phase alters by a small amount the staggered magnetization m_{AF}, which drops by approximately 1% (see Figure 6.4a).

a)

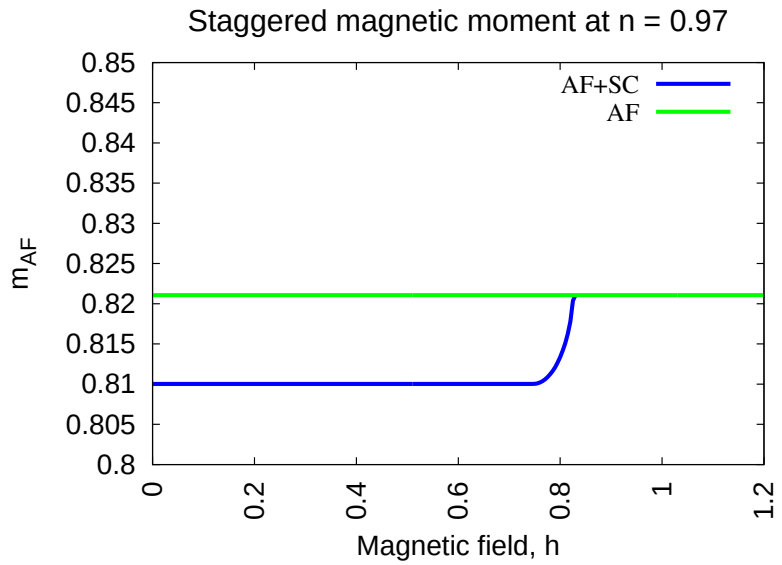

b)

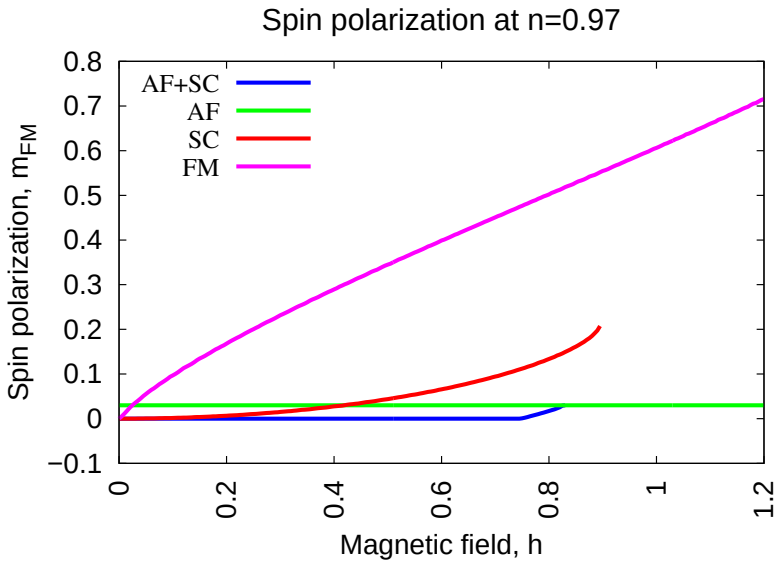

Figure 6.4: Magnetic moment, staggered (a) and spin-polarization (b) for the selected phases. Obviously, the staggered moment of the SC and FM phases is 0, and has not been plotted in (a). The magnetic moment value is insensitive to the projection (i.e., it is the same in both the correlated $|\Psi\rangle$ and the uncorrelated $|\Psi_0\rangle$ states).

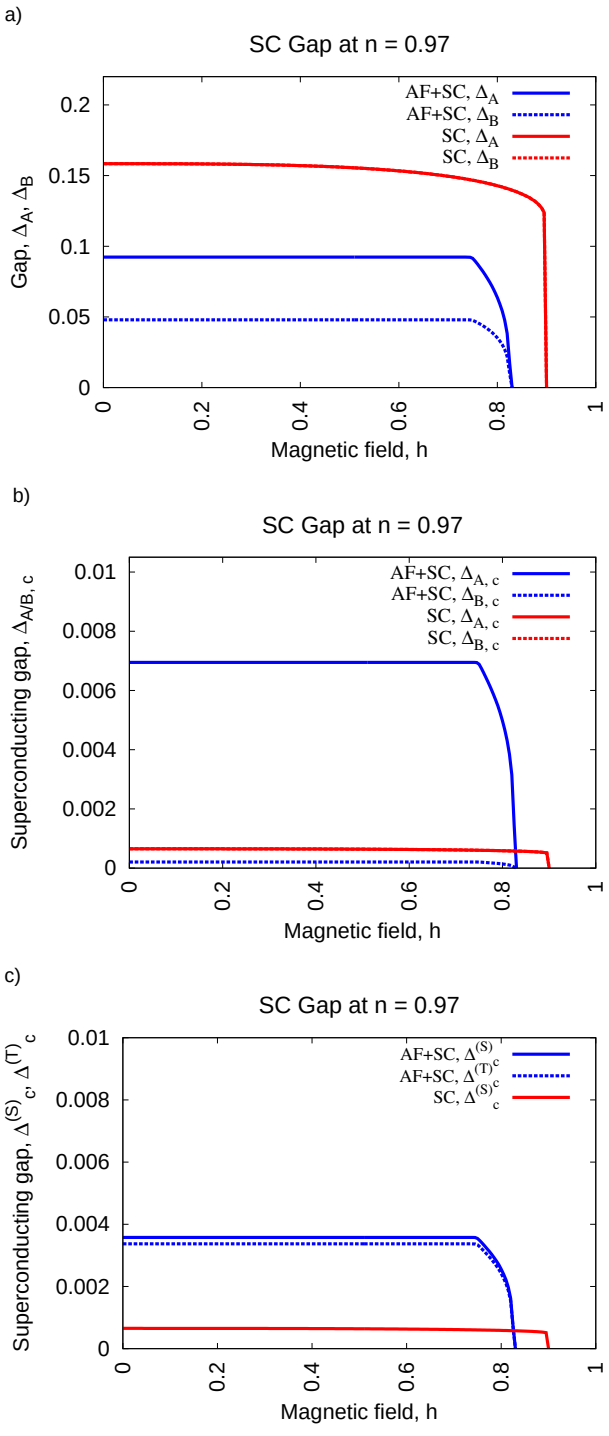

Figure 6.5: Superconducting gaps versus magnetic field for AF+SC and SC phases. (a) Δ_A and Δ_B gaps obtained for the uncorrelated wave function $|\Psi_0\rangle$; (b) and (c) gaps for the state specified by the correlated wave function (labeled as Δ_c), as given by Eq. (6.4). (b) shows the sublattice-specific Δ_A and Δ_B gaps, and (c) shows the singlet and triplet components of the gap. Note that the superconducting gaps (Δ_c) are enhanced in the AF+SC state (with respect to the SC state).

In Figure 6.5 various superconducting gaps are shown. Namely we exhibit both the "uncorrelated" gap for the wave function $|\Psi_0\rangle$, as well as the gap for the correlated wave function $|\Psi\rangle$, the latter defined by Eq. (6.4) and labeled as Δ_c. Note that in the SC phase the sublattice gaps are equal ($\Delta_A = \Delta_B$), what amounts to the absence of the triplet component. Note that although the uncorrelated gaps (Δ_A, Δ_B) are larger in the pure SC phase than in the AF+SC phase, the correlated gaps ($\Delta_c^{(S)}$, $\Delta_c^{(T)}$) are much larger in the AF+SC phase than in the pure SC phase. This very important conclusion means that magnetism supports superconductivity in the present situation. The opposite is not true as the staggered moment is slightly larger in the AF phase than in the AF+SC phase.

The picture with large antiferromagnetic magnetization m_{AF} (Figure 6.4) and small superconducting gap (Figure 6.5) is consistent with the energy curves displayed in Figure 6.3. To shift the energy balance towards the SC phase one could decrease t', increase J, and/or include the intersite attraction ($V\sum_{\langle ij\rangle}\hat{n}_i\hat{n}_j$) in the starting Hamiltonian (this would stabilize further the d-wave superconducting state [79]). It seems that even doing so, antiferromagnetism would still remain the predominant phenomenon. This may represent an apparent feature of the Gutzwiller scheme used [147], in which magnetization is not changed by the projection, as follows directly from Eq. (6.6).

Finally, in Figure 6.6 we plot the quasiparticle energies (bands) for the states discussed above for $n = 0.97$. The crossing of one of the bands with the zero energy line at the S point of the Brillouin zone in Figure 6.6bc means that the quasiparticles will be spontaneously created, a circumstance leading to nonzero spin-polarization (cf. Figure 6.4), similarly as in the case of the FFLO state [20] (cf. also Chapter 4 and Figure 4.1).

6.5 A brief summary

In this Chapter we have carried out a detailed analysis of the coexistence of antiferromagnetism and superconductivity within microscopic t-J model, with the Zeeman term included. The strong correlations were accounted for by means of the extended Gutzwiller projection method. We have obtained the phase diagram on the band filling-magnetic field plane, in which for the band fillings in the range $n \approx 0.935-0.970$ and with the increasing magnetic field, a series of transitions takes place. Namely, the system evolves from the coexisting phase, through the antiferromagnetic phase, to the normal state with nonzero spin polarization (ferromagnetic state). Also, the onset of superconducting order limits the AF order parameter. These features resemble the experimental findings in the $CeCo(In_{1-x}Cd_x)_5$ [7, 146] and $CeRhSi_3$ [9] heavy fermion systems. Additionally, both antiferromagnetism and superconductivity originate from the same electrons. The driving force for both of these orders is the (real-space) exchange coupling term. This is clearly visible by e.g. the circumstance that the presence of antiferromagnetism enhances superconducting order parameter. Note that the real-space pairing is the pairing without "boson glue", i.e. without *paramagnons*. It is the mechanism of pairing

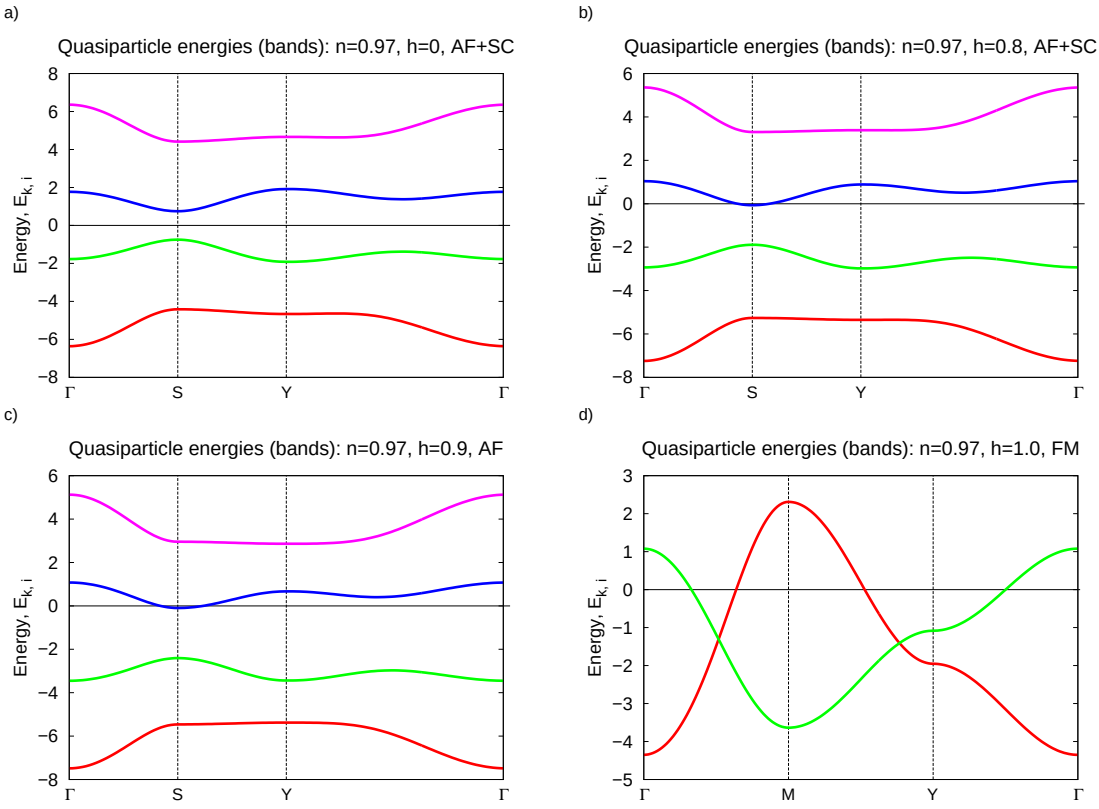

Figure 6.6: Quasiparticle energies (bands) for phases obtained at $n = 0.97$: (a) AF+SC phase, (b) AF+SC phase with nonzero spin-polarization, (c) AF phase, and (d) FM phase (for a different path in the Brillouin zone). Note that in (a-c) two of the energies $E_{\mathbf{k}i}$ (those with $E_{\mathbf{k}i} > 0$) describe quasiparticle states, and the other two represent quasihole states. Also, in (d) only two energies are displayed, as the Brillouin zone is not the folded (magnetic) one, but the full Brillouin zone, because there is no antiferromagnetism in this case. The red curve in (d) describes a quasiparticle with $\sigma =\uparrow$, and the green curve describes a quasihole with $\sigma =\downarrow$. The fully gapped electronic structure in (a)-(c) is caused by the magnetic (renormalized Slater) gap appearance in the AF+SC and the AF phases. Energy scale is in units of J.

arising entirely from interelectron correlations.

As said earlier, it would be very interesting to perform similar analysis within the Periodic Anderson Model, as this might allow for a comparison with the experiments [work along this line is in progress [165]]. Also, testing other Gutzwiller schemes seems important, as well as verifying if the strong antiferromagnetism dominating superconductivity and the tendency towards saturated ferromagnetism are only the characteristic feature of the utilized scheme, or represent a universal tendency of the projected t-J model. For that purpose, the inclusion of realistic, orbitally degenerate f level structure, not just pseudospin Γ_7 doublet of Ce^{3+}, would be desirable.

Chapter 7

Summary and conclusions

7.1 A brief summary

In this Thesis we have analyzed unconventional superconductivity in a system with strong correlations and in an applied Zeeman field. We have concentrated here mainly on concrete predictions for a given model situation by taking into account known (but not tested so far) novel characteristics of the quasiparticle states in the strong-correlation limit and (in the quoted paper, Ref. 95), the real-space pairing among the quasiparticles. We have shown that the *correlations may stabilize the FFLO phase* and explained the *mechanism* of its stabilization. This mechanism is universal, and hence correlations may stabilize other high-field low-temperature (HFLT) phases as well.

We have also performed the detailed analysis of the conductance across a normal metal - strongly-correlated superconductor junction (NSJ). It turns out that the conductance in the case with strong correlations differs essentially (from that in the uncorrelated case), and the differences should be detectable experimentally. Therefore, our analysis provides among others a *test for the presence of strong correlations in the superconducting state*.

Finally, we have studied the coexistence of antiferromagnetism (AF) and superconductivity (SC) within t-J model for a system with strong correlations and in an applied magnetic field. We have obtained a phase diagram on the band filling - magnetic field plane. At band filling close to unity, *our results resemble those obtained recently in the heavy fermion system* $CeCo(In_{1-x}Cd_x)_5$. The last topic is particularly relevant to the strong-correlation limit as in that situation magnetism and pairing are intimately connected by the same exchange interaction.

7.2 Relation to experiment

Our results indicate that strong-correlations may be viewed as one of the driving forces for the appearance of the FFLO and other HFLT phases. Existence of such phases has been suggested for: (i) heavy fermion systems: $CeCoIn_5$ [12, 13, 16, 17, 26], $PuRhGa_5$ [34], Ce_2PdIn_8 [35] (see Ref. 1, Sec. V.B.1 for a more detailed account), (ii) organic superconductors κ-$(BEDT\text{-}TTF)_2Cu(NCS)_2$ [31, 32],

β''-$(ET)_2SF_5CH_2CF_2SO_3$ [33], and others (see References in Ref. 32), and (iii) pnictide superconductor LiFeAs [36]. Obviously, our model is too simplified to account for a fully quantitative behavior of e.g. the HFLT phase of $CeCoIn_5$. On the other hand, the mere fact that the FFLO phase is stabilized by the correlations is, in our view, an important observation and calls for its reexamination within more sophisticated models (see the next Section).

Our analysis of conductance of NSJ for a strongly-correlated superconductor provides a test for the presence of strong correlations in superconductors. Namely, the splitting of the spin-specific features of the NSJ conductance is twice the Zeeman energy only in the non-correlated case. The most promising for experimental verification seems the analysis of situation for the BCS phase, (100) contact, and high Z, as then the spin-specific features are most clearly visible and orbital effects of the magnetic field on the normal side of the junction are not so problematic as in the situation for the FFLO phase (the latter requires much higher magnetic fields). Measurements of NSJ conductance in strongly-correlated systems and in applied magnetic fields have already been performed [138, 139], but only in the low-Z limit, in which the spin-specific features are not so clearly visible as for the high Z.

Finally, our analysis of AF and SC coexistence within the t-J model provides results being in qualitative agreement with those obtained recently in the $CeCo(In_{1-x}Cd_x)_5$ system. Namely, with the increasing magnetic field the system evolves from coexisting phase, through AF phase, towards spin-polarized normal state. To be able to compare those results with the experiment more directly, an analysis within the Periodic Anderson Model (PAM) should be performed [165]. We should be able to see a progress along these lines in the near future.

7.3 Outlook: future projects

There is a number of projects which can be viewed as continuation of the work carried out by us in this Thesis. Among them are the following:

- It would be desirable to account for the incommensurate SDW appearing in the vicinity of the HFLT phase in $CeCoIn_5$ within a strong-correlation approach. For example, to tackle this problem, the model proposed by Yanase and Sigrist [79] could be analyzed in the Gutzwiller method in a range of parameters reflecting better the experimental values (i.e. $8\,t < U < 16\,t$, instead of $U = t$, as assumed in Ref. 79). Such model is solved by utilizing the Bogolyubov-de Gennes (BdG) equations, and in effect the theory is formulated in real space, a circumstance that permits an analysis of the LO type of the FFLO state. The Gutzwiller method has already been applied in connection with solving of the BdG equations in Refs. 166 and 167. On the other hand, the numerical complexity of such approach can become a major problem to resolve.

- By considering the t-J-U model [168, 169] within the Gutzwiller approach and in an applied Zeeman field, the phase diagram obtained by Aperis *et al.*

[80] might be revised within our approach taking into account correlations and assuming a smaller number of phenomenological terms in the starting Hamiltonian. Such formulation can be carried through explicitly with the help of the method similar to that presented in Chapter 6. The principal difficulty is connected with an appropriate formulation of the Gutzwiller method in that situation.

- The scheme presented in Chapter 6 can be applied to PAM, which would allow for a more direct comparison with the experiment, as PAM is considered as a minimal model for studying heavy-fermion systems. Such work is in the process [165].

- The Andreev reflection in the strongly-correlated situation should be studied for a more realistic situation. Namely, the analysis could be performed within a tight-binding approximation (as e.g. in Ref. 170) or in a multichannel model [141] taking into account both light and heavy itinerant electrons, as well as the localized f-electron states on the SC side of the junction.

- It would be interesting to study systematically a nonzero-temperature situation by using an extended Gutzwiller approximation. Such formulations have been discussed in Refs. 171–174 for simple situations in the standard version of GA.

- Finally, the strong correlations should be incorporated into a *reliable* single-electron (band) scheme (for example in the full potential Korringa-Kohn-Rostoker (FP-KKR) method [175–178]) to account for e.g. the wave-function readjustment in the correlated state [for model calculations see Refs. 179–181]. The existing approaches LDA+DMFT [182, 183] and LDA+U [184, 185] incorporate the correlation aspects of the problem in, strictly speaking, a non-consistent manner (due to the so-called Coulomb energy double-counting problem).

Work along these lines is planned in our group within the project "*TEAM*" in the near future.

Appendix A

Explicit expression for W

We provide here the expression for $W \equiv \langle \hat{\mathcal{H}}_{tJ} \rangle_0$. This expression can be divided into parts coming from different terms of Hamiltonian with $W_t \equiv \sum_{ij\sigma} t_{ij} \langle c^\dagger_{i\sigma} c_{j\sigma} \rangle$ and $W_J \equiv J \sum_{\langle ij \rangle} (\langle S^z_i S^z_j \rangle + \langle S^x_i S^x_j + S^y_i S^y_j \rangle)$, as follows $W = W_t + W_J - \Lambda h m_{FM}$. The expressions for W_J and W_t are given by

$$
\begin{aligned}
W_J \;=\; & 2J\Lambda\Big(-\frac{4(\chi_{AB\downarrow}\chi_{AB\uparrow} + \Delta_A\Delta_B)}{\sqrt{m^4_{AF} + (m^2_{FM} - (-2+n)^2)^2 - 2m^2_{AF}(m^2_{FM} + (-2+n)^2)}} \\
& + \frac{1}{4}\Big((-m_{AF} + m_{FM})(m_{AF} + m_{FM}) \\
& - \big(4\big(\Delta^2_A(-1 + m_{AF} - m_{FM})(-1 + m_{AF} + m_{FM}) \\
& \times (2 + m_{AF} - m_{FM} - n)(2 + m_{AF} + m_{FM} - n) \\
& + \chi^2_{AB\uparrow}(1 + m_{AF} - m_{FM})(-1 + m_{AF} + m_{FM}) \\
& \times (2 + m_{AF} + m_{FM} - n)(-2 + m_{AF} - m_{FM} + n) \\
& + \chi^2_{AB\downarrow}(-1 + m_{AF} - m_{FM})(1 + m_{AF} + m_{FM}) \\
& \times (2 + m_{AF} - m_{FM} - n)(-2 + m_{AF} + m_{FM} + n) \\
& + \Delta^2_B(1 + m_{AF} - m_{FM})(1 + m_{AF} + m_{FM}) \\
& \times (-2 + m_{AF} - m_{FM} + n)(-2 + m_{AF} + m_{FM} + n)\big)\big) \\
& / \big((2 + m_{AF} - m_{FM} - n)(2 + m_{AF} + m_{FM} - n) \\
& \times (-2 + m_{AF} - m_{FM} + n)(-2 + m_{AF} + m_{FM} + n)\big)\big)\Big)
\end{aligned}
\tag{A.1}
$$

and

$$
\begin{aligned}
W_t \;=\;& 2\Lambda(-4(1-n)(\frac{4\chi_{AB\downarrow}\Delta_A\Delta_B+\chi_{AB\uparrow}(4\chi_{AB\downarrow}^2+m_{AF}^2-(2+m_{FM}-n)^2)}{(m_{AF}^2-(2+m_{FM}-n)^2)\sqrt{-m_{AF}^2+(-2+m_{FM}+n)^2}}\\
&+\frac{4\chi_{AB\uparrow}\Delta_A\Delta_B+\chi_{AB\downarrow}(4\chi_{AB\uparrow}^2+m_{AF}^2-(-2+m_{FM}+n)^2)}{\sqrt{-m_{AF}^2+(2+m_{FM}-n)^2}(m_{AF}^2-(-2+m_{FM}+n)^2)})t\\
&+(2(-1+n)(-\frac{(\chi_{BB\uparrow}(-4\chi_{BB\downarrow}^2+(-2+m_{AF}-m_{FM}+n)^2))}{(2+m_{AF}-m_{FM}-n)}\\
&+\frac{\chi_{BB\downarrow}(-2+m_{AF}-m_{FM}+n)(-4\chi_{BB\uparrow}^2+(-2-m_{AF}+m_{FM}+n)^2)^2}{-2-m_{AF}+m_{FM}+n})t')\\
&/(-2+m_{AF}-m_{FM}+n)^2\\
&+(2(-1+n)(\chi_{AA\uparrow}(-4\chi_{AA\downarrow}^2+(2+m_{AF}+m_{FM}-n)^2)(-2+m_{AF}+m_{FM}+n)\\
&-\chi_{AA\downarrow}(2+m_{AF}+m_{FM}-n)(-4\chi_{AA\uparrow}^2+(-2+m_{AF}+m_{FM}+n)^2))t')\\
&/((2+m_{AF}+m_{FM}-n)^2(-2+m_{AF}+m_{FM}+n)^2)). \qquad \text{(A.2)}
\end{aligned}
$$

Appendix B

Code performing the summation over the folded Brillouin zone

```
1  double f_beta(void) {
2  double result = 0;
3
4  const int MAX_NX = (int) L/2 - 1;
5  const int MIN_NX = - (int) L/2 + 1;
6
7  int nx, ny, nxp;
8
9  #ifdef FLAG_PARALLEL
10
11   double resultV[MAX_NX - MIN_NX + 1];
12
13   gsl_vector *evalk[MAX_NX - MIN_NX + 1];
14   gsl_matrix *Mk[MAX_NX - MIN_NX + 1];
15
16   for (nx = MIN_NX; nx <= MAX_NX; nx++) {
17     resultV[nx - MIN_NX] = 0;
18     evalk[nx - MIN_NX] = gsl_vector_calloc(4);
19     Mk[nx - MIN_NX] = gsl_matrix_calloc(4, 4);
20   }
21
22   #pragma omp parallel for shared(resultV, evalk, Mk) private(nx, ny, nxp)
23   for (nx = MIN_NX; nx <= 0; nx++) {
24
25     for (ny = -(MAX_NX - abs(nx)); ny <= MAX_NX - abs(nx) + 1; ny++)
26       compute_f_beta_atk(&resultV[nx - MIN_NX], Mk[nx - MIN_NX], evalk[nx - MIN_NX
             ], nx, ny);
27     nxp = nx + (int)L/2;
28     for (ny = -(MAX_NX - abs(nxp)); ny <= MAX_NX - abs(nxp) + 1; ny++)
29       compute_f_beta_atk(&resultV[nxp - MIN_NX], Mk[nxp - MIN_NX], evalk[nxp -
             MIN_NX], nxp, ny);
30     }
31   for (nx = MIN_NX; nx <= MAX_NX; nx++) {
32     result += resultV[nx - MIN_NX];
33     gsl_vector_free (evalk[nx - MIN_NX]);
34     gsl_matrix_free (Mk[nx - MIN_NX]);
35   }
36
37 #else
38   gsl_vector *evalk = gsl_vector_calloc(4);
39   gsl_matrix *Mk = gsl_matrix_calloc(4, 4);
40
41   for (nx = MIN_NX; nx <= MAX_NX; nx++) {
42     for (ny = -(MAX_NX - abs(nx)); ny <= MAX_NX - abs(nx) + 1; ny++) {
43       compute_f_beta_atk(&result, Mk, evalk, nx, ny);
44       }
```

```
45      }
46
47    gsl_vector_free (evalk);
48    gsl_matrix_free (Mk);
49  #endif
50  return result;
51  }
52  /*****************************************************************************/
53  void compute_f_beta_atk(double *result, gsl_matrix *Mk, gsl_vector *evalk, int nx,
        int ny) {
54  const double LIM_EXP = 40.;
55  double temp;
56
57  buildMk(Mk, n2k(nx), n2k(ny));
58  diagonalize(Mk, evalk);
59
60  for (int i=0; i<4; i++) {
61    temp = - gsl_vector_get(evalk, i) * beta;
62    if (temp > LIM_EXP)      *result += temp;
63    else if (temp < -LIM_EXP) *result += exp(temp);
64    else                      *result += log(1. + exp( temp ));
65    }
66  }
```

The `double f_beta(void)` function computes $f_\beta(\vec{\lambda})$ as defined in Eq. (6.48). The procedure `buildMk(Hk, n2k(nx), n2k(ny))` in line 57 builds the $\mathbf{M_k}$ matrix (as defined in Eq. (6.22)) for a given $\mathbf{k}$ point.

The code presented here can be further optimized by utilizing the symmetry of the $\mathbf{k}$ space. Namely the transformations $k_x \to -k_x$ and $k_y \to -k_y$ do not change any energies (as all energies appearing e.g. in $\mathbf{M_k}$ or $\mathcal{F}$ depend on $\mathbf{k}$ via $\cos k_x$ and $\cos k_y$ factors). This allows to reduce the summations to a quarter of the reduced Brillouin zone, and would amount to reduction of time of calculations by about a factor of 4. We did not utilize this symmetry. Also, collapsing the nested for loops[1] (lines: 23 and 25, 28) would lead to some calculation-time improvement. On the other hand, the processor usage for the presented code was above 95%, and therefore, we do not expect an essential improvement from collapsing, as its effect is only a better distribution of the computation work among threads.

[1] Collapsing means bringing them to a form of one for loop with a single index and calculating nx and ny from this index. Such loops are more efficiently parallelized.

Bibliography

[1] C. Pfleiderer, Rev. Mod. Phys. **81**, 1551 (2009).

[2] J. Wosnitza, J. Low Temp. Phys. **146**, 641 (2007).

[3] E. Bauer, G. Hilscher, H. Michor, C. Paul, E. W. Scheidt, A. Gribanov, Y. Seropegin, H. Noël, M. Sigrist, and P. Rogl, Phys. Rev. Lett. **92**, 027003 (2004).

[4] H. Mukuda, S. Nishide, A. Harada, K. Iwasaki, M. Yogi, M. Yashima, Y. Kitaoka, M. Tsujino, T. Takeuchi, R. Settai, Y. Ōnuki, E. Bauer, K. M. Itoh, and E. E. Haller, J. Phys. Soc. Jpn. **78**, 014705 (2009).

[5] M. Sigrist, Physica B: Condensed Matter **280**, 154 (2000).

[6] G. Luke, Y. Fudamoto, K. Kojima, M. Larkin, J. Merrin, B. Nachumi, Y. Uemura, Y. Maeno, Z. Mao, Y. Mori, H. Nakamura, and M. Sigrist, Nature **394**, 558 (1998).

[7] S. Nair, O. Stockert, U. Witte, M. Nicklas, R. Schedler, K. Kiefer, J. D. Thompson, A. D. Bianchi, Z. Fisk, S. Wirth, and F. Steglich, Proc. Natl. Acad. Sci. U. S. A. **107**, 9537 (2010).

[8] G. F. Chen, K. Matsubayashi, S. Ban, K. Deguchi, and N. K. Sato, Phys. Rev. Lett. **97**, 017005 (2006).

[9] N. Kimura, K. Ito, K. Saitoh, Y. Umeda, H. Aoki, and T. Terashima, Phys. Rev. Lett. **95**, 247004 (2005).

[10] S. Saxena, P. Agarwal, K. Ahilan, F. Grosche, R. Haselwimmer, M. Steiner, E. Pugh, I. Walker, S. Julian, P. Monthoux, G. Lonzarich, A. Huxley, I. Sheikin, D. Braithwaite, and J. Flouquet, Nature **406**, 587 (2000).

[11] D. Aoki, A. Huxley, E. Ressouche, D. Braithwaite, J. Flouquet, J.-P. Brison, E. Lhotel, and C. Paulsen, Nature **413**, 613 (2001).

[12] K. Kakuyanagi, M. Saitoh, K. Kumagai, S. Takashima, M. Nohara, H. Takagi, and Y. Matsuda, Phys. Rev. Lett. **94**, 047602 (2005).

[13] K. Kumagai, M. Saitoh, T. Oyaizu, Y. Furukawa, S. Takashima, M. Nohara, H. Takagi, and Y. Matsuda, Phys. Rev. Lett. **97**, 227002 (2006).

[14] Y. Matsuda and H. Shimahara, J. Phys. Soc. Jpn. **76**, 051005 (2007).

[15] B.-L. Young, R. R. Urbano, N. J. Curro, J. D. Thompson, J. L. Sarrao, A. B. Vorontsov, and M. J. Graf, Phys. Rev. Lett. **98**, 036402 (2007).

[16] M. Kenzelmann, T. Strässle, C. Niedermayer, M. Sigrist, B. Padmanabhan, M. Zolliker, A. D. Bianchi, R. Movshovich, E. D. Bauer, J. L. Sarrao, and J. D. Thompson, Science **321**, 1652 (2008).

[17] G. Koutroulakis, M. D. Stewart, V. F. Mitrović, M. Horvatić, C. Berthier, G. Lapertot, and J. Flouquet, Phys. Rev. Lett. **104**, 087001 (2010).

[18] H. Tsunetsugu, M. Sigrist, and K. Ueda, Rev. Mod. Phys. **69**, 809 (1997).

[19] T. Park, M. J. Graf, L. Boulaevskii, J. L. Sarrao, and J. D. Thompson, Proc. Natl. Acad. Sci. U. S. A. **105**, 6825 (2008).

[20] P. Fulde and R. A. Ferrell, Phys. Rev. **135**, A550 (1964).

[21] A. Larkin and Y. Ovchinnikov, J. Exp. Theor. Phys. **47**, 1136 (1964); Sov. Phys. JETP **20**, 762 (1965).

[22] K. Maki, Phys. Rev. **148**, 362 (1966).

[23] L. W. Gruenberg and L. Gunther, Phys. Rev. Lett. **16**, 996 (1966).

[24] A. Bianchi, R. Movshovich, C. Capan, P. G. Pagliuso, and J. L. Sarrao, Phys. Rev. Lett. **91**, 187004 (2003).

[25] C. F. Miclea, M. Nicklas, D. Parker, K. Maki, J. L. Sarrao, J. D. Thompson, G. Sparn, and F. Steglich, Phys. Rev. Lett. **96**, 117001 (2006).

[26] K. Kumagai, H. Shishido, T. Shibauchi, and Y. Matsuda, Phys. Rev. Lett. **106**, 137004 (2011).

[27] V. F. Mitrović, M. Horvatić, C. Berthier, G. Knebel, G. Lapertot, and J. Flouquet, Phys. Rev. Lett. **97**, 117002 (2006).

[28] N. Curro, B.-L. Young, R. Urbano, and M. Graf, J. Low Temp. Phys. **158**, 635 (2010).

[29] J. Spehling, R. H. Heffner, J. E. Sonier, N. Curro, C. H. Wang, B. Hitti, G. Morris, E. D. Bauer, J. L. Sarrao, F. J. Litterst, and H.-H. Klauss, Phys. Rev. Lett. **103**, 237003 (2009).

[30] M. Kenzelmann, S. Gerber, N. Egetenmeyer, J. L. Gavilano, T. Strässle, A. D. Bianchi, E. Ressouche, R. Movshovich, E. D. Bauer, J. L. Sarrao, and J. D. Thompson, Phys. Rev. Lett. **104**, 127001 (2010).

[31] J. Singleton, J. A. Symington, M.-S. Nam, A. Ardavan, M. Kurmoo, and P. Day, J. Phys.: Condens. Matter **12**, L641 (2000).

[32] B. Bergk, A. Demuer, I. Sheikin, Y. Wang, J. Wosnitza, Y. Nakazawa, and R. Lortz, Phys. Rev. B **83**, 064506 (2011).

[33] K. Cho, B. E. Smith, W. A. Coniglio, L. E. Winter, C. C. Agosta, and J. A. Schlueter, Phys. Rev. B **79**, 220507 (2009).

[34] P. Javorský, E. Colineau, F. Wastin, F. Jutier, J.-C. Griveau, P. Boulet, R. Jardin, and J. Rebizant, Phys. Rev. B **75**, 184501 (2007).

[35] J. K. Dong, H. Zhang, X. Qiu, B. Y. Pan, Y. F. Dai, T. Y. Guan, S. Y. Zhou, D. Gnida, D. Kaczorowski, and S. Y. Li, ArXiv e-prints (2010), arXiv:1008.0679 [cond-mat.supr-con] .

[36] K. Cho, H. Kim, M. A. Tanatar, Y. J. Song, Y. S. Kwon, W. A. Coniglio, C. C. Agosta, A. Gurevich, and R. Prozorov, Phys. Rev. B **83**, 060502 (2011).

[37] R. Casalbuoni and G. Nardulli, Rev. Mod. Phys. **76**, 263 (2004).

[38] K. Machida, T. Mizushima, and M. Ichioka, Phys. Rev. Lett. **97**, 120407 (2006).

[39] J. Kinnunen, L. M. Jensen, and P. Törmä, Phys. Rev. Lett. **96**, 110403 (2006).

[40] T. K. Koponen, T. Paananen, J.-P. Martikainen, M. R. Bakhtiari, and P. Törmä, New J. Phys. **10**, 045014 (2008).

[41] J. L. Sarrao and J. D. Thompson, J. Phys. Soc. Jpn. **76**, 051013 (2007).

[42] J. Thompson, R. Movshovich, Z. Fisk, F. Bouquet, N. Curro, R. Fisher, P. Hammel, H. Hegger, M. Hundley, M. Jaime, P. Pagliuso, C. Petrovic, N. Phillips, and J. Sarrao, J. Magn. Magn. Mater. **226-230**, 5 (2001).

[43] H. Shishido, R. Settai, D. Aoki, S. Ikeda, H. Nakawaki, N. Nakamura, T. Iizuka, Y. Inada, K. Sugiyama, T. Takeuchi, K. Kindo, T. C. Kobayashi, Y. Haga, H. Harima, Y. Aoki, T. Namiki, H. Sato, and Y. Ōnuki, J. Phys. Soc. Jpn. **71**, 162 (2002).

[44] C. Petrovic, P. G. Pagliuso, M. F. Hundley, R. Movshovich, J. L. Sarrao, J. D. Thompson, Z. Fisk, and P. Monthoux, J. Phys. Condens. Matter **13**, L337 (2001).

[45] P. Monthoux and G. G. Lonzarich, Phys. Rev. B **59**, 14598 (1999); Phys. Rev. B **63**, 054529 (2001).

[46] J. Paglione, M. A. Tanatar, D. G. Hawthorn, F. Ronning, R. W. Hill, M. Sutherland, L. Taillefer, and C. Petrovic, Phys. Rev. Lett. **97**, 106606 (2006).

[47] A. McCollam, S. R. Julian, P. M. C. Rourke, D. Aoki, and J. Flouquet, Phys. Rev. Lett. **94**, 186401 (2005).

[48] D. Hall, E. C. Palm, T. P. Murphy, S. W. Tozer, Z. Fisk, U. Alver, R. G. Goodrich, J. L. Sarrao, P. G. Pagliuso, and T. Ebihara, Phys. Rev. B **64**, 212508 (2001).

[49] A. Koitzsch, I. Opahle, S. Elgazzar, S. V. Borisenko, J. Geck, V. B. Zabolotnyy, D. Inosov, H. Shiozawa, M. Richter, M. Knupfer, J. Fink, B. Büchner, E. D. Bauer, J. L. Sarrao, and R. Follath, Phys. Rev. B **79**, 075104 (2009).

[50] W. K. Park, J. L. Sarrao, J. D. Thompson, and L. H. Greene, Phys. Rev. Lett. **100**, 177001 (2008).

[51] R. Movshovich, M. Jaime, J. D. Thompson, C. Petrovic, Z. Fisk, P. G. Pagliuso, and J. L. Sarrao, Phys. Rev. Lett. **86**, 5152 (2001).

[52] K. Izawa, H. Yamaguchi, Y. Matsuda, H. Shishido, R. Settai, and Y. Ōnuki, Phys. Rev. Lett. **87**, 057002 (2001).

[53] J. Costa-Quintana, F. López-Aguilar, and M. M. Sánchez-López, Physica C **408-410**, 268 (2004).

[54] J. Costa-Quintana and F. López-Aguilar, J. Phys.: Condens. Matter **16**, 6941 (2004).

[55] J. L. Wang, Z. Zeng, and H. Q. Lin, J. Appl. Phys. **99**, 08M505 (2006).

[56] T. P. Murphy, D. Hall, E. C. Palm, S. W. Tozer, C. Petrovic, Z. Fisk, R. G. Goodrich, P. G. Pagliuso, J. L. Sarrao, and J. D. Thompson, Phys. Rev. B **65**, 100514 (2002).

[57] H. Radovan, N. Fortune, T. Murphy, S. Hannahs, E. Palm, S. Tozer, and D. Hall, Nature **425**, 51 (2003).

[58] R. Movshovich, A. Bianchi, C. Capan, M. Jaime, and R. Goodrich, Nature **427**, 802 (2004).

[59] N. J. Curro, Rep. Prog. Phys. **72**, 026502 (2009).

[60] V. F. Mitrović, G. Koutroulakis, M. Klanjšek, M. Horvatić, C. Berthier, G. Knebel, G. Lapertot, and J. Flouquet, Phys. Rev. Lett. **101**, 039701 (2008).

[61] K. Kakuyanagi, K. Kumagai, and Y. Matsuda, Phys. Rev. Lett. **101**, 039702 (2008).

[62] R. Movshovich, Y. Tokiwa, N. Kurita, F. Ronning, E. Bauer, A. Bianchi, P. Papin, and Z. Fisk, J. Supercond. Nov. Magn. **22**, 291 (2009).

[63] Y. Tokiwa, R. Movshovich, F. Ronning, E. D. Bauer, P. Papin, A. D. Bianchi, J. F. Rauscher, S. M. Kauzlarich, and Z. Fisk, Phys. Rev. Lett. **101**, 037001 (2008).

[64] Y. Tokiwa, R. Movshovich, F. Ronning, E. D. Bauer, A. D. Bianchi, Z. Fisk, and J. D. Thompson, Phys. Rev. B **82**, 220502 (2010).

[65] R. Ikeda, Phys. Rev. B **81**, 060510 (2010).

[66] A. Bianchi, M. Kenzelmann, L. DeBeer-Schmitt, J. White, E. Forgan, J. Mesot, M. Zolliker, J. Kohlbrecher, R. Movshovich, E. Bauer, J. Sarrao, Z. Fisk, C. Petrović, and M. Eskildsen, Science **319**, 177 (2008).

[67] R. Ikeda, Y. Hatakeyama, and K. Aoyama, Phys. Rev. B **82**, 060510 (2010).

[68] Y. Hatakeyama and R. Ikeda, ArXiv e-prints (2011), arXiv:1103.1735 [cond-mat.supr-con] .

[69] Q. Cui, C.-R. Hu, J. Y. T. Wei, and K. Yang, Phys. Rev. B **73**, 214514 (2006).

[70] Y. Tanaka, Y. Asano, M. Ichioka, and S. Kashiwaya, Phys. Rev. Lett. **98**, 077001 (2007).

[71] J. Spałek and P. Gopalan, Phys. Rev. Lett. **64**, 2823 (1990).

[72] P. Korbel, J. Spałek, W. Wójcik, and M. Acquarone, Phys. Rev. B **52**, R2213 (1995).

[73] J. Spałek and W. Wójcik, *Spectroscopy of the Mott Insulators and Correlated Metals*, edited by A. Fujimori and Y. Tokura, Vol. 119 (Springer-Verlag, Berlin, 1995) pp. 41–65.

[74] R. Doradziński and J. Spałek, Phys. Rev. B **58**, 3293 (1998).

[75] J. Bauer and A. C. Hewson, Phys. Rev. B **76**, 035118 (2007).

[76] S. Onari, H. Kontani, and Y. Tanaka, J. Phys. Soc. Jpn. **77**, 023703 (2008).

[77] I. Sheikin, A. Gröger, S. Raymond, D. Jaccard, D. Aoki, H. Harima, and J. Flouquet, Phys. Rev. B **67**, 094420 (2003).

[78] M. Takashita, H. Aoki, T. Terashima, S. Uji, K. Maezawa, R. Settai, and Y. Ōnuki, J. Phys. Soc. Jpn. **65**, 515 (1996).

[79] Y. Yanase and M. Sigrist, J. Phys. Soc. Jpn. **78**, 114715 (2009); J. Phys.: Condens. Matter **23**, 094219 (2011); J. Phys.: Conf. Ser. **150**, 052287 (2009).

[80] A. Aperis, G. Varelogiannis, and P. B. Littlewood, Phys. Rev. Lett. **104**, 216403 (2010).

[81] Z.-J. Ying, M. Cuoco, C. Noce, and H.-Q. Zhou, Phys. Rev. B **78**, 104523 (2008).

[82] J. Kaczmarczyk, M. Sc. Thesis, Jagiellonian University, Kraków (2007).

[83] J. Kaczmarczyk and J. Spałek, Phys. Rev. B **79**, 214519 (2009).

[84] J. Jędrak, J. Kaczmarczyk, and J. Spałek, ArXiv e-prints (2010), arXiv:1008.0021 [cond-mat.str-el] .

[85] D. Vollhardt, Rev. Mod. Phys. **56**, 99 (1984).

[86] G. Kotliar and A. E. Ruckenstein, Phys. Rev. Lett. **57**, 1362 (1986).

[87] M. C. Gutzwiller, Phys. Rev. Lett. **10**, 159 (1963); Phys. Rev. **134**, A923 (1964); Phys. Rev. **137**, A1726 (1965).

[88] B. Edegger, V. N. Muthukumar, and C. Gros, Adv. Phys. **56**, 927 (2007).

[89] J. Spałek, A. Datta, and J. M. Honig, Phys. Rev. B **33**, 4891 (1986); J. Spalek, Phys. Rev. Lett. **59**, 728 (1987).

[90] J. Spałek, Phys. Rev. B **37**, 533 (1988).

[91] F. C. Zhang, C. Gros, T. M. Rice, and H. Shiba, Supercond. Sci. Technol. **1**, 36 (1988).

[92] D. Poilblanc, Phys. Rev. B **72**, 060508 (2005).

[93] M. Raczkowski, D. Poilblanc, R. Frésard, and A. M. Oleś, Phys. Rev. B **75**, 094505 (2007); M. Raczkowski, M. Capello, D. Poilblanc, R. Frésard, and A. M. Oleś, Phys. Rev. B **76**, 140505 (2007); M. Raczkowski, M. Capello, and D. Poilblanc, Acta Phys. Polon. A **115**, 77 (2009).

[94] M. Raczkowski and D. Poilblanc, Phys. Rev. Lett. **103**, 027001 (2009).

[95] M. M. Maśka, M. Mierzejewski, J. Kaczmarczyk, and J. Spałek, Phys. Rev. B **82**, 054509 (2010).

[96] F. Gebhard, Phys. Rev. B **44**, 992 (1991).

[97] J. Bünemann, F. Gebhard, and R. Thul, Phys. Rev. B **67**, 075103 (2003).

[98] C. Li, S. Zhou, and Z. Wang, Phys. Rev. B **73**, 060501 (2006).

[99] J. Spałek, phys. stat. sol. (b) **243**, 78 (2006).

[100] J. Spałek, Phys. Rev. B **38**, 208 (1988); J. Spałek and P. Gopalan, J. Phys. (France) **50**, 2869 (1989); J. Karbowski and J. Spałek, Phys. Rev. B **49**, 1454 (1994).

[101] Y. Nagaoka, Phys. Rev. **147**, 392 (1966).

[102] G. Carleo, S. Moroni, F. Becca, and S. Baroni, Phys. Rev. B **83**, 060411 (2011).

[103] F. Becca and S. Sorella, Phys. Rev. Lett. **86**, 3396 (2001).

[104] H. Park, K. Haule, C. A. Marianetti, and G. Kotliar, Phys. Rev. B **77**, 035107 (2008).

[105] T. Hanisch, G. S. Uhrig, and E. Müller-Hartmann, Phys. Rev. B **56**, 13960 (1997).

[106] G. Knebel, D. Aoki, J.-P. Brison, L. Howald, G. Lapertot, J. Panarin, S. Raymond, and J. Flouquet, phys. stat. sol. (b) **247**, 557 (2010).

[107] J. Jędrak and J. Spałek, Phys. Rev. B **83**, 104512 (2011).

[108] G. Rickayzen, *Theory of Superconductivity* (John Wiley & Sons, 1965).

[109] P. G. de Gennes, *Superconductivity of Metals and Alloys* (Westview Press, 1999).

[110] H. Shimahara, Phys. Rev. B **50**, 12760 (1994).

[111] J. Kaczmarczyk and J. Spałek, J. Phys.: Condens. Matter **22**, 355702 (2010).

[112] A. Aperis, G. Varelogiannis, P. B. Littlewood, and B. Simons, J. Supercond. Nov. Magn. **22**, 115 (2009).

[113] T. Yokoyama, S. Onari, and Y. Tanaka, J. Phys. Soc. Jpn. **77**, 064711 (2008).

[114] H. Shimahara, Phys. Rev. B **62**, 3524 (2000).

[115] H. Shimahara, J. Phys. Soc. Jpn. **71**, 1644 (2002).

[116] A. Andreev, Zh. Eksp. Teor. Fiz. **46**, 1823 (1964); Sov. Phys. JETP **19**, 1228 (1964).

[117] G. E. Blonder, M. Tinkham, and T. M. Klapwijk, Phys. Rev. B **25**, 4515 (1982).

[118] J. Kaczmarczyk, M. Sadzikowski, and J. Spałek, Physica C **471**, 193 (2011).

[119] T. Partyka, M. Sadzikowski, and M. Tachibana, Physica C **470**, 277 (2010).

[120] D. Zhang, C. S. Ting, and C.-R. Hu, Phys. Rev. B **70**, 172508 (2004).

[121] V. Lukic and E. J. Nicol, Phys. Rev. B **76**, 144508 (2007).

[122] Y. Tanaka and S. Kashiwaya, Phys. Rev. Lett. **74**, 3451 (1995).

[123] C. Bruder, Phys. Rev. B **41**, 4017 (1990).

[124] S. Kashiwaya and Y. Tanaka, Rep. Prog. Phys. **63**, 1641 (2000).

[125] K. Argyropoulos and A. Dimoulas, Physica C **405**, 77 (2004).

[126] W. K. Park and L. H. Greene, J. Phys.: Condens. Matter **21**, 103203 (2009).

[127] G. Goll, Adv. Solid State Phys. **45**, 213 (2006).

[128] G. Deutscher and P. Nozières, Phys. Rev. B **50**, 13557 (1994).

[129] M. A. N. Araújo and P. D. Sacramento, Phys. Rev. B **77**, 134519 (2008).

[130] M. A. N. Araújo and A. H. Castro Neto, Phys. Rev. B **75**, 115133 (2007).

[131] M. G. Burt, Phys. Rev. B **50**, 7518 (1994).

[132] N. A. Mortensen, K. Flensberg, and A.-P. Jauho, Phys. Rev. B **59**, 10176 (1999).

[133] G. Annunziata, M. Cuoco, C. Noce, A. Romano, and P. Gentile, Phys. Rev. B **80**, 012503 (2009); G. Annunziata, M. Cuoco, P. Gentile, A. Romano, and C. Noce, Phys. Rev. B **83**, 094507 (2011).

[134] S. Chaudhuri and P. F. Bagwell, Phys. Rev. B **51**, 16936 (1995).

[135] H. Hoppe, U. Zülicke, and G. Schön, Phys. Rev. Lett. **84**, 1804 (2000).

[136] T. D. Moore and D. A. Williams, Phys. Rev. B **59**, 7308 (1999).

[137] J. Kačmarčík, P. Szabó, P. Samuely, K. Flachbart, A. Nader, and A. Briggs, Physica B **259-261**, 985 (1999).

[138] W. K. Park, J. L. Sarrao, J. D. Thompson, L. D. Pham, Z. Fisk, and L. H. Greene, Physica B **403**, 731 (2008).

[139] W. K. Park, L. D. Pham, A. D. Bianchi, C. Capan, Z. Fisk, and L. H. Greene, J. Phys.: Conf. Ser. **150**, 052208 (2009).

[140] V. Dmitriev, L. Rybaltchenko, E. Khristenko, L. Ishchenko, Z. Bukowski, and R. Troć, Acta Phys. Polon. A **114**, 263 (2008); V. Dmitriev, L. Rybaltchenko, L. Ishchenko, E. Khristenko, Z. Bukowski, and R. Troć, Low Temp. Phys. **33**, 1009 (2007).

[141] M. Fogelström, W. K. Park, L. H. Greene, G. Goll, and M. J. Graf, Phys. Rev. B **82**, 014527 (2010).

[142] E. Demler, W. Hanke, and S.-C. Zhang, Rev. Mod. Phys. **76**, 909 (2004).

[143] P. A. Lee, N. Nagaosa, and X.-G. Wen, Rev. Mod. Phys. **78**, 17 (2006).

[144] P. Monthoux, D. Pines, and G. Lonzarich, Nature **450**, 1177 (2007).

[145] G. Knebel, D. Aoki, D. Braithwaite, B. Salce, and J. Flouquet, Phys. Rev. B **74**, 020501 (2006).

[146] R. R. Urbano, B.-L. Young, N. J. Curro, J. D. Thompson, L. D. Pham, and Z. Fisk, Phys. Rev. Lett. **99**, 146402 (2007).

[147] N. Fukushima, Phys. Rev. B **78**, 115105 (2008).

[148] P. D. Sacramento, J. Phys.: Condens. Matter **15**, 6285 (2003).

[149] J. V. Alvarez and F. Yndurain, Phys. Rev. Lett. **98**, 126406 (2007).

[150] J. Spałek, Acta Phys. Polon. A **111**, 409 (2007).

[151] P. W. Anderson, P. A. Lee, M. Randeria, T. M. Rice, N. Trivedi, and F. C. Zhang, J. Phys.: Cond. Matter **16**, R755 (2004).

[152] N. Fukushima, J. Phys. A: Math. Theor. **44**, 075002 (2011).

[153] P. Fazekas, *Lecture Notes on Electron Correlation and Magnetism* (World Scientific Publishing, 1999) chapter 7.

[154] B. Kyung, Phys. Rev. B **62**, 9083 (2000).

[155] G. C. Psaltakis and E. W. Fenton, J. Phys. C **16**, 3913 (1983).

[156] S. Tsonis, P. Kotetes, G. Varelogiannis, and P. B. Littlewood, J. Phys.: Cond. Matter **20**, 434234 (2008).

[157] M. Ogata, J. Phys. Soc. Jpn. **66**, 3375 (1997).

[158] F. Loder, A. P. Kampf, and T. Kopp, Phys. Rev. B **81**, 020511 (2010).

[159] J. Jędrak and J. Spałek, Phys. Rev. B **81**, 073108 (2010); J. Jędrak and J. Spałek, ArXiv e-prints (2008), arXiv:0804.1376 [cond-mat.str-el] ; J. Kaczmarczyk, J. Jędrak, and J. Spałek, Acta Phys. Polon. A **118**, 261 (2010).

[160] J. Jędrak and J. Spałek, Phys. Rev. B **83**, 104512 (2011).

[161] Q.-H. Wang, Z. D. Wang, Y. Chen, and F. C. Zhang, Phys. Rev. B **73**, 092507 (2006).

[162] K.-Y. Yang, W. Q. Chen, T. M. Rice, M. Sigrist, and F.-C. Zhang, New J. Phys. **11**, 055053 (2009).

[163] T. Koretsune and M. Ogata, Phys. Rev. Lett. **89**, 116401 (2002); J. Phys. Soc. Jpn. **72**, 2437 (2003).

[164] W. O. Putikka, M. U. Luchini, and M. Ogata, Phys. Rev. Lett. **69**, 2288 (1992).

[165] O. Howczak, Ph. D. Thesis, Jagiellonian University, Kraków, in preparation.

[166] H. Tsuchiura and M. Ogata, J. Phys.: Conf. Ser. **150**, 052272 (2009).

[167] A. Garg, M. Randeria, and N. Trivedi, ArXiv e-prints (2006), arXiv:cond-mat/0609666 .

[168] F. C. Zhang, Phys. Rev. Lett. **90**, 207002 (2003).

[169] J. Y. Gan, Y. Chen, Z. B. Su, and F. C. Zhang, Phys. Rev. Lett. **94**, 067005 (2005).

[170] K.-Y. Yang, K. Huang, W.-Q. Chen, T. M. Rice, and F.-C. Zhang, Phys. Rev. Lett. **105**, 167004 (2010).

[171] J. Spałek, A. M. Oleś, and J. M. Honig, Phys. Rev. B **28**, 6802 (1983).

[172] J. Spałek, A. Datta, and J. M. Honig, Phys. Rev. B **33**, 4891 (1986).

[173] K. Seiler, C. Gros, T. M. Rice, K. Ueda, and D. Vollhardt, J. Low Temp. Phys. **64**, 195 (1986).

[174] J. Spałek, Phys. Rev. Lett. **59**, 728 (1987).

[175] A. Bansil, S. Kaprzyk, P. E. Mijnarends, and J. Toboła, Phys. Rev. B **60**, 13396 (1999).

[176] T. Stopa, S. Kaprzyk, and J. Toboła, J. Phys.: Condens. Matter **16**, 4921 (2004).

[177] B. Wiendlocha, J. Tobola, S. Kaprzyk, and A. Kolodziejczyk, Phys. Rev. B **83**, 094408 (2011).

[178] B. Wiendlocha, Ph. D. Thesis, AGH University of Science and Technology, Kraków (2009).

[179] J. Kurzyk, Ph. D. Thesis, Jagiellonian University, Kraków (2007).

[180] J. Kurzyk, W. Wójcik, and J. Spałek, Eur. Phys. J. B **66**, 385 (2008).

[181] J. Spałek, J. Kurzyk, R. Podsiadły, and W. Wójcik, Eur. Phys. J. B **74**, 63 (2010).

[182] V. I. Anisimov, A. I. Poteryaev, M. A. Korotin, A. O. Anokhin, and G. Kotliar, J. Phys.: Condens. Matter **9**, 7359 (1997).

[183] A. Georges, G. Kotliar, W. Krauth, and M. J. Rozenberg, Rev. Mod. Phys. **68**, 13 (1996).

[184] V. I. Anisimov, J. Zaanen, and O. K. Andersen, Phys. Rev. B **44**, 943 (1991).

[185] A. I. Liechtenstein, V. I. Anisimov, and J. Zaanen, Phys. Rev. B **52**, R5467 (1995).